MECHANISMS AND CONTROLS OF TRACE GAS RELEASES FROM A NORTHERN PEATLAND

by

Elizabeth J. Fechner

B.A. Environmental Sciences,
University of Virginia (1986)

SUBMITTED TO THE DEPARTMENT OF
CIVIL ENGINEERING
IN PARTIAL FULFILLMENT OF THE REQUIREMENTS
FOR THE DEGREE OF

MASTER OF SCIENCE
IN CIVIL ENGINEERING

at the

MASSACHUSETTS INSTITUTE OF TECHNOLOGY
February, 1991

Signature of Author _____
Department of Civil Engineering
January 28, 1991

Certified by _____
Professor Harold F. Hemond
Thesis Supervisor

Accepted by _____
Ole S. Madsen
Department Committee on Graduate Studies

MECHANISMS AND CONTROLS OF TRACE GAS RELEASES FROM A NORTHERN PEATLAND

by

Elizabeth J. Fechner

Submitted to the Department of Civil Engineering
on January 28, 1991 in partial fulfillment of the
requirements for the Degree of Master of Science in Civil Engineering

ABSTRACT

Atmospheric concentrations of methane, a greenhouse gas, have been steadily increasing in recent years. Northern peatlands are acknowledged to be a significant non-anthropogenic source of methane. An intensive study of a northern peatland, Thoreau's Bog in Concord, Massachusetts, was undertaken to measure magnitude and seasonality of fluxes of methane and to elucidate the importance of ebullition and reoxidation.

Clear annual patterns in porewater CH_4, N_2, and CO_2 concentrations were found. Much of the seasonal fluctuation in porewater concentrations of CH_4 can be explained by porewater temperature fluctuations and the resultant changes in gas partitioning between liquid and bubble phases. Variation in CH_4 sources and sinks seems to be secondary in importance. For CO_2, changes in sources and sinks play a much larger role in affecting the annual cycle of aqueous CO_2 because the solubility of CO_2 is so high.

Atmospheric pressure was found to affect the volume of the bubble phase in the floating peat mat of the bog. Estimates of bubble volume were made based on changes in the buoyancy of the peat mat. Potential parameters that might regulate bubble volume by triggering episodes of ebullition were also investigated.

By analysis of peat porosity and methane concentration profiles in the unsaturated zone, and by use of a propane tracer, both atmospheric release rates and reoxidation rates of CH_4 were measured without changing in situ conditions either by triggering bubble efflux or by altering peat surface boundary conditions. CH_4 flux from water-saturated, methanogenic sediment to the unsaturated zone was of the order of 2.4 moles m^{-2} yr^{-1}, over 3 times the CH_4 flux to the atmosphere. Most reoxidation appears to occur between the water table and about 6 cm below the moss surface. Methane concentrations and methane reoxidation rates are unevenly distributed within the unsaturated zone, probably following patterns of upward transport of CH_4 by bubbles via fissures and tubes. Methane profiles can be greatly altered by walking on the peatland surface near the measurement location. A new technique for measuring effective diffusion coefficients in peat using propane as a tracer is described.

Thesis Supervisor: Dr. Harold Hemond Title: Professor of Civil Engineering

ACKNOWLEDGEMENTS

My sincerest and deepest thanks go to my advisor, Professor Harold Hemond, for whom it was a pleasure to work. His combination of intellect, patience, and humor is remarkable. I am very appreciative of the opportunity afforded me to work with him at Thoreau's Bog.

I am also indebted to the Parsons Foundation and Mr. Cecil Green for Parsons and Green Fellowships.

I have enjoyed knowing many people at the Parsons Lab; several deserve special recognition for their help and friendship: Lynn Roberts, Heekyung Kim, Yu Chin, and Tom Carlin. I especially want to acknowledge my very close friendship with Dianne Tobey Covault.

This thesis would not have been completed without a vast amount of love and support from my family, especially from my husband, Mr. Benjamin S. Levy, my parents, Dr. Robert E. Fechner and Mrs. Loretta B. Fechner, my sister, Mrs. Cynthia F. Moser, and my grandparents, Dr. and Mrs. Albert H. Fechner.

> But all at once it dawned on me that this
> Was the real point, the contrapuntal theme;
> Just this: not text, but texture; not the dream
> But a topsy-turvical coincidence,
> Not flimsy nonsense, but a web of sense.
> Yes! It sufficed that I in life could find
> Some kind of link-and-bobolink, some kind
> Of correlated pattern in the game,
> Plexed artistry, and something of the same
> Pleasure in it as they who played it found.
>
> Vladimir Nabokov, Pale Fire

TABLE OF CONTENTS

Abstract 2

Acknowledgements 3

Table of Contents 4

List of Figures 6

List of Tables 9

CHAPTER 1

Introduction 11
Materials and Methods 15
Results 20
Discussion 36
References 50

CHAPTER 2

Introduction 53
Materials and Methods 55
Results 58
Discussion 79
References 83

CHAPTER 3

Introduction 85
Materials and Methods 88
Results 94
Discussion 106
References 114

APPENDICES

A Molar Concentrations of N_2, CH_4, and CO_2 in Well Porewaters 116

APPENDICES (continued)

B Temperatures of Well Porewaters 126

C Partial Pressures of Porewater Gases 130

D Mat, Water, Pressure, and Wind Data for Four Selected Periods 134

E Propane and Methane Profiles from Propane Tracer Tests 140

LIST OF FIGURES

Fig. 1-1: Locations of Well Nests at Thoreau's Bog 17
Fig. 1-2: Fast Fourier Transform of Methane Data 21
Fig. 1-3: Temporal Variations in Temperature at 0.61 m Depth 23
Fig. 1-4: Temporal Variations in Temperature at 0.91 m Depth 24
Fig. 1-5: Temporal Variations in Temperature at 1.22 m Depth 25
Fig. 1-6: Temporal Variations in Porewater Nitrogen at 0.68 m Depth 26
Fig. 1-7: Temporal Variations in Porewater Nitrogen at 0.92 m Depth 27
Fig. 1-8: Temporal Variations in Porewater Nitrogen at 1.36 m Depth 28
Fig. 1-9: Temporal Variations in Porewater Methane at 0.68 m Depth 29
Fig. 1-10: Temporal Variations in Porewater Methane at 0.92 m Depth 30
Fig. 1-11: Temporal Variations in Porewater Methane at 1.36 m Depth 31
Fig. 1-12: Temporal Variations in Porewater Carbon Dioxide at 0.68 m Depth 32
Fig. 1-13: Temporal Variations in Porewater Carbon Dioxide at 0.92 m Depth 33
Fig. 1-14: Temporal Variations in Porewater Carbon Dioxide at 1.36 m Depth 34
Fig. 1-15: Temperature-dependent Partitioning of N_2 at 0.68 m Depth 38
Fig. 1-16: Temperature-dependent Partitioning of N_2 at 0.92 m Depth 39
Fig. 1-17: Temperature-dependent Partitioning of N_2 at 1.36 m Depth 40
Fig. 1-18: Temperature-dependent Partitioning of CH_4 at 0.68 m Depth 41
Fig. 1-19: Temperature-dependent Partitioning of CH_4 at 0.92 m Depth 42
Fig. 1-20: Temperature-dependent Partitioning of CH_4 at 1.36 m Depth 43
Fig. 1-21: Temperature-dependent Partitioning of CO_2 at 0.68 m Depth 44
Fig. 1-22: Temperature-dependent Partitioning of CO_2 at 0.92 m Depth 45
Fig. 1-23: Temperature-dependent Partitioning of CO_2 at 1.36 m Depth 46

Fig. 2-1: Peat Porosity Experiment 57
Fig. 2-2: Depth to Mat versus Depth to Water,
June 24 to December 10, 1988 59
Fig. 2-3: Depth to Mat versus Depth to Water,
March 16 to December 8, 1989 60
Fig. 2-4: Temporal Variations in Mat and Water Heights,
6/29/88 to 7/6/88 61
Fig. 2-5: Temporal Variations in Mat and Water Heights,
8/11/88 to 8/23/88 62
Fig. 2-6: Temporal Variations in Mat and Water Heights,
6/23/89 to 6/29/89 63
Fig. 2-7: Temporal Variations in Mat and Water Heights,
7/29/89 to 8/7/89 64
Fig. 2-8: Corrected Mat Levels versus Pressure,
6/29/88 to 7/6/88 66
Fig. 2-9: Corrected Mat Levels versus Pressure,
8/11/88 to 8/23/88 67
Fig. 2-10: Corrected Mat Levels versus Pressure,
6/23/89 to 6/29/89 68
Fig. 2-11: Corrected Mat Levels versus Pressure,
7/29/89 to 8/7/89 69
Fig. 2-12: Corrected Mat Level Residuals versus
Pressure Change w.r.t. Time, 6/29/88 to 7/6/88 71
Fig. 2-13: Corrected Mat Level Residuals versus
Pressure Change w.r.t. Time, 8/11/88 to 8/23/88 72
Fig. 2-14: Corrected Mat Level Residuals versus
Pressure Change w.r.t. Time, 6/23/89 to 6/29/89 73
Fig. 2-15: Corrected Mat Level Residuals versus
Pressure Change w.r.t. Time, 7/29/89 to 8/7/89 74
Fig. 2-16: Corrected Mat Level Residuals versus
Wind Speed, 6/29/88 to 7/6/88 75
Fig. 2-17: Corrected Mat Level Residuals versus
Wind Speed, 8/11/88 to 8/23/88 76
Fig. 2-18: Corrected Mat Level Residuals versus
Wind Speed, 6/23/89 to 6/29/89 77
Fig. 2-19: Corrected Mat Level Residuals versus
Wind Speed, 7/29/89 to 8/7/89 78
Fig. 3-1: Peat Porosity Experiment 91
Fig. 3-2: Unsaturated Zone Profiles Taken from Platform 95
Fig. 3-3: Unsaturated Zone Profiles Taken from Platform 96
Fig. 3-4: Unsaturated Zone Profiles Taken Remotely 97
Fig. 3-5: Undisturbed and Disturbed Unsaturated Zone
Profiles 98
Fig. 3-6: Unsaturated Zone Profiles Taken Remotely 99

Fig. 3-7: Unsaturated Zone Profiles Taken Remotely and from Platform 100
Fig. 3-8: Unsaturated Zone Profiles Taken Remotely 101
Fig. 3-9: Flux Box Experiment, Disturbed Sampling after 30 min. 104
Fig. 3-10: Propane Tracer Tests, 10/11/90 and 11/16/90 105
Fig. 3-11: Methane Profiles from Propane Tracer Tests, 10/25/90, 11/1/90, and 11/16/90 107

LIST OF TABLES

Table 1-1: Depths of Wells at Thoreau's Bog 16
Table 1-2: Temperature and Porewater Gas Concentration Data Filtered by a Fast Fourier Transform 35
Table 2-1: Bubble Volume Calculations 81
Table 3-1: Methane Fluxes from Northern Peatlands, Measured Using Flux Chambers 86
Table 3-2: Methane Fluxes in the Unsaturated Zone 109

CHAPTER 1

The Saturated Zone

INTRODUCTION

Recent measurements of tropospheric gases have shown that the concentrations of carbon dioxide (CO_2), methane (CH_4), and other trace gases such as nitrous oxide (N_2O) have increased within the last century (Khalil and Rasmussen, 1987; Blake and Rowland, 1988; Matthews and Fung, 1987). Much of the increase is attributed to anthropogenic activities. The increased concentrations of these gases in the atmosphere is of great concern because these gases trap the infrared radiation emitted by the Earth, thereby causing increases in the Earth's average surface temperatures. This so-called "greenhouse effect" could initiate a positive feedback mechanism by enhancing sources of certain atmospheric trace gases, leading to further temperature increases.

Atmospheric CO_2 has increased by approximately 12% since 1960 (Keeling et al., 1989), or approximately 0.4% per year (Dickinson and Cicerone, 1986). Current levels of CO_2 in the atmosphere are approximately 3.5×10^5 ppbv (Dickinson and Cicerone, 1986). Most of the increase in atmospheric CO_2 can be attributed to fossil fuel combustion and the burning of forests and wood. Atmospheric CH_4 has increased at a rate of about 1.5% per year for the past 10 years (Seiler, 1984); current levels are approximately 1700 ppbv (Stauffer et al., 1988). About 50% to 70% of CH_4 present in the atmosphere is from anthropogenic sources such as rice paddies and herds of cattle. The other 30% to 50% is due primarily to fluxes from northern peatlands and subtropical, tropical, and other wetland sources (Wahlen et al., 1989). The influence from wetland

sources is reflected in the seasonal fluctuations in atmospheric CH_4 concentrations, with higher concentrations in the summer (Khalil and Rasmussen, 1990; Matthews and Fung, 1987). Molecule for molecule, CH_4 is about 20 times more effective than CO_2 in creating the greenhouse effect because the "window" through which 8-12 μm radiation passes is still relatively open, so every CH_4 molecule makes a greater difference. CO_2 has almost "closed" the window through which 12-18 μm wavelength radiation escapes (Dickinson and Cicerone, 1986).

Northern peatlands, which may contribute upwards of 30% of the atmospheric CH_4 flux, lie approximately between 45° N and 65° N in Alaska, Canada, the Soviet Union, the United Kingdom, and Scandinavia. Northern peatlands are characterized by long-term accumulations of detrital organic carbon, called peat. This accumulation occurs because the input of carbon from the production of organic matter has exceeded the amount of carbon mineralized through the decomposition of organic matter. Carbon mineralization is inhibited by the anaerobic, acidic conditions that usually exist in peatlands.

Northern peatlands cover an area in excess of 3×10^6 km^2 (Matthews and Fung, 1987). They contain approximately 170×10^{15} g of carbon in biomass and detrital material, which represents about 20% of the carbon pool in the atmosphere (Miller, 1981). If global temperatures were to rise due to the greenhouse effect, thereby altering the climate, a significant fraction of the carbon stored in peatlands could be released as atmospheric CO_2 and CH_4, thereby leading to further temperature increases.

The reactions which produce CH_4 and CO_2 in peatlands are anaerobic and are mediated by microorganisms called methanogens. Methanogenic bacteria belong to a distinct group known as archaeobacteria, which require highly reducing (a redox potential of less than -330 mV) and highly anaerobic (less than 2 ppm oxygen) environments to grow (Williams and Crawford, 1985). Almost all methanogenic bacteria reduce CO_2 to CH_4:

$$H_2CO_3^{\bullet} + 4\ H_2 \rightarrow CH_4 + 3\ H_2O \qquad (1\text{-}1)$$

Many methanogens also convert acetate to CH_4:

$$H^+ + CH_3COO\text{-} + H_2O \rightarrow CH_4 + H_2CO_3^{\bullet} \qquad (1\text{-}2)$$

These are the two major methanogenic pathways (Winfrey and Zeikus, 1979; Atlas, 1984). Methanogenesis is temperature-dependent, with increased numbers of methanogenic bacteria and higher rates of CH_4 production occurring at higher temperatures (Zeikus and Winfrey, 1976; Williams and Crawford, 1984; Crill et al., 1988).

The contribution of the methanogenic activity of northern peatlands to the overall CH_4 flux to the atmosphere has been estimated mainly through the use of flux chambers and peat core incubation experiments. Flux chambers are boxes put over an area of wetland to trap gases, which are then analyzed. The limitations of flux chambers, including potentially non-representative coverage of spatial heterogeneity, alteration of microclimatic conditions, and changes of concentration gradients have been noted by other workers (Cicerone and Shetter, 1981). Flux chambers have proven useful, however, in establishing the approximate magnitude of the wetland CH_4 flux.

Harriss et al. (1985) used a flux chamber in northern peatlands in Minnesota and measured CH_4 emission rates from 3 x 10^{-3} to 1.94 g m^{-2} day^{-1}. Crill et al. (1988) measured fluxes in a variety of Minnesota peatlands and found late spring and summer fluxes ranging from 1 x 10^{-2} to 0.9 g m^{-2} d^{-1}. Sebacher et al. (1986) measured CH4 fluxes from Alaskan tundra bogs, an alpine fen, and a subarctic boreal marsh. Emission rates for tundra ranged from 4.9 x 10^{-3} to 0.1 g m^{-2} d^{-1}; rates were 0.3 g m^{-2} d^{-1} for an alpine fen, and 0.1 g m^{-2} d^{-1} for the boreal marsh. Emission rates were logarithmically related to water levels. Whalen and Reeburgh (1988) used flux chambers at arctic tundra sites in Alaska and measured mean annual fluxes ranging from 0.47 g m^{-2} yr^{-1} to 8 g m^{-2} yr^{-1}.

Yavitt et al. (1988) studied CH_4 production in peat cores from moss-dominated peatlands in the Appalachian Mountains and found annual CH_4 production ranged from 2.7 to 17.5 mol m^{-2}, with low winter temperatures decreasing CH_4 production in the winter.

While flux chamber data confirm the importance of the CH_4 flux from northern peatlands, they do not allow for predictions of future fluxes under altered climate conditions. Understanding the controls of CH_4 production and the pathways of release with the potentially mitigating reactions along those pathways is the only way to fully quantify the importance of northern peatlands to the greenhouse effect. Our work on trace gas fluxes was done at Thoreau's Bog, located in Concord, MA. Thoreau's Bog is an ombrotrophic Sphagnum bog typical of northern peatlands with respect to vegetation (Hemond, 1980) and porewater chemistry (Gorham et al., 1985; Hemond, 1980). The vegetation is

dominated by Sphagnum spp. and ericaceous shrubs; the porewater is acidic and chemically dominated by humic substances. The bog is approximately 0.38 hectares in size, located in a larger wetland complex of 3.6 hectares. It is a classical floating-mat bog in the remnant of a kettle hole pond, with the peat mat in the center of the bog fully supported by the buoyancy of the peat itself with its associated gas-filled voids. The thickness of the peat mat varies from approximately 2 m near the edge to 0.5 m near the center of the bog. Thoreau's Bog is surrounded by a lagg, or moat of water, less than 1 m deep.

We measured CH_4, CO_2, and N_2 porewater concentrations at different depths at different locations in the bog over a year's time. We also took temperature profiles at those locations to look for temperature dependencies in the gas concentrations. The importance of ebullition versus diffusion and the role of reoxidation in the flux of CH_4 to the atmosphere are discussed in later chapters.

MATERIALS AND METHODS

Six well nests with a total of 20 wells are located at Thoreau's Bog. The wells are constructed of Schedule 40, 1/2" PVC with slots at the bottom; the well screen is isolated by a PVC cap on the bottom of the well and a black rubber plug at the top, through which a 1/4" stainless steel sampling tube extends from the top of the well to approximately half way down the well screen. Wells are installed at depths ranging from 0.3 m to 1.8 m. See Table 1-1 for a summary of

well depths at each location, and Figure 1-1 for a map of well nest locations.

A Teflon (R) rod was placed in each well to prevent ice formation in the

Table 1-1: Depths of Wells at Thoreau's Bog.

WELL NEST	DEPTHS OF WELLS (m)*	WELL NEST	DEPTHS OF WELLS (m)*
D	0.68	A	1.30
D	0.93	A	1.57
D	1.37	A	2.04
C	0.67	G	0.68
C	0.92	G	0.92
C	1.42	G	1.42
AC	0.68	P	0.30
AC	0.92	P	0.68
A	0.68	P	0.91
A	0.91	P	1.27

*Measured from top of PVC fitting sticking above the peat surface to bottom of PVC cap on bottom of well.

stainless steel tube during winter; thus porewaters could still be sampled even

Figure 1-1: Locations of Well Nests at Thoreau's Bog

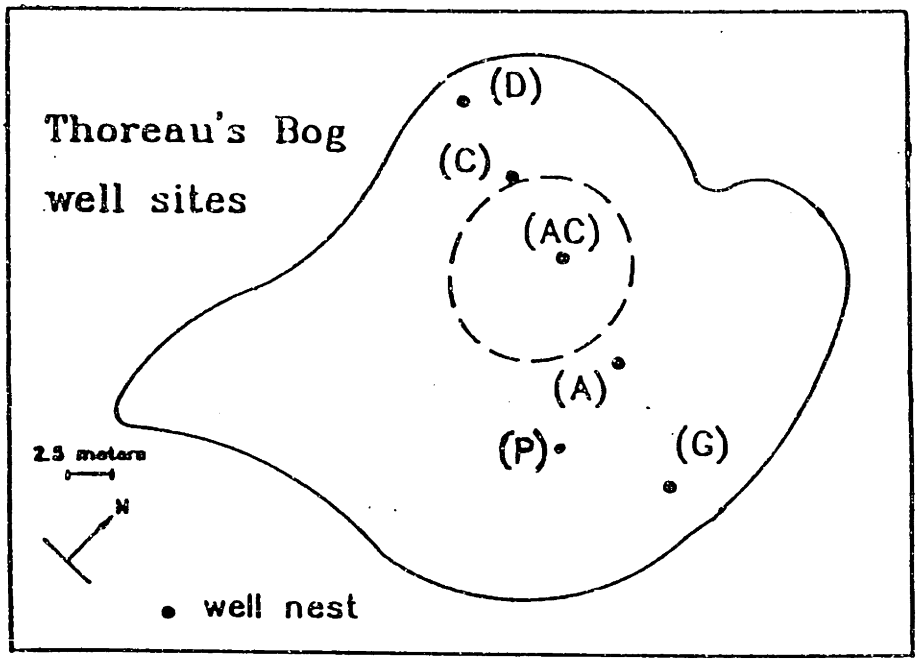

when the surface of the peat mat was frozen.

Porewater samples were taken approximately every 14 days in glass Popper(R) syringes fitted with 3-way Luer lok(R) valves. To prevent air contamination, a well adapter consisting of a Cajon (R) fitting on one end to form an airtight seal around the stainless steel well tube and a luer(R) fitting on the other end was used. Syringes were flushed with between 30 and 300 ml and then a 10 ml porewater sample was withdrawn; syringes were stored in ice water in a cooler for analysis within 24 hours of sampling. Samples taken between January 1 and March 23, 1990 were held for 24 hours before analysis; after March 23, 1990, samples were analyzed the same day. We found that holding certain samples for 24 hours could lead to an increase in CH_4 concentrations; apparently, since porewaters were not filtered, methanogens on particulate matter were being pulled into the syringe.

Porewater samples were analyzed by warming them up to ambient lab temperature in a water bath, recording the water volume in each syringe, injecting 10 ml of helium into each syringe, and placing the syringes for 25 minutes on a wrist-action shaker to allow the water and headspace gases to equilibrate. The final headspace volume was then recorded for samples taken on and after March 23, 1990. The headspace was then injected through a sampling loop onto a 1/8" x 1.5' stainless steel column with carbosieve S 80/100 as the packing material. Ultra-pure helium was used as the carrier gas, at a flow rate of 30 ml/min, and the column temperature was maintained at 100° C. N_2, CH_4, and CO_2 were detected by a thermal conductivity detector, and peak heights quantified by a

Hewlett Packard Integrator (Model HP3394A). Standards were made in gas-tight 1 L glass bottles using certified CH_4, CO_2, and N_2 in He. Standards equilibrated at least 2 hours before analysis; analysis of samples drawn from standard bottles over time showed 2 hours to be sufficient for equilibration. Standards were analyzed before, during, and after the samples, and three standards were made for each gas to allow an accurate standard curve to be made. Lab temperature and pressure were recorded to allow porewater gas concentrations to be calculated based on temperature-dependent Bunsen coefficient equations (Wiesenburg and Guinasso, 1979; Weiss, 1970; Weiss, 1974). Peak heights for each gas were converted to partial pressures based on the standard curves, and syringe headspace volume readings were corrected for atmospheric pressure on and after March 23, 1990. Before that date, headspace volumes after equilibration were not measured, and no atmospheric pressure correction was made. Analysis of pressure-corrected and non-pressure-corrected data from the April 12, 1990 and April 28, 1990 data sets showed 1% or less error on 2/3 of the points. Pressure corrections without corresponding headspace volume corrections were shown to lead to even greater errors; therefore data before March 23, 1990 have no atmospheric pressure correction whatsoever.

Temperature profiles were taken at each well nest with a 6 ft 1/8" O.D. stainless steel temperature probe connected to a hand-held thermistor which recorded temperature in tenths of degrees Fahrenheit. During the winter when the peat mat was frozen, the probe was placed down each well approximately 2 cm above the bottom of the well to measure temperature. On January 14, 1990,

temperatures were measured at a well nest both in the wells and at equivalent well depths in a hole through the ice; no significant differences in temperatures were found. When the peat mat was not frozen, temperature measurements were taken at 0.15 m, 0.3 m, 0.46 m, 0.61 m, 0.91 m, 1.22 m, 1.52 m, and 1.83 m depths at each well nest.

RESULTS

For each gas (N2, CH4, and CO2), porewater concentrations at 0.68 m, 0.92 m, and 1.36 m depths were averaged across the six well nest sites on each day of sampling. Temperatures measured at each well nest at 0.61 m, 0.91 m, and 1.22 m depths were also averaged across the bog. These average values are shown in Appendices A and B.

In order to smooth the averaged data and extract annual patterns from high frequency noise due to sampling and analysis error, a fast Fourier transform was applied to the averaged data. Since such a transform requires 2^n sampling points, the 24 data points spanning a year were simply repeated to provide 64 sampling points. In the transformed data, the zero frequency reperesents the annual mean; the third frequency, with the second highest magnitude and a period of approximately a year, represents the annual fluctuations about this mean (see Figure 1-2).

Because there are not several complete yearly cycles of data, the fast Fourier transform underestimates the annual period for the three porewater gases

Figure 1-2: Fast Fourier Transform of Methane Data

Filtering of METHANE data.

Read in data file.

$M \equiv READPRN\begin{bmatrix} CH2 \\ PRN \end{bmatrix}$ $n = 64$

Unfiltered Time Series

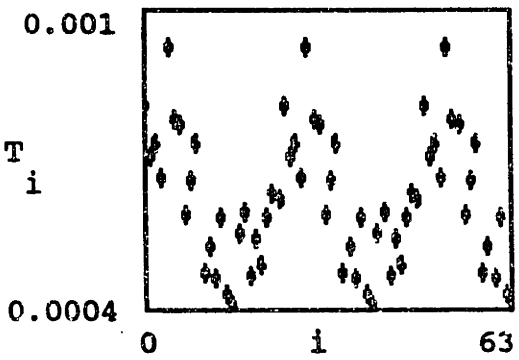

Fourier transform of data and high and low-pass freq.

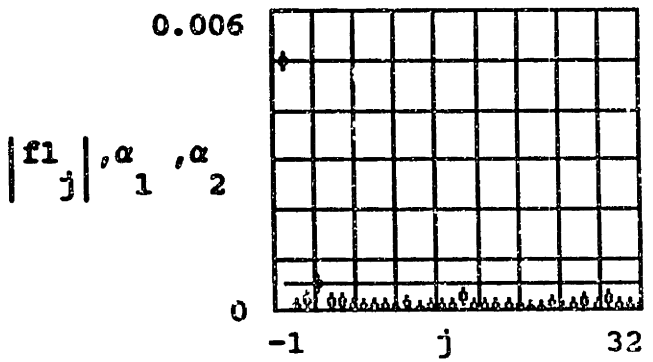

and temperature as approximately 300 days. Obviously, the average period has to be 365 days for temperature and temperature-dependent processes. The transform fits three cycles of sine waves to 2 2/3 years' worth of repeated data points; the second sine wave cycle provides the best fit to the data because the phase error due to the shorter cycle is minimized in the middle. All subsequent calculations are based on transformed data from the second sine wave cycle. The original data and the filtered data for the temperature readings and each of the 3 gases are shown in Figures 1-3 through 1-14. Table 1-2 shows the amplitudes and ranges for the filtered data.

The average partial pressures at each depth for N_2, CH_4, and CO_2 were calculated for each sampling day based on measured temperatures and temperature-dependent Bunsen coefficients (Wiesenburg and Guinasso, 1979; Weiss, 1970; Weiss, 1974). These partial pressures as well as the partial pressure of water at each measured temperature (Weast, 1990) are presented in Appendix C.

Figure 1–3: Temporal Variations in Temperature at 0.61 m Depth

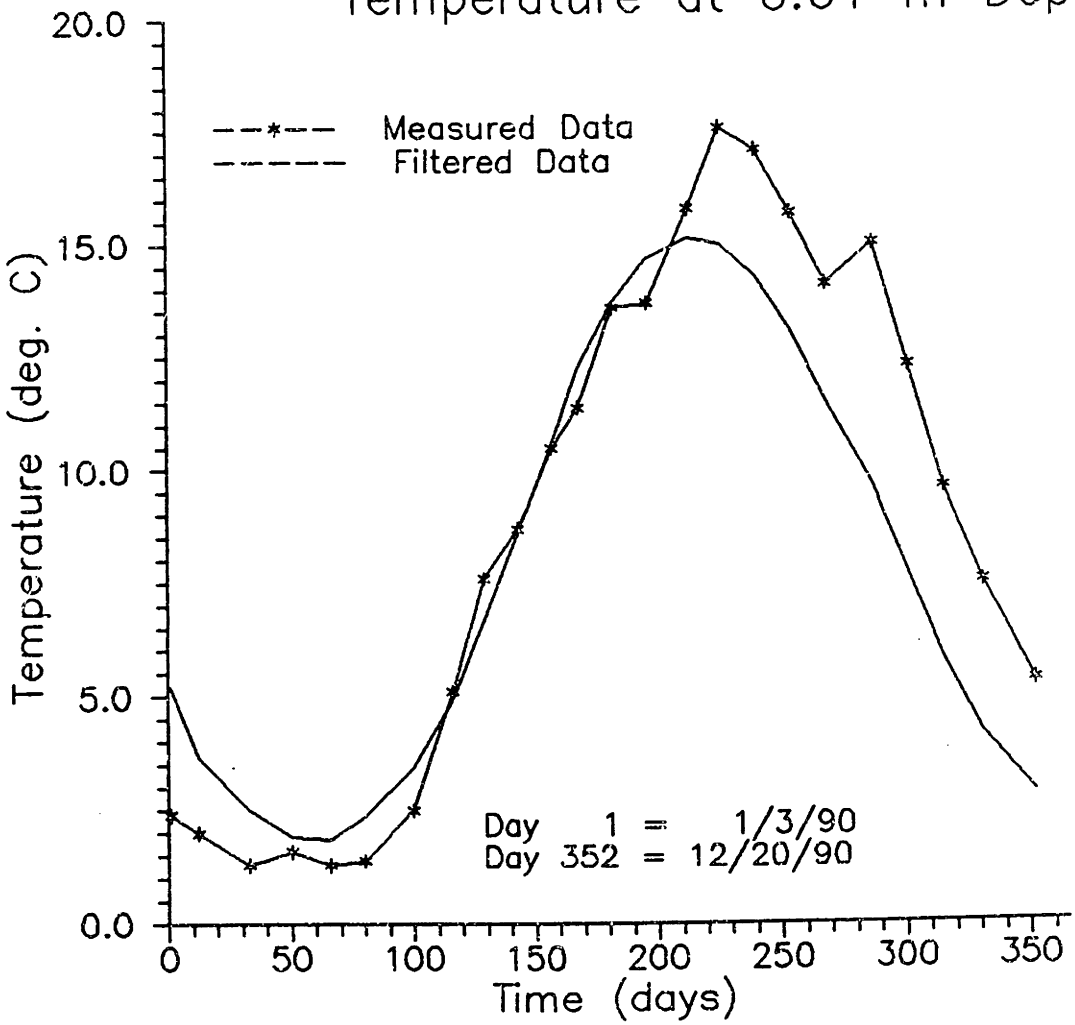

Figure 1—4: Temporal Variations in Temperature at 0.91 m Depth

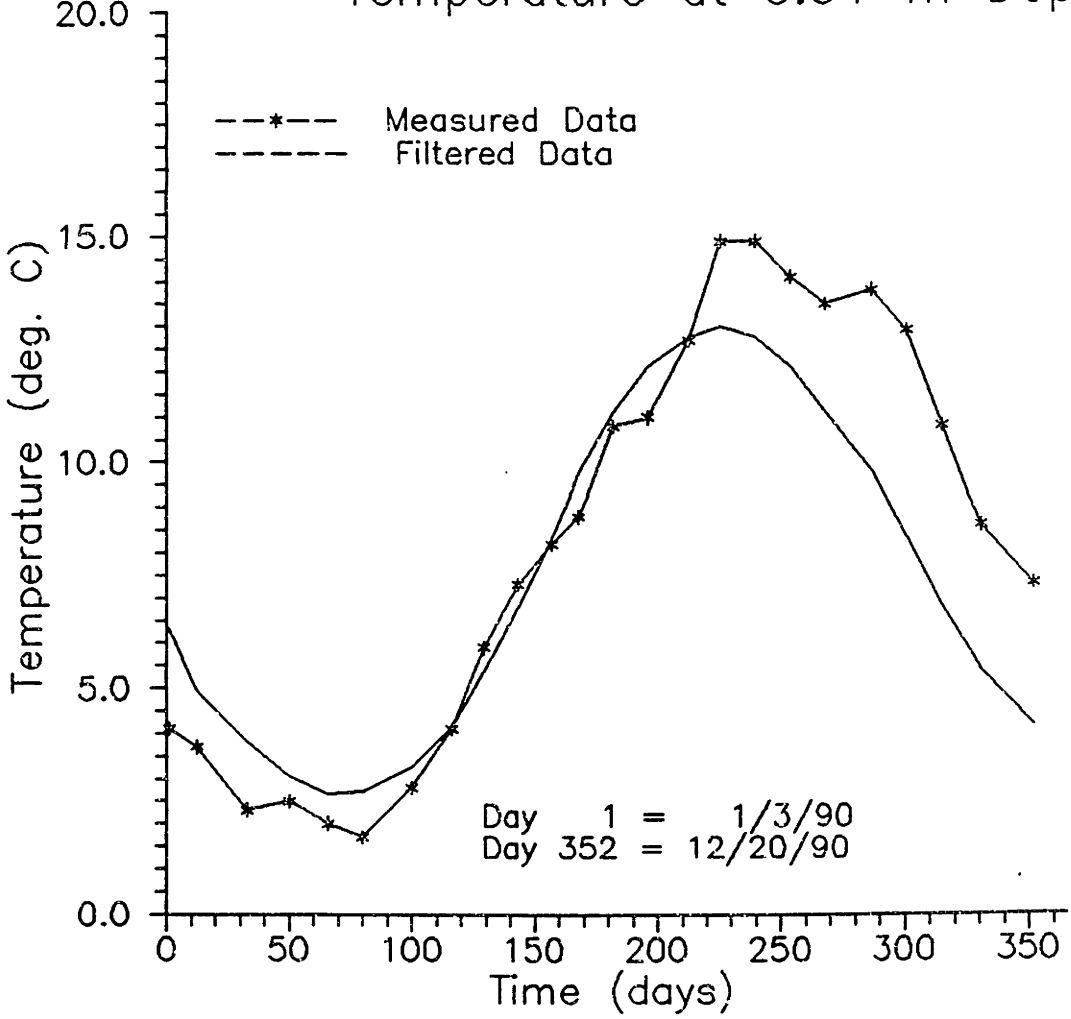

Figure 1–5: Temporal Variations in Temperature at 1.22 m Depth

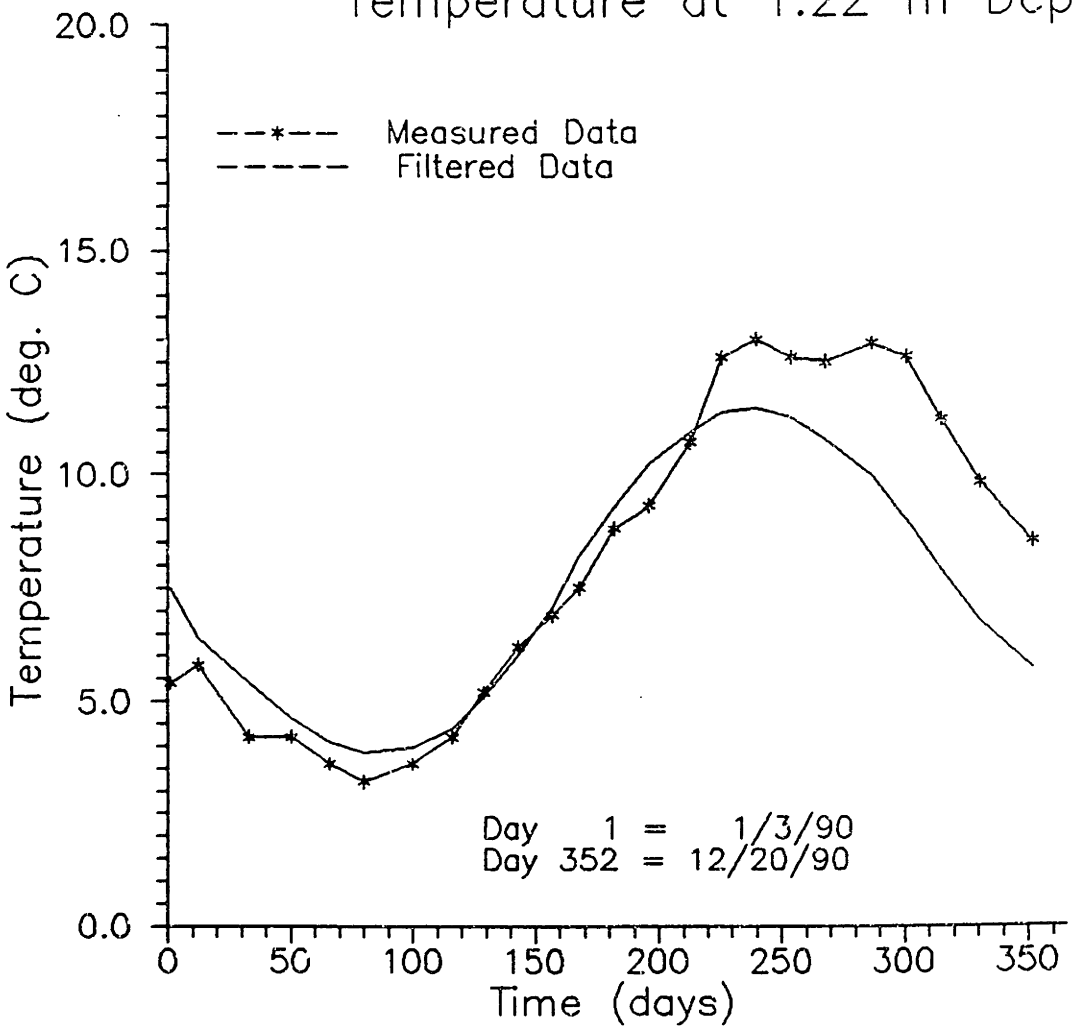

Figure 1–6: Temporal Variations in Porewater Nitrogen at 0.68 m Depth

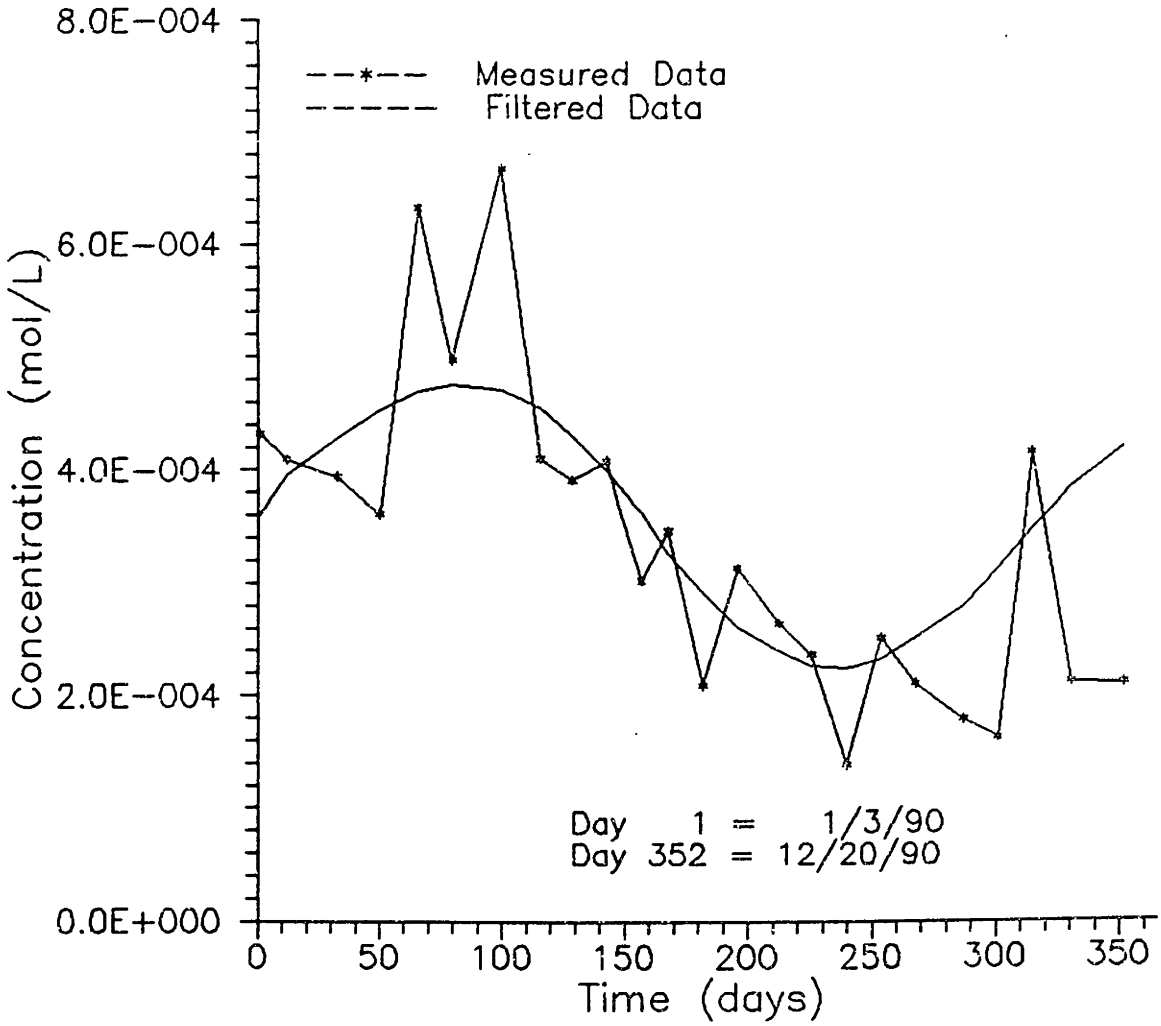

Figure 1–7: Temporal Variations in Porewater Nitrogen at 0.92 m Depth

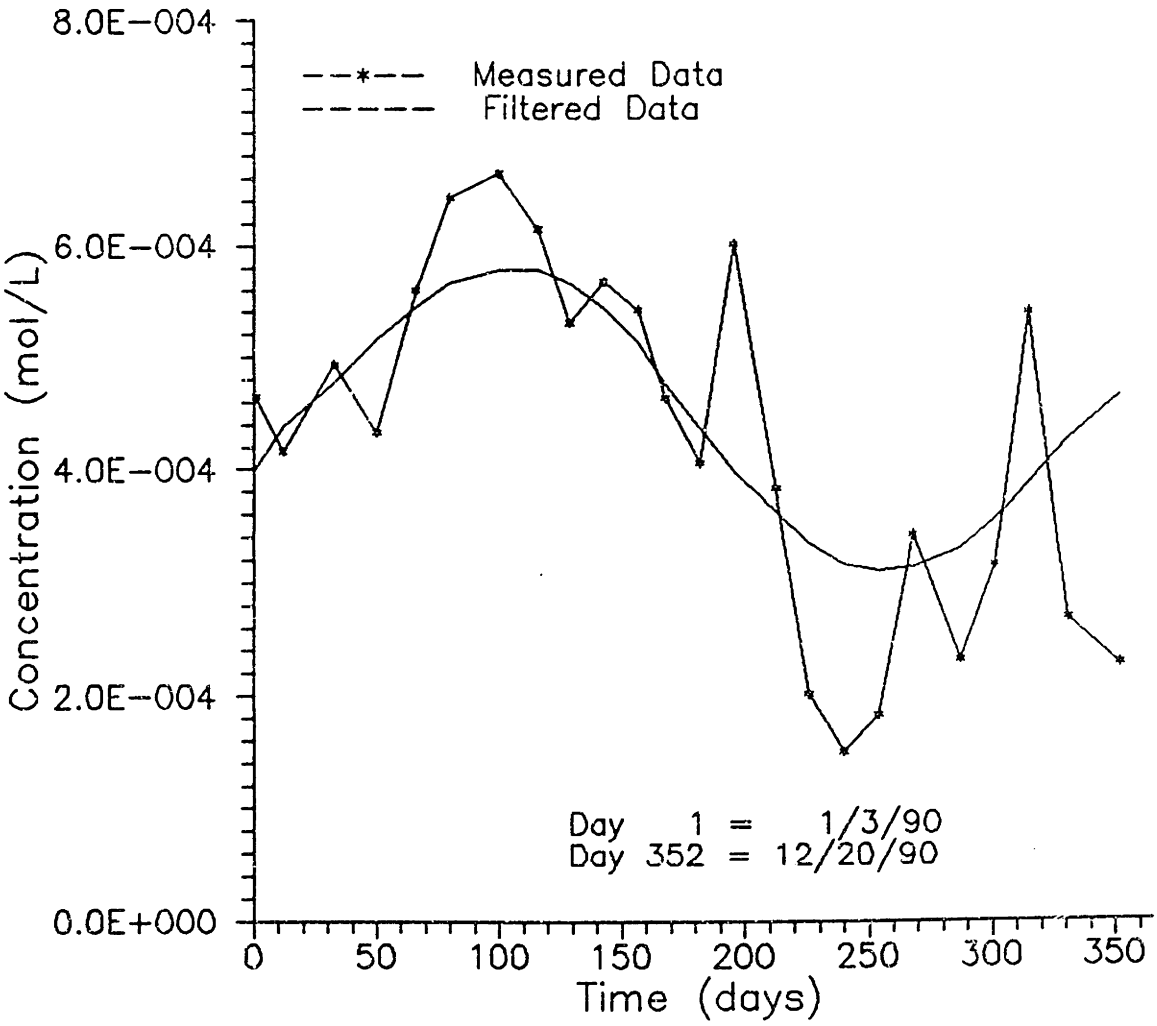

Figure 1–8: Temporal Variations in Porewater Nitrogen at 1.36 m Depth

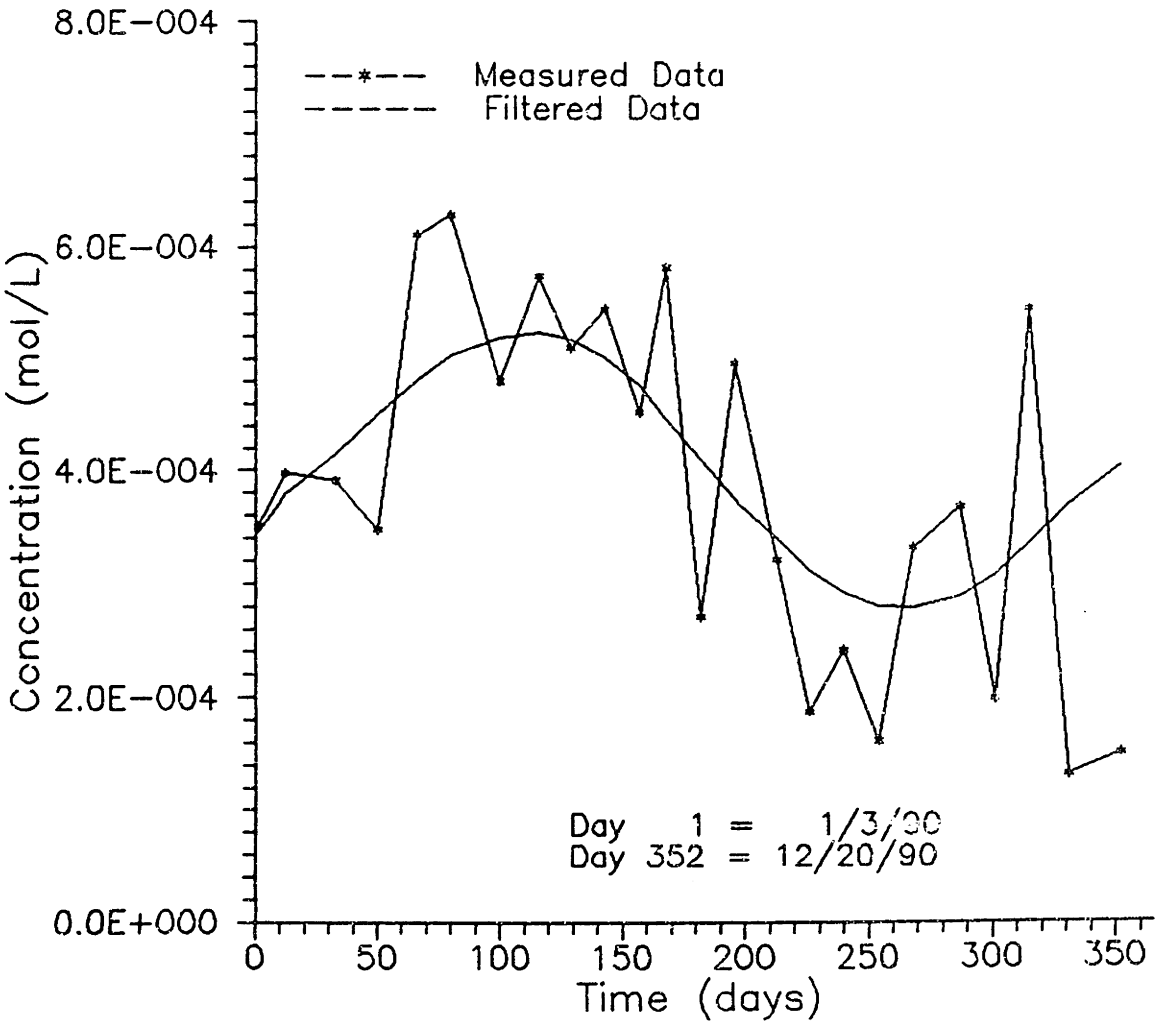

Figure 1–9: Temporal Variations in Porewater Methane at 0.68 m Depth

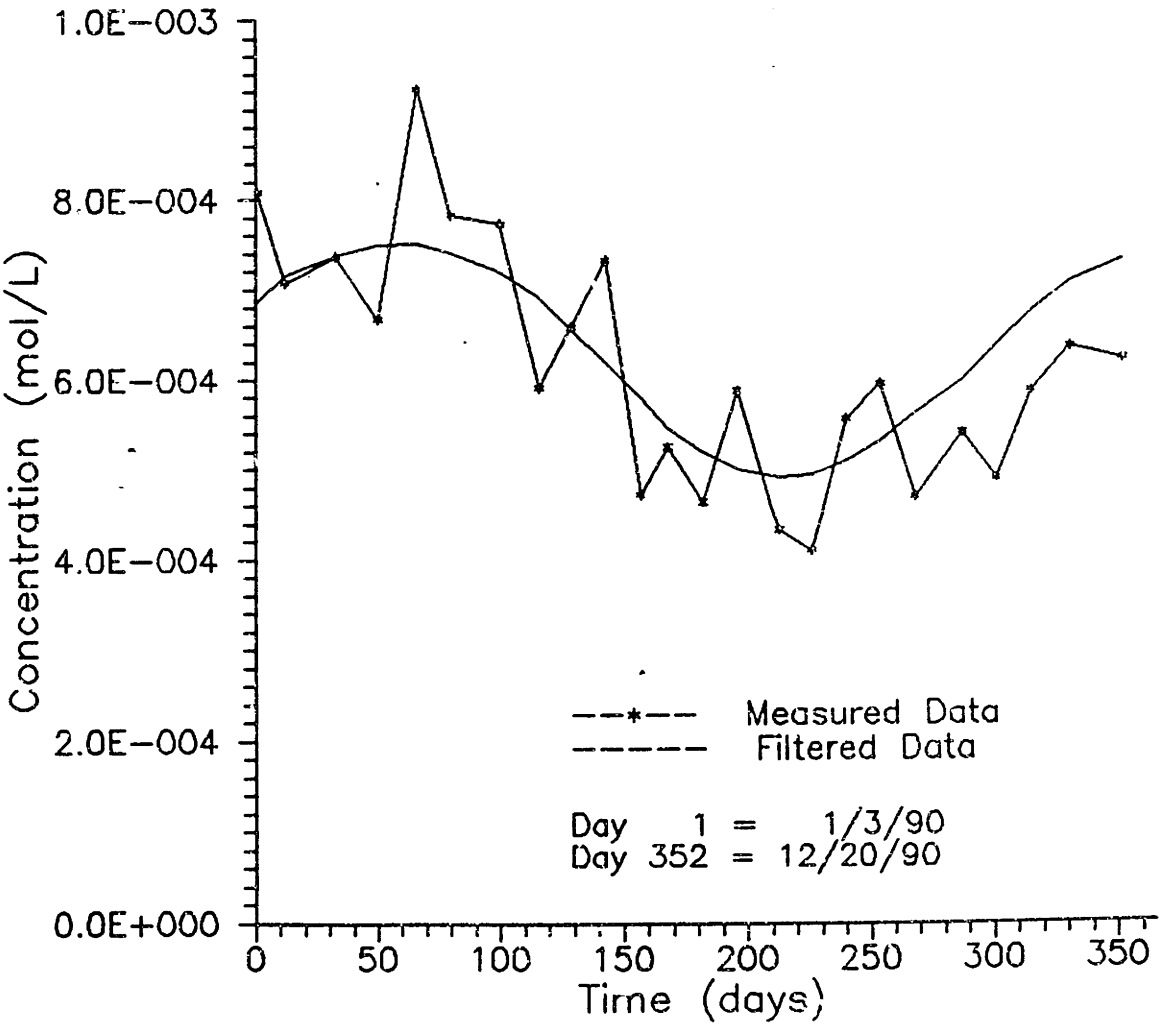

Figure 1–10: Temporal Variations in Porewater Methane at 0.92 m Depth

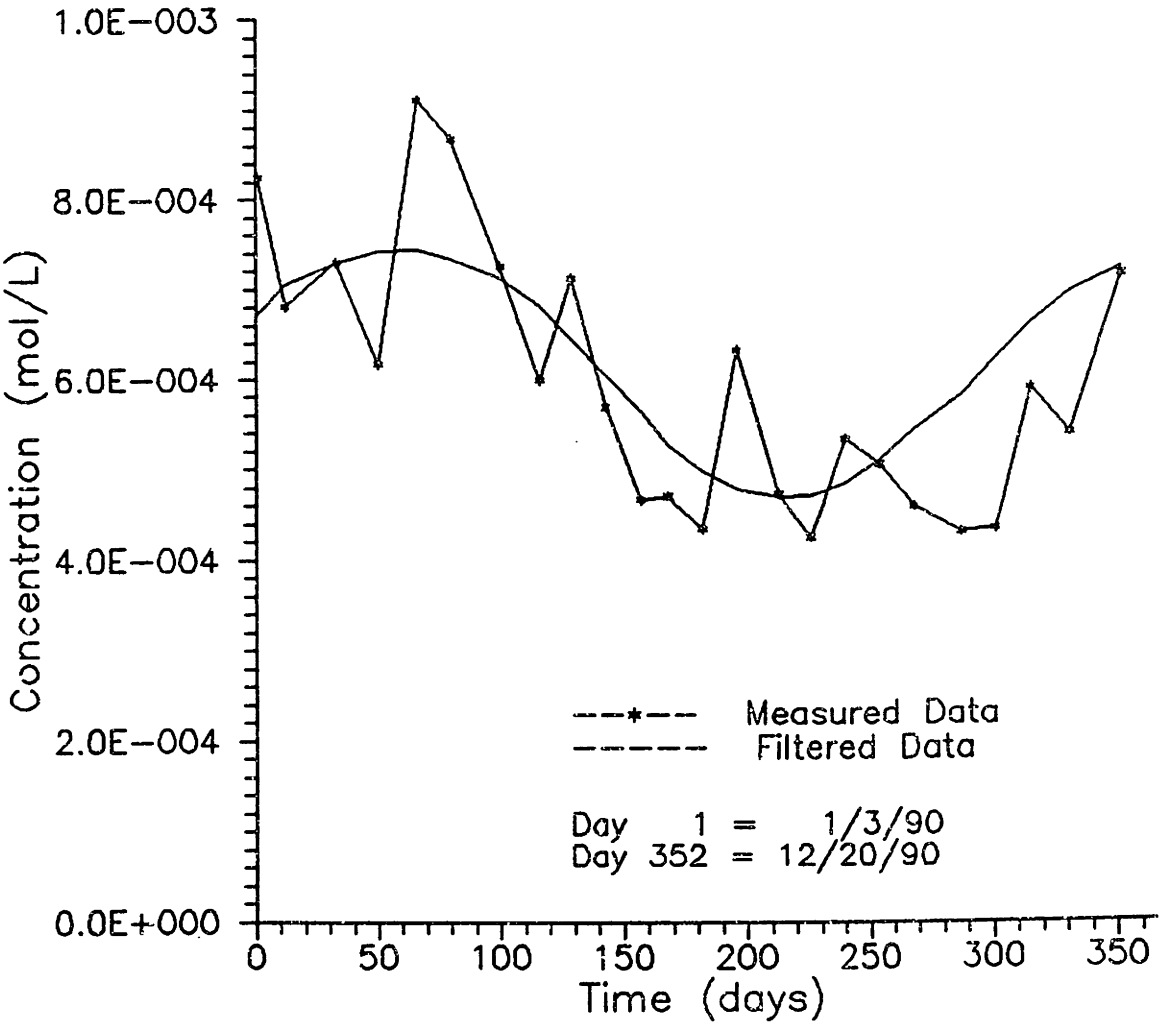

Figure 1–11: Temporal Variations in Porewater Methane at 1.36 m Depth

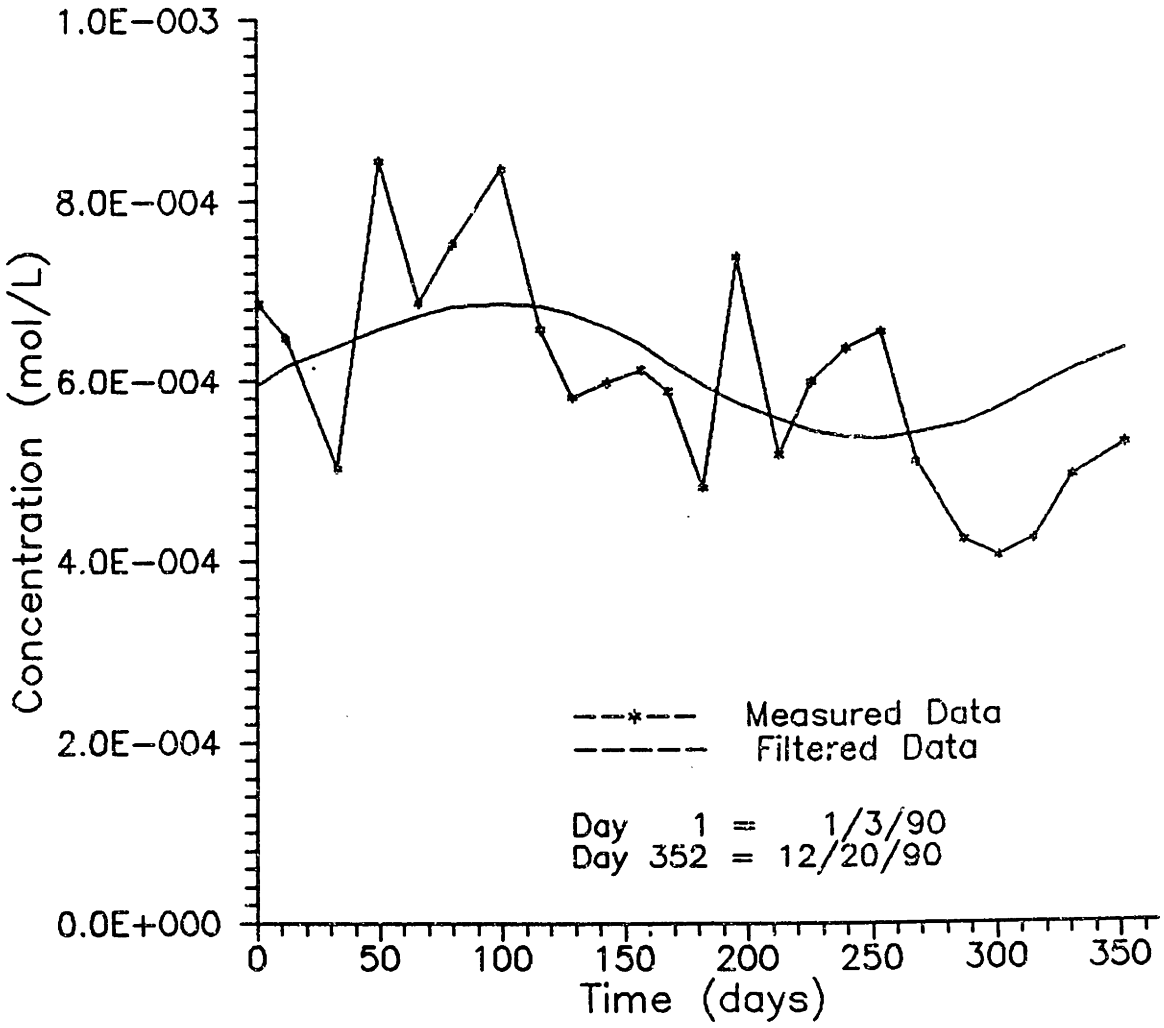

Figure 1–12: Temporal Variations in Porewater Carbon Dioxide at 0.68 m Depth

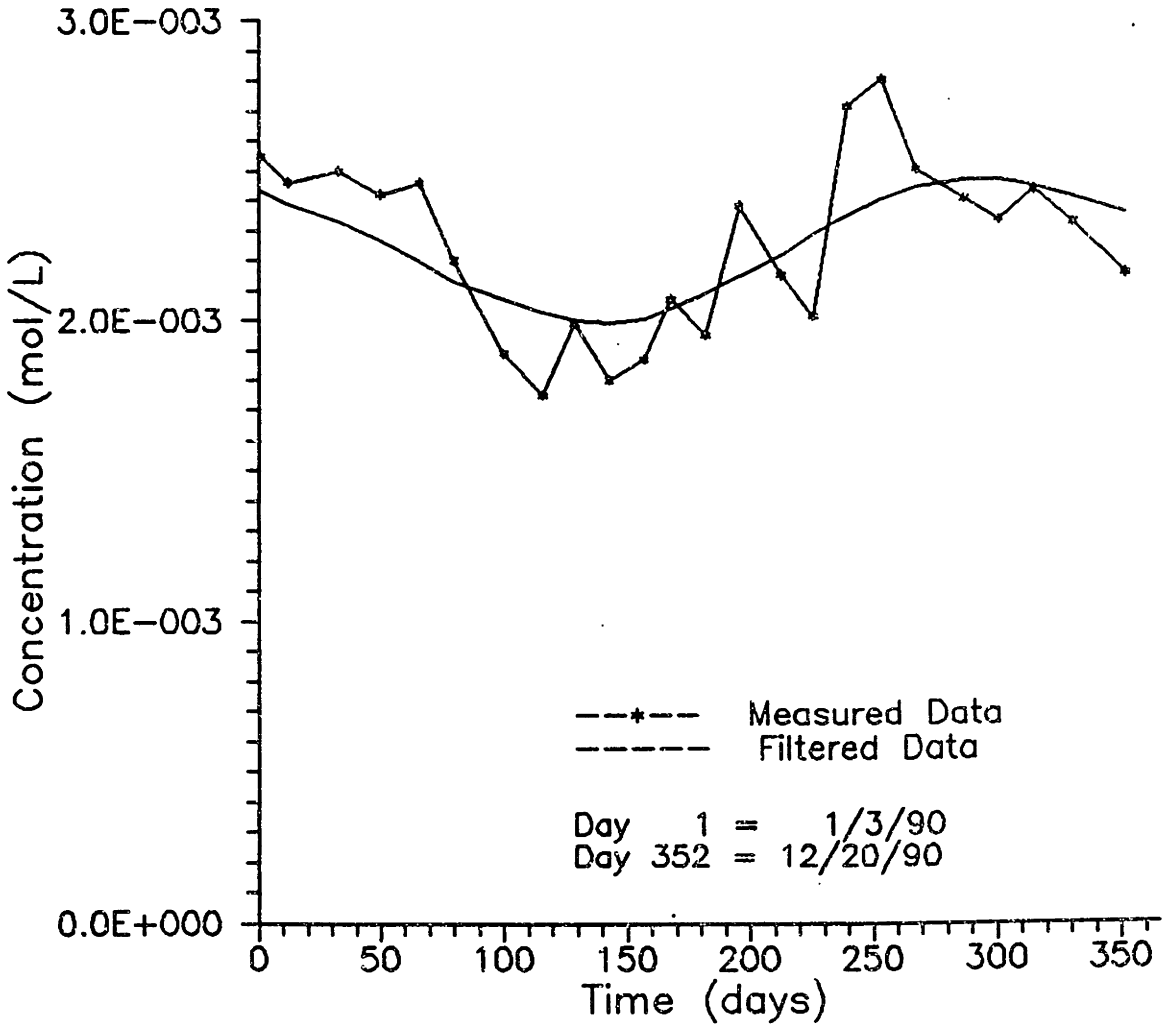

Figure 1–13: Temporal Variations in Porewater Carbon Dioxide at 0.92 m Depth

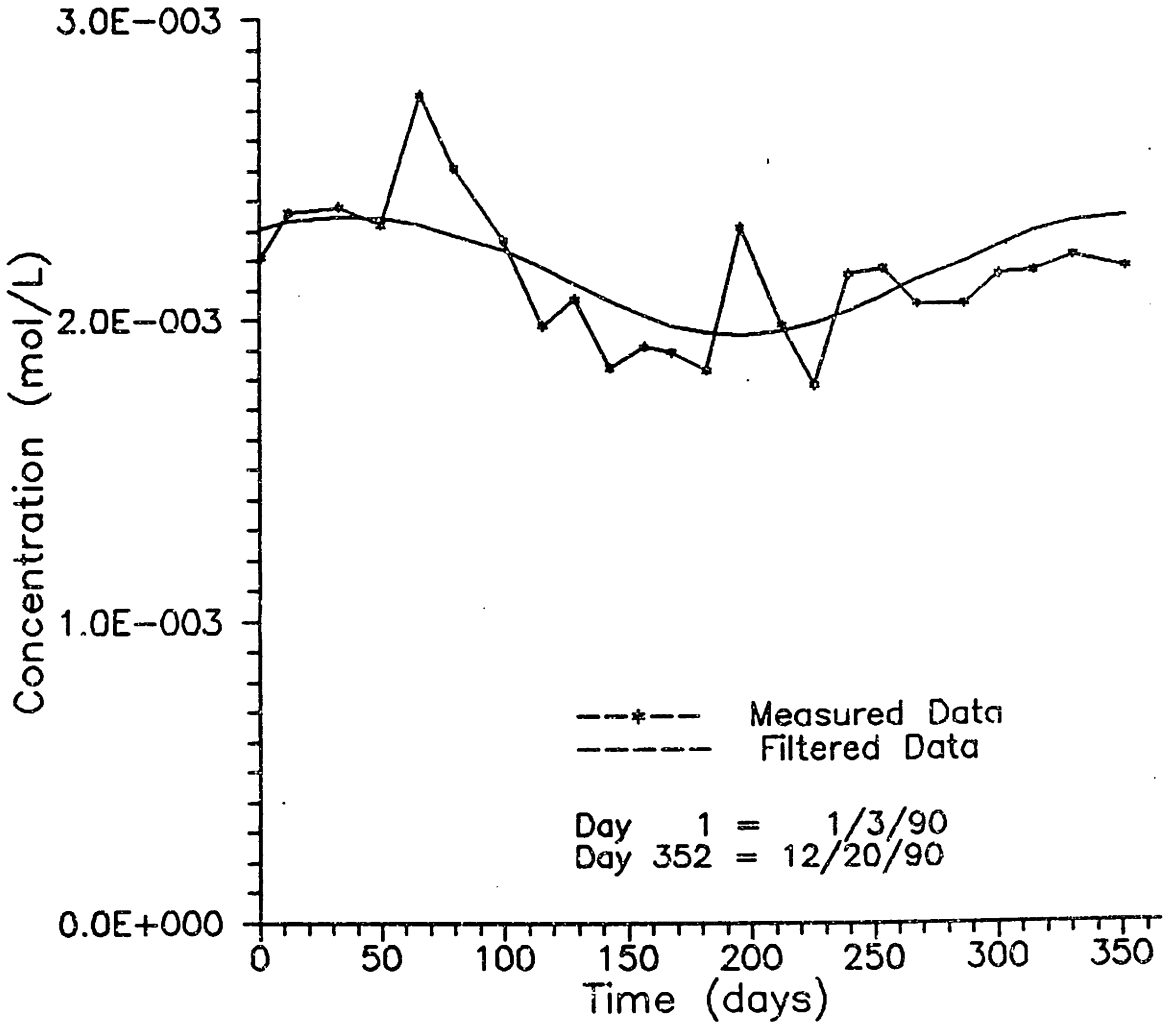

Figure 1–14: Temporal Variations in Porewater Carbon Dioxide at 1.36 m Depth

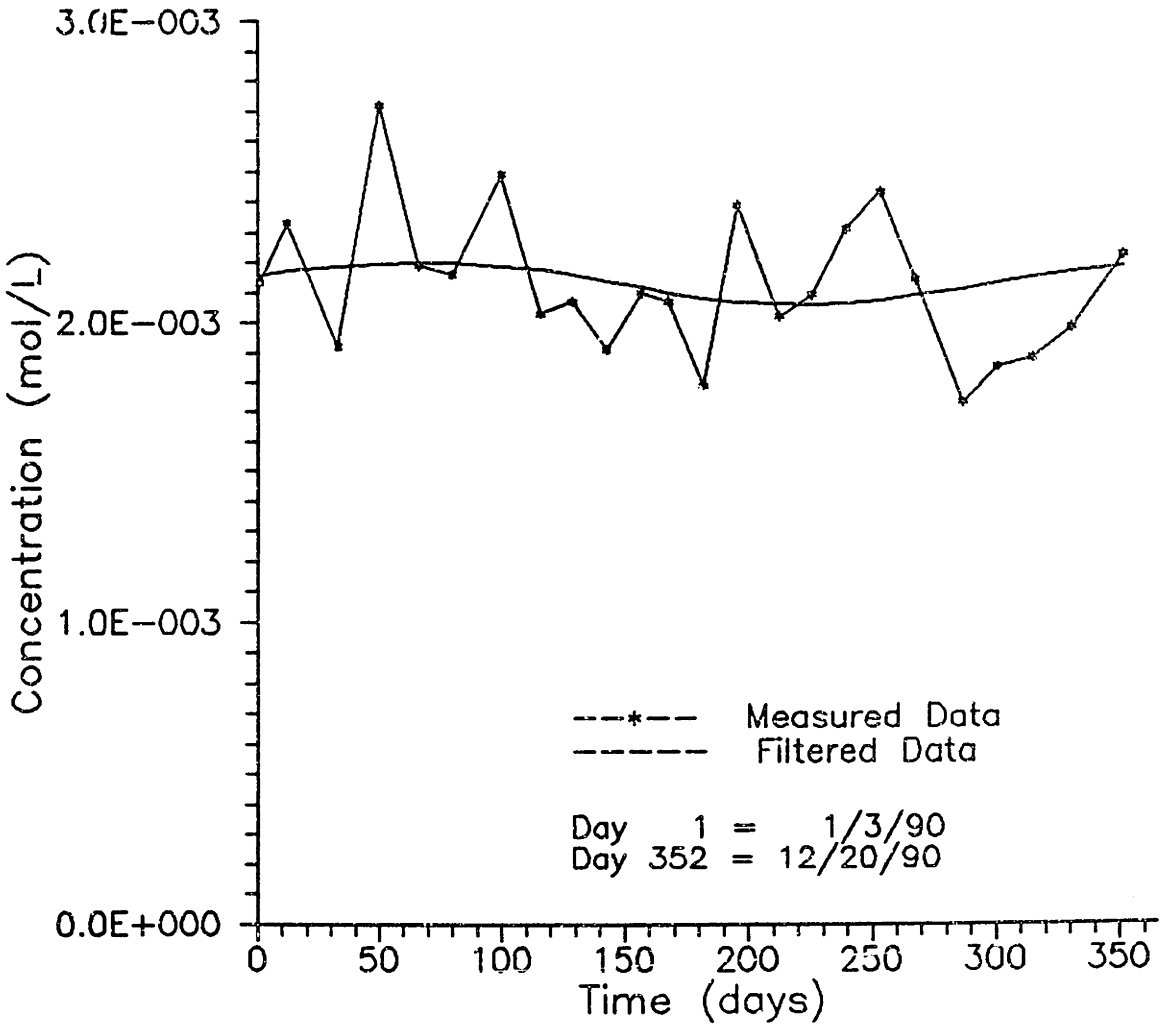

Table 1-2: Temperature and Porewater Gas Concentration Data Filtered by a Fast Fourier Transform.

	DEPTH(m)	AMPLITUDE	RANGE
TEMP	0.61	6.67° C	1.8 - 15.1° C
TEMP	0.91	5.18° C	2.6 - 13.0° C
TEMP	1.22	3.82° C	3.8 - 11.5° C
N_2	0.68	1.26×10^{-4} M	2.23×10^{-4} - 4.75×10^{-4} M
N_2	0.92	1.35×10^{-4} M	3.1×10^{-4} - 5.79×10^{-4} M
N_2	1.36	1.23×10^{-4} M	2.78×10^{-4} - 5.24×10^{-4} M
CH_4	0.68	1.30×10^{-4} M	4.92×10^{-4} - 7.52×10^{-4} M
CH_4	0.92	1.38×10^{-4} M	4.68×10^{-4} - 7.44×10^{-4} M
CH_4	1.36	0.76×10^{-4} M	5.35×10^{-4} - 6.86×10^{-4} M
CO_2	0.68	2.36×10^{-4} M	1.99×10^{-3} - 2.46×10^{-3} M
CO_2	0.92	1.99×10^{-4} M	1.95×10^{-3} - 2.35×10^{-3} M
CO_2	1.36	0.70×10^{-4} M	2.06×10^{-3} - 2.2×10^{-3} M

DISCUSSION

As shown in Figures 1-3 through 1-5 and Table 1-2, with depth the annual variation in temperature has a progressively smaller amplitude and an increasing phase lag. This is expected since the main driving force --atmospheric temperatures changes-- is damped with depth. The methane data also show a phase lag relative to surface temperature at 0.68 m and 1.36 m depths, and have a smaller amplitude at 1.36 m depth than at 0.68 m and 0.92 m depths. The nitrogen data at all three depths have approximately the same amplitude and a slight phase lag relative to surface temperature (see Table 1-2). For CO_2, there is a much larger phase lag relative to surface temperature and the amplitude decreases with depth.

Figures 1-3 through 1-14 clearly show that there is a strong inverse relationship between temperature and concentrations of CH_4 and N_2 in the porewaters, and a weaker inverse relationship between temperature and CO_2. There are two possible reasons for these annual fluctuations in gas porewater concentrations. First, there may be an annual fluctuation in the magnitude of source and sink strengths such that the sum of the source and sink fluctuations produces the annual fluctuations we detect. Secondly, Bunsen coefficients vary significantly with temperature, and since we have very strong evidence for the presence of bubbles in the bog (see Chapter 2), the annual fluctuations in porewater concentrations may reflect equilibrium partitioning between liquid and gas (bubble) phases, assuming the gas phase exists throughout the year. Looking

at the average sums of partial pressures of N_2, CH_4, CO_2, and water vapor with depth, the mean at 1.36 m is 0.8 atm, at 0.92 m, 0.9 atm, and at 0.68 m, 0.8 atm (see Appendix D). These average pressures are nearly sufficient to overcome the necessary hydrostatic and atmospheric pressure (approximately 1.1 atm) for bubble formation to occur.

In order to elucidate how much variability in porewater gas concentrations could be explained by changes in temperature and solubility, a porewater concentration for each gas was selected based on the closest intersection of an original data point with the filtered data curve. The equilibrium partial pressures in the gas bubble phase were then calculated from the original porewater concentrations, based on the temperature-dependent Bunsen coefficients, a water porosity of 0.2, and a gas filled porosity of 0.1 (see Chapter 2). For each gas, the moles of gas present in the liquid and gas phases were added, and this total mole value was taken as constant for the entire year. The moles of gas were then allowed to partition between the gas and liquid phases according to the filtered temperature data and temperature-dependent Bunsen coefficients. These predicted partitioning data were plotted with the filtered data, as shown in Figures 1-15 through 1-23, and a linear regression performed. The r^2 values are shown on the figures.

For CH_4, the smoothed data are highly correlated both in amplitude and in phase with the predicted temperature-dependent partitioning data. This suggests that the contribution of CH_4 sources and sinks to annual fluctuations is not as important as the temperature-induced partitioning of CH_4 between liquid and gas

Figure 1-15: Temperature-dependent Partitioning of N_2 at 0.68 m Depth

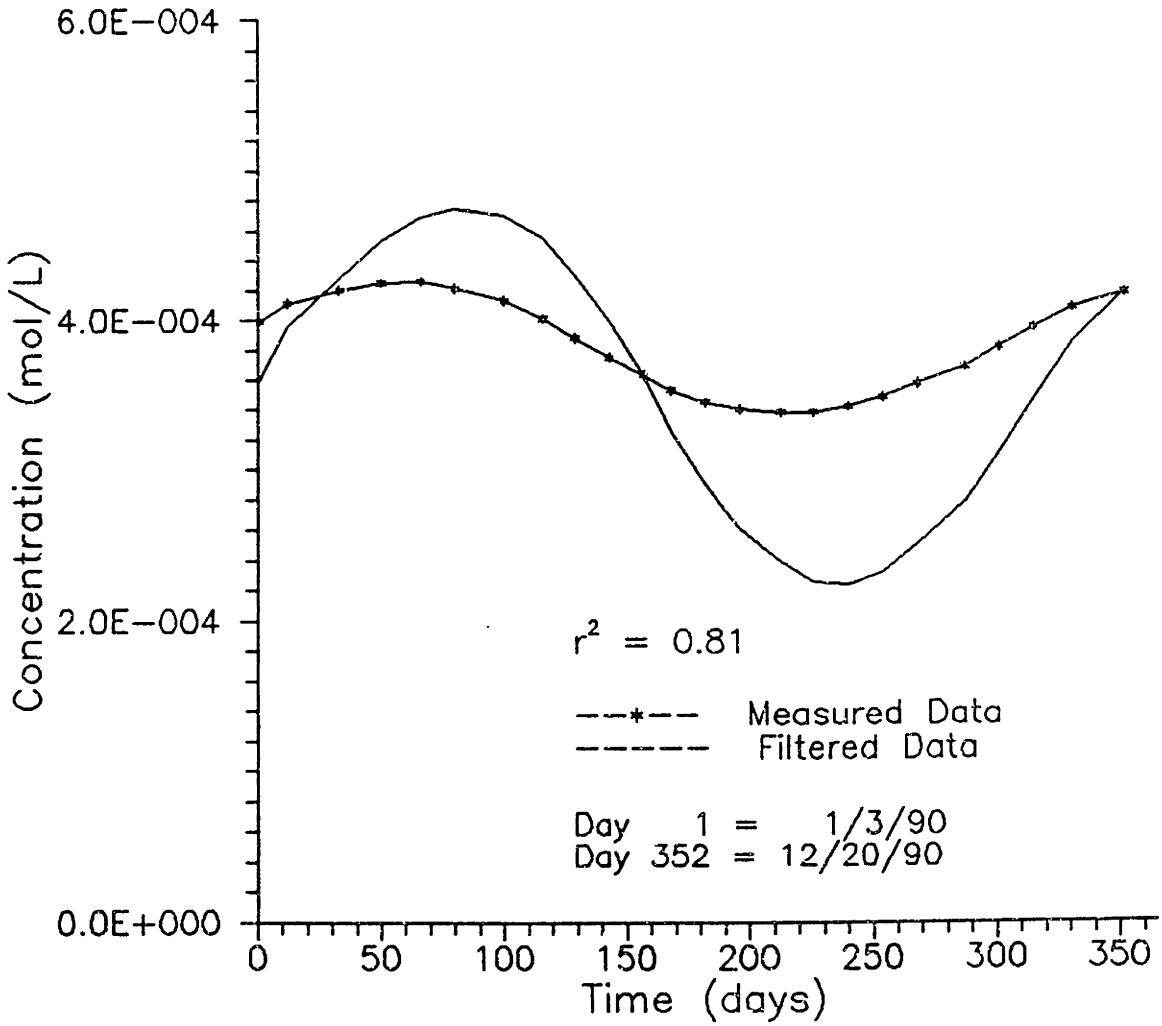

Figure 1-16: Temperature-dependent Partitioning of N_2 at 0.92 m Depth

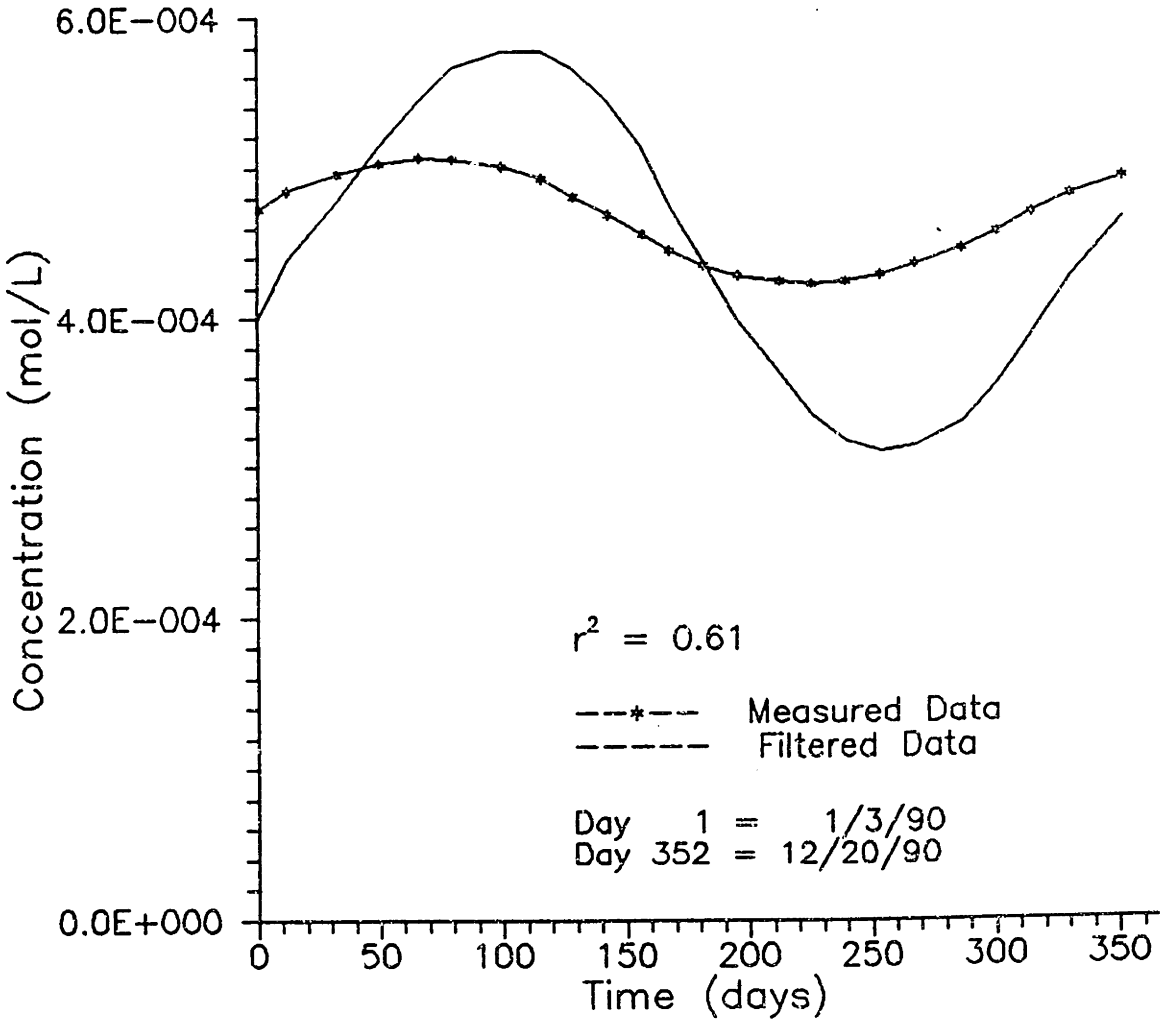

Figure 1-17: Temperature-dependent Partitioning of N_2 at 1.36 m Depth

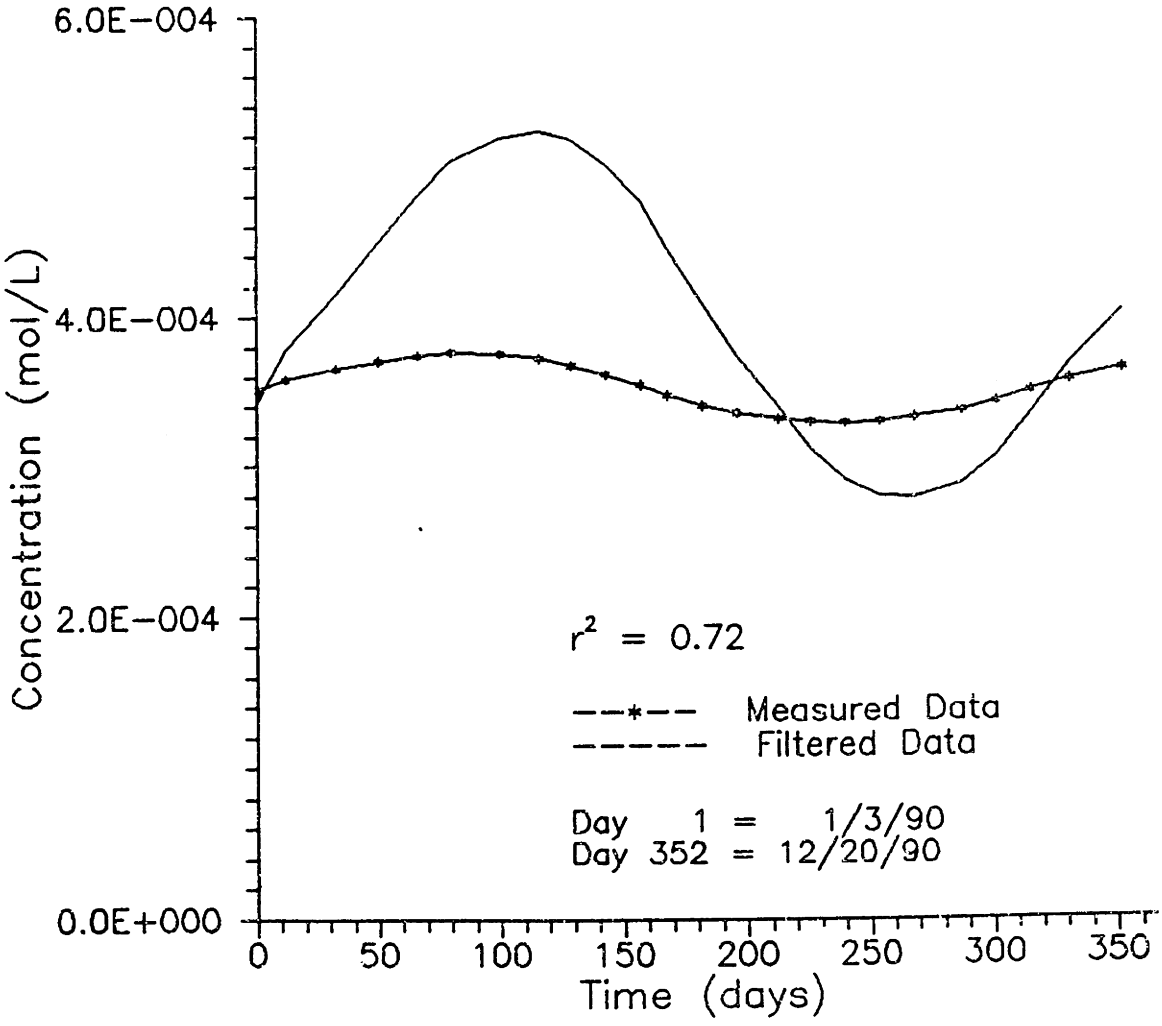

Figure 1–18: Temperature–dependent Partitioning of CH_4 at 0.68 m Depth

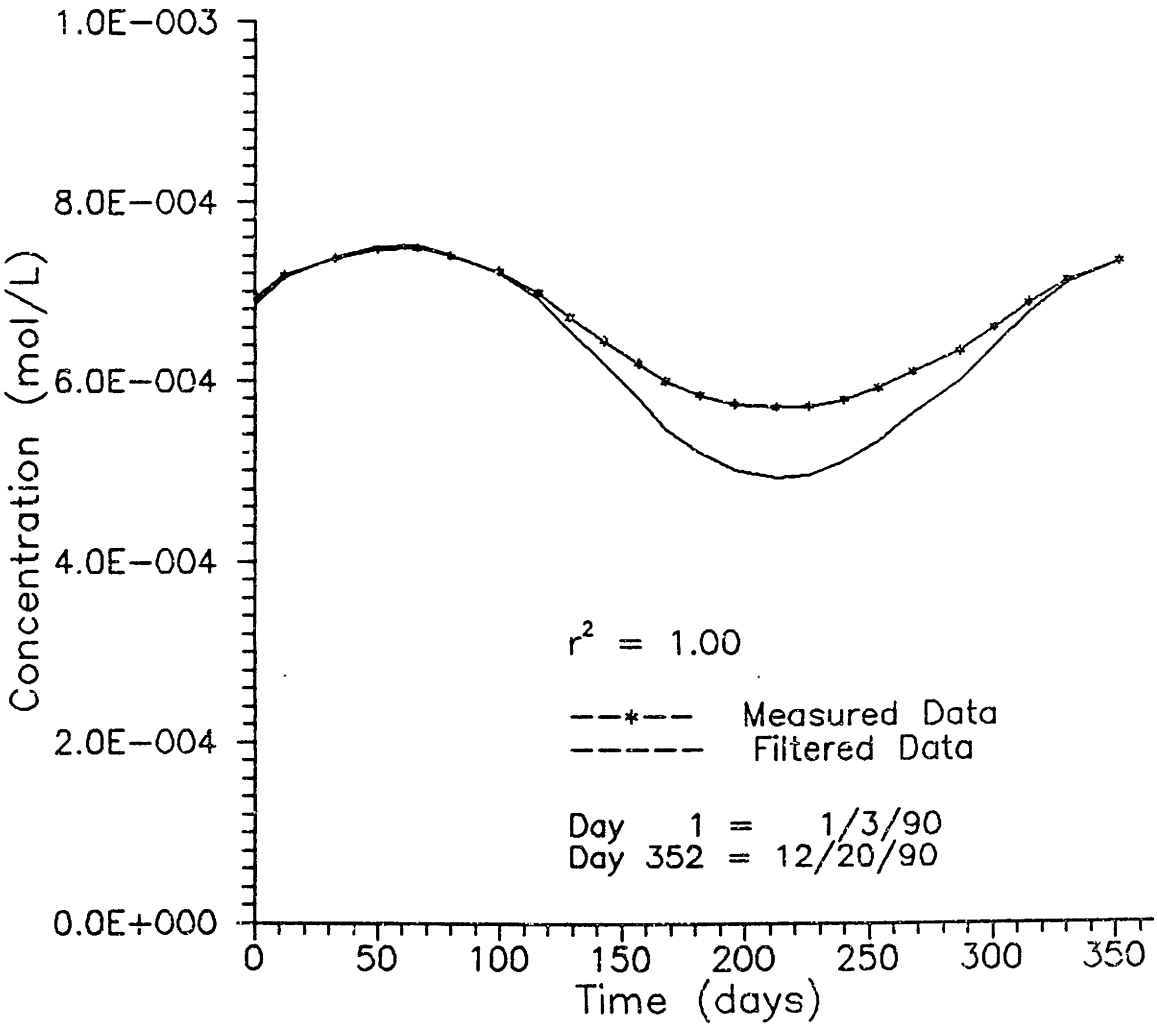

Figure 1–19: Temperature–dependent Partitioning of CH_4 at 0.92 m Depth

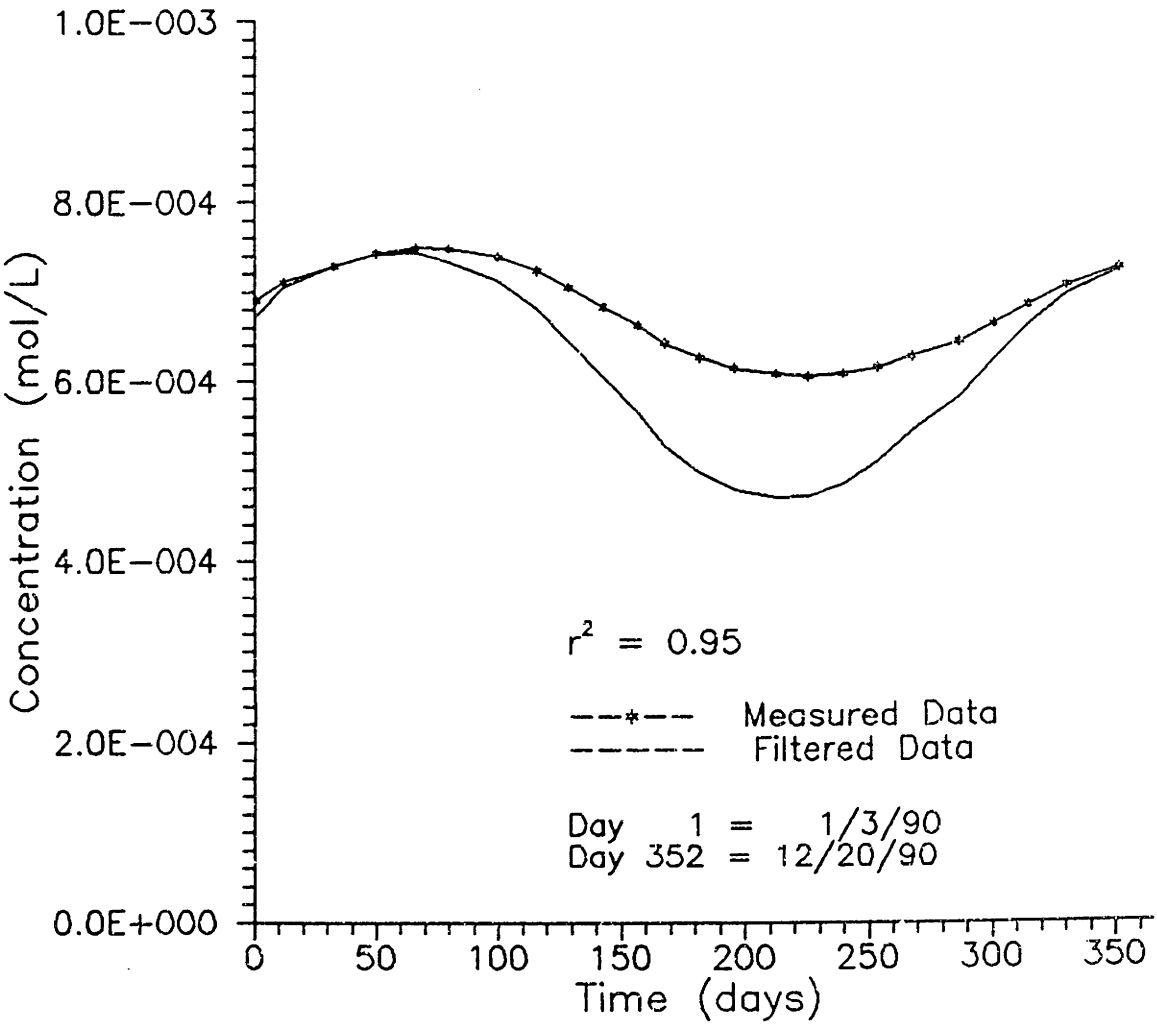

Figure 1–20: Temperature–dependent Partitioning of CH_4 at 1.36 m Depth

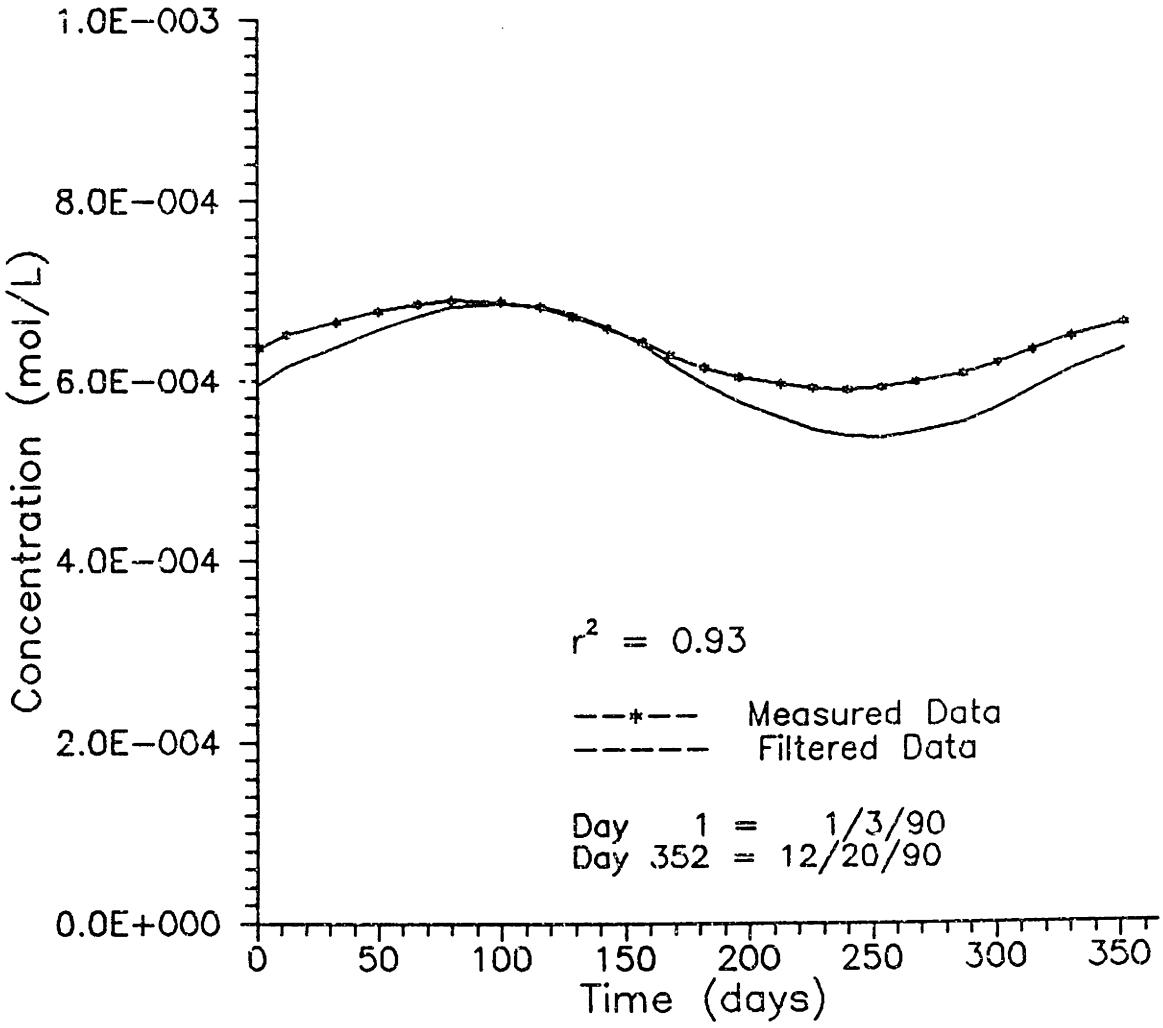

Figure 1–21: Temperature–dependent Partitioning of CO_2 at 0.68 m Depth

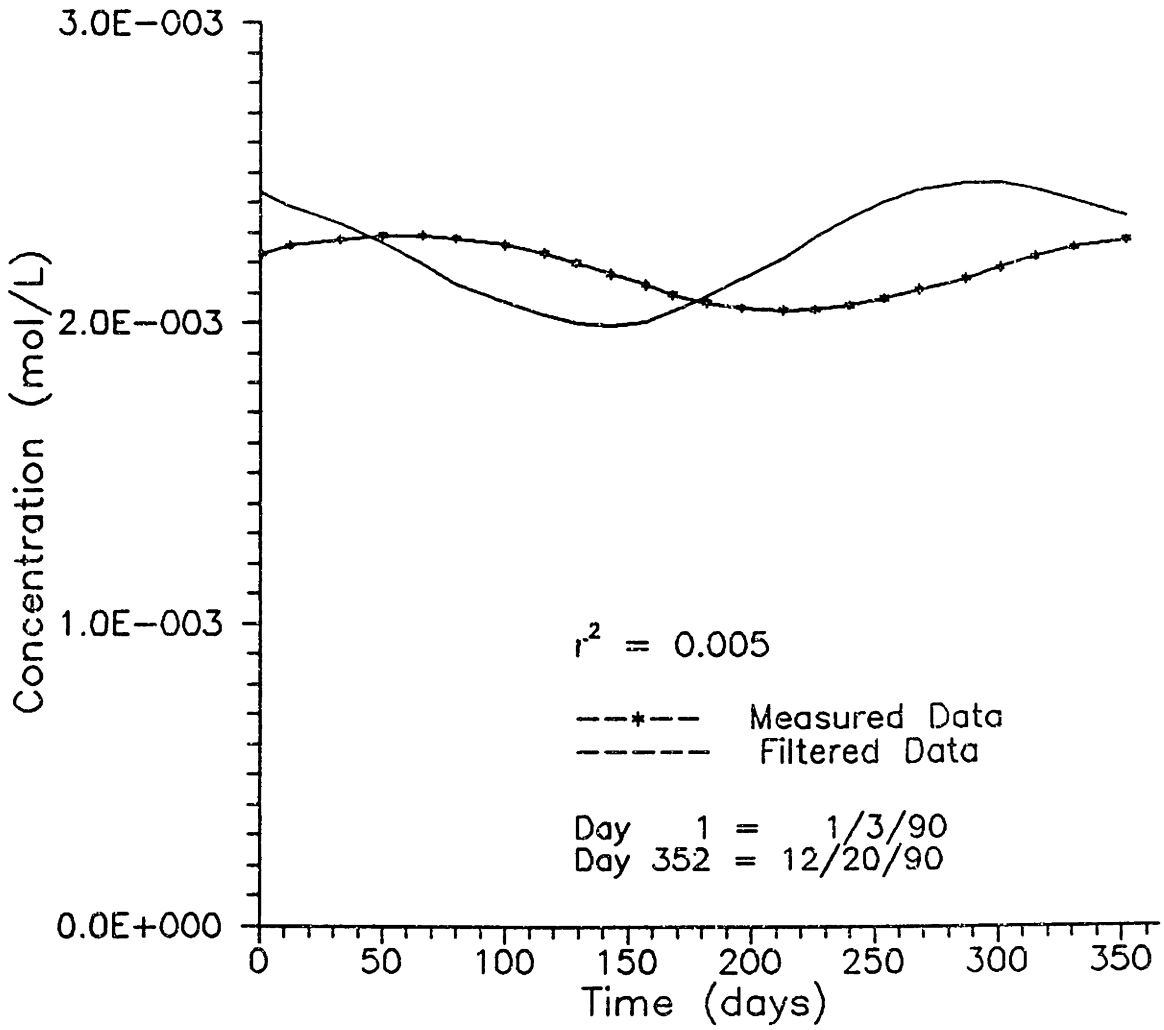

Figure 1-22: Temperature-dependent Partitioning of CO_2 at 0.92 m Depth

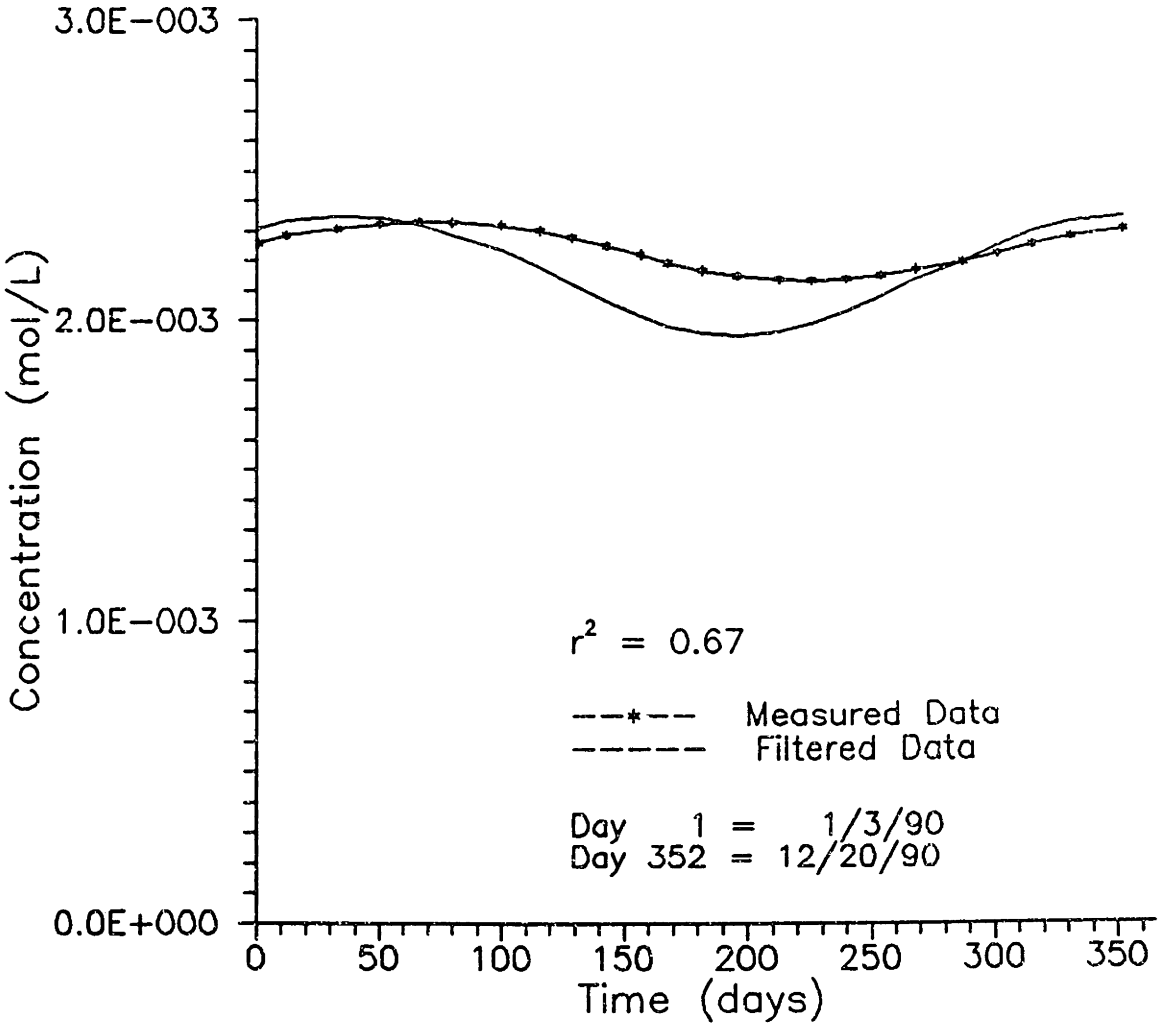

Figure 1–23: Temperature–dependent Partitioning of CO_2 at 1.36 m Depth

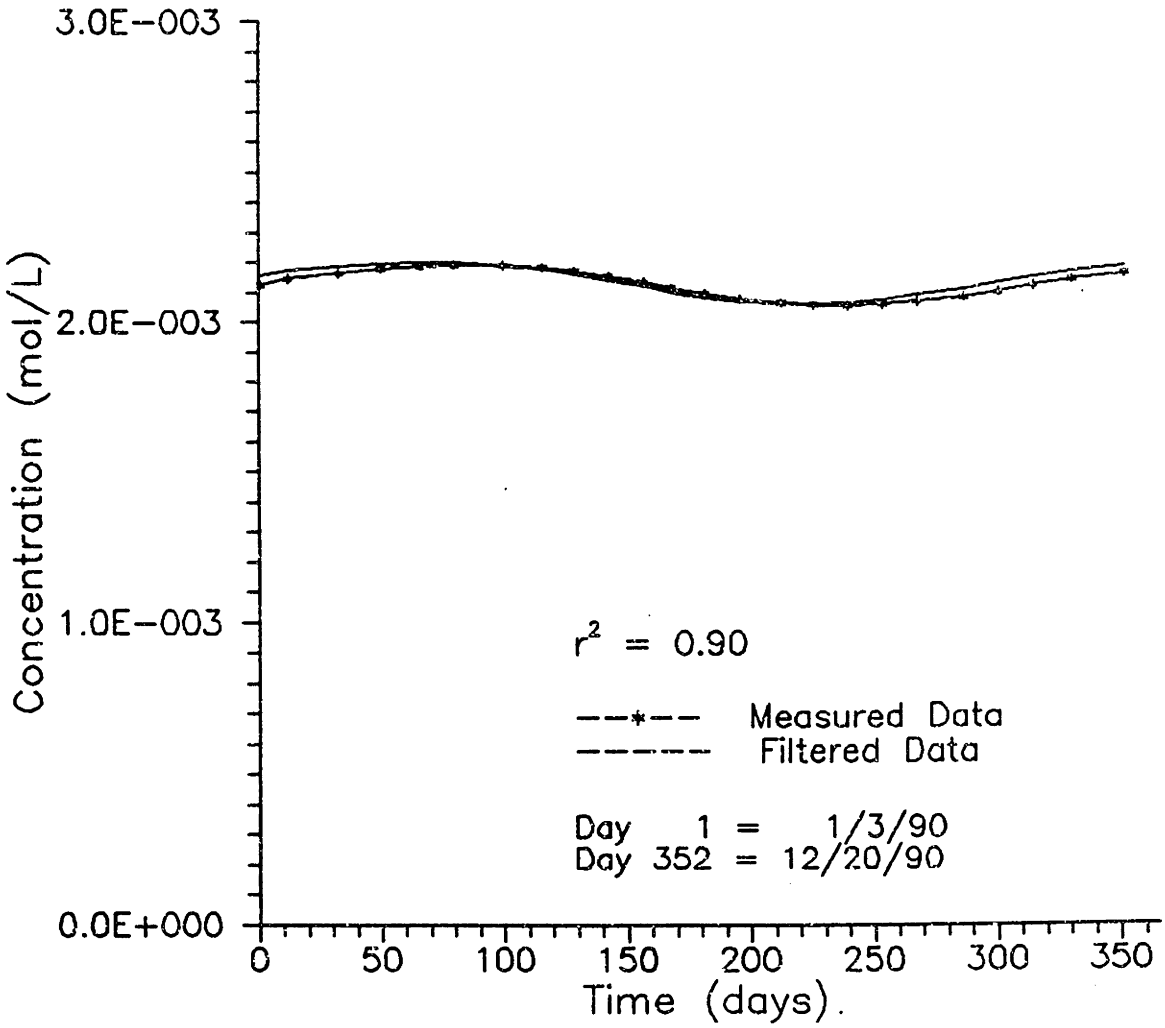

phases. The amplitude of the fluctuation of CH_4 concentrations in the water is almost as great as the CH_4 concentrations themselves. Due to low solubility, approximately 90% of CH_4 would be present in the gas bubble phase for this ratio of water volume to gas volume.

We would expect N_2 to have the strongest correlation between the smoothed data and the predicted partitioning data since there is a constant large atmospheric source. For N_2, however, the predicted water concentrations are much more constant, thereby alternately underestimating and overestimating actual smoothed data. This may occur because there is a strong seasonality in the replenishment of N_2 to the bog based on temperature-dependent diffusion, precipitation, and thermally-driven convection in the late fall. Or, since air contamination of porewater is very difficult to totally eliminate during sampling, the amplitude of the smoothed N_2 data may actually be systematically overestimated during the colder months.

As expected for CO_2, there is less of a correlation between temperature and concentration. As shown in Table 1-2, the amplitude of change in CO_2 porewater concentrations is small compared to the total CO_2 concentration in the water; therefore CO_2 porewater concentrations will be much more sensitive to changes in sources and sinks than to temperature changes because the solubility of CO_2 is so high. Approximately 75% of the CO_2 present is in the liquid phase. The strongest correlation occurs at 1.36 m, but this could be due to a correlation with CH_4 production more than a temperature dependency. At 0.68 m and 0.92 m, the predicted amplitude is about the same as the amplitude of the smoothed

data, but there is an unexplained phase lag.

Much of the seasonal fluctuation in porewater concentrations of N_2 and CH_4 can be explained by temperature fluctuations and the resultant changes in gas partitioning between liquid and bubble phases. Although this simple model does not take into account methane production, which would tend to increase with increasing temperatures, or changes in bubble volume due to changes in temperature, much of the seasonal flux of CH_4 in porewaters is accounted for by temperature-dependent partitioning. Variation in CH_4 sources and sinks seems to be secondary in importance for this simple model; there is no need to invoke variations in CH_4 sources and sinks with temperature fluctuations, changes in substrate, etc., although these undoubtedly occur in the actual ecosystem. For CO_2, changes in sources and sinks will play a much larger role in affecting annual cycles because the solubility of CO_2 is so high.

REFERENCES

Blake, D.R. and F.S. Rowland. 1988. Continuing worldwide increase in tropospheric methane, 1978 to 1987. Science, 239: 1129-1131

Cicerone, R.J. and J.D. Shetter. 1981. Sources of atmospheric methane: Measurements in rice paddies and a discussion. Journal of Geophysical Research, 86(C8): 7203-7209.

Crill, P.M., K.B. Bartlett, R.C. Harriss, E. Gorham, E.S. Verry, D.I. Sebacher, L. Madzar, and W. Sanner. 1988. Methane flux from Minnesota peatlands. Global Biogeochemical Cycles, 2(4): 371-384.

Dickinson, R.E. and R.J. Cicerone. 1986. Future global warming from atmospheric trace gases. Nature, 319: 109-115.

Gorham, E., S.J. Eisenreich, J. Ford, and M.V. Santelmann. 1985. The chemistry of bog waters. In: Chemical Processes in Lakes, Werner Stumm (Ed.), John Wiley and Sons, Inc., pp. 339-363.

Harriss, R.C., E. Gorham, D.I. Sebacher, K.B. Barlett, and P.A. Flebbe. 1985. Methane flux from northern peatlands. Nature, 315: 652-654.

Hemond, H.F. 1980. Biogeochemistry of Thoreau's Bog, Concord, Massachusetts. Ecological Monographs, 50(4): 507-526.

Keeling, C.D., R.B. Bacastow, A.F. Carter, S.C. Piper, T. P. Whorf, M. Heimann, W.G. Mook, and H. Roeloffzen. 1989. A three-dimensional model of atmospheric CO_2 transport based on observed winds: 1.Analysis of observational data. In: Aspects of Climate Variability in the Pacific and the Western Americas, D.H. Peterson (ed.), Geophysical Monograph 55:165-235.

Khalil, M.A.K. and R.A. Rasmussen. 1987. Atmospheric methane: Trends over the last 10,000 years. Atmospheric Environment, 21(11): 2445-2452.

Khalil, M.A.K. and R.A. Rasmussen. 1990. Atmospheric methane: Recent global trends. Environ. Sci. Technol., 24: 549-553.

Miller, P. C. 1981. Carbon Balance in Northern Ecosystems and the Potential Effect of Carbon Dioxide Induced Climatic Change. U.S. Dept. of Energy, CONF-8003118, UC-11.

Matthews, E. and I. Fung. 1987. Methane emission from natural wetlands: Global distribution, area, and environmental characteristics of sources. Global Biogeochemical Cycles, 1(1): 61-86.

Sebacher, D.I., R.C. Harriss, K.B. Bartlett, S.M. Sebacher, and S.S. Grice. 1986. Atmospheric methane sources: Alaskan tundra bogs, an alpine fen, and a subarctic boreal marsh. Tellus, 38B: 1-10.

Seiler, W. 1984. Contribution of biological processes to the global budget of CH_4 in the atmosphere. In: Current Perspectives in Microbial Ecology, M.J. Klug and C.A. Reddy (Eds.), American Society for Microbiology, Washington, D.C.

Stauffer, B., E. Lochbronner, H. Oeschger, and J. Schwander. 1988. Methane concentration in the glacial atmosphere was only half that of the preindustrial Holocene. Nature, 332: 812-814.

Wahlen, M., N. Tanaka, R. Henry, B. Deck, J. Zeglen, J.S. Vogel, J. Southon, A. Shemesh, R. Fairbanks, W. Broecker. 1989. Carbon-14 in methane sources and in atmospheric methane: The contribution from fossil carbon. Science, 245: 286-290.

Weast, R.C. 1990. [Editor in Chief]. CRC Handbook of Chemistry and Physics, 70th edition, CRC Press, Inc., Boca Raton, Florida.

Weiss, R.F. 1970. The solubility of nitrogen, oxygen and argon in water and seawater. Deep-Sea Research, 17: 721-735.

Weiss, R.F. 1974. Carbon dioxide in water and seawater: The solubility of a non-ideal gas. Marine Chemistry, 2: 203-215.

Whalen, S.C. and W.S. Reeburgh. 1988. A methane flux time series for tundra environments. Global Biogeochemical Cycles, 2(4): 399-409.

Wiesenburg, D.A. and N.L. Guinasso, Jr. 1979. Equilibrium solubilities of methane, carbon monoxide, and hydrogen in water and sea water. Journal of Chemical and Engineering Data, 24(4): 356-360.

Williams, R.T. and R.L. Crawford. 1984. Methane production in Minnesota peatlands. Applied and Environmental Microbiology, 47(6): 1266-1271.

Williams, R.T. and R.L. Crawford. 1985. Methanogenic bacteria, including an acid-tolerant strain, from peatlands. Applied and Environmental

Microbiology, 50(6): 1542-1544.

Winfrey, M.R. 1984. Microbial production of methane. In: Petroleum Microbiology, R.M. Atlas (Ed.), Macmillan Publishing Co., New York.

Winfrey, M.R. and J.G. Zeikus. 1979. Microbial methanogenesis and acetate metabolism in a meromictic lake. Applied and Environmental Microbiology, 37(2): 213-221.

Yavitt, J.B., G.E. Lang, and D.M. Downey. 1988. Potential methane production and methane oxidation rates in peatland ecosystems of the Appalachian Mountains, United States. Global Biogeochemical Cycles, 2(3): 253-268.

Zeikus, J.G. and M.R. Winfrey. 1976. Temperature limitation of methanogenesis in aquatic sediments. Applied and Environmental Microbiology, 31(1): 99-107.

CHAPTER 2

Ebullition

INTRODUCTION

Methane can leave the saturated zone of Thoreau's Bog in two ways: through diffusion and through ebullition. Ebullition, or bubbling, is thought to occur through discrete bubble tubes in the peat mat, and may be a more rapid method of vertical gas transport through water than diffusion. In general, bubbles form when the pressures of gases at depth exceed the sum of the atmospheric pressure and the hydrostatic pressure. At Thoreau's Bog, it has been proposed that biogenically produced CH_4, and N_2 that has been transported by diffusion and advection into the bog from the atmosphere, together form bubbles that transport CH_4 to the unsaturated zone (Army, 1987). Once the bubbles reach the unsaturated zone, they burst, and CH_4 either diffuses up to the peat surface or it is oxidized to CO_2 by methanotrophs in the aerated unsaturated zone (see Chapter 3).

Quantification of bubble composition and bubbling rates is inherently difficult due to the heterogeneous and episodic nature of bubbling. Nevertheless, other workers studying CH_4 ebullition in other ecosystems have noted the importance of ebullition to the overall CH_4 flux. Chanton and Martens (1988) found in a tidal freshwater estuary that ebullitive CH_4 fluxes are depleted in $^{13}CH_4$ relative to fluxes due to molecular diffusion; they propose that this occurs because bubbles transport the CH_4 rapidly through the upper zones where microbial methane oxidation would enrich the CH_4 in ^{13}C. They also noted that the rate of methanogenesis strongly influences the ebullitive flux and that the

ebullitive flux is highly seasonal. Martens et al. (1980) documented the presence in a small marine basin of abiogenic bubble tube structures which lead to summertime CH_4 transport rates three times greater than those due to molecular diffusion alone. In floating grass mats in the tropical Amazon, ebullition, when it occurred, was found to dominate CH_4 release to the atmosphere; it accounted for 64% of the total CH_4 flux from the site (Bartlett et al., 1988). Devol et al. (1988) also studied wetlands on the Amazon floodplain and noted that ebullition was the dominant transport mechanism, accounting for 85% of the total CH_4 flux to the atmosphere.

In order to characterize ebullition at Thoreau's Bog, we exploited the fact that bubble production affects the elevation of the bog's floating peat mat. At Thoreau's Bog, a portion of the peat mat is supported by buoyancy, i.e., the mat is floating in the water that fills the kettle hole beneath it. Buoyancy is caused by both the peat itself and bubbles present in the peat mat. Mat elevation data were recorded remotely, thereby circumventing problems of site disturbance, which could trigger the release of bubbles. From changes in the mat level (mat buoyancy), estimates of the volume of bubbles in the mat were made, as well as estimates of the temporal variability of ebullition. We found that some mat buoyancy changes are correlated with atmospheric pressure, most likely due to compressibility of bubbles.

MATERIALS AND METHODS

Thoreau's Bog is equipped with both a mat level recorder and a water stage recorder. Both recorders are Stevens Type F recorders, run on 32 day cycles, with a 1:1 relationship between changes in stage and changes recorded on the charts. The mat level recorder is located on the rigid platform, and a 1 m long stake is driven into the mat below so that the stake moves up and down with the mat. The water stage recorder is located in the lagg and uses a float and stilling well.

Data from these chart recorders were digitized using a Calcomp 9000 digitizer board; resolution is of the order of less than a millimeter. Data were digitized at 8 hour time intervals, the smallest time increment on the chart, and time was recorded to the nearest half-hour. The digitized data were then plotted using Lotus 1-2-3 to check that the original shape of the stage record had been correctly mapped. Although the digitized data cannot fully capture the fluctuations in the mat buoyancy, visual inspection of the recorder charts shows that as the mat level is falling, there are regular intervals of stage decrease, evidently due to evapotranspiration from the peat mat occurring during daylight hours. These fluctuations are very small compared to the overall changes in the mat level.

Atmospheric pressure data recorded hourly at Hanscom Air Force Base (HAFB) in Bedford, MA were obtained from the National Center for Climatic Data. HAFB is located approximately 2.4 km to the east of Thoreau's Bog.

When pressure readings on the half-hour were required, the arithmetic mean of the previous and subsequent hourly readings was taken.

Four 12.7 cm diameter peat cores were taken from different locations in the bog to measure porosity near the water table. The experimental set-up for these 4 cores is shown in Figure 2-1. At the beginning of the experiment, water was added to a height several centimeters above the initial water table, and the core was allowed to equilibrate so that the water level in the core was the same as the water level in the tank. The weight of the peat core at that water level was recorded; the water level was then lowered, the core allowed to re-equilibrate, and a new weight recorded. The final reading was taken at a water level several centimeters below the original water table. It was assumed that any changes in the weight of water held above the water table by capillary forces were small compared to changes in the buoyant force.

By using the changes in the buoyant force (as measured by the scale) and the changes in the water level in the tank, the porosity, n, was calculated for each depth increment using the following relationship:

$$n = 1 - \frac{\Delta F_B}{\Delta z g A \rho_w} \qquad (2\text{-}1)$$

where: F_B = buoyant force

z = depth of core submerged

A = cross sectional area of core

Figure 2-1: Peat Porosity Experiment

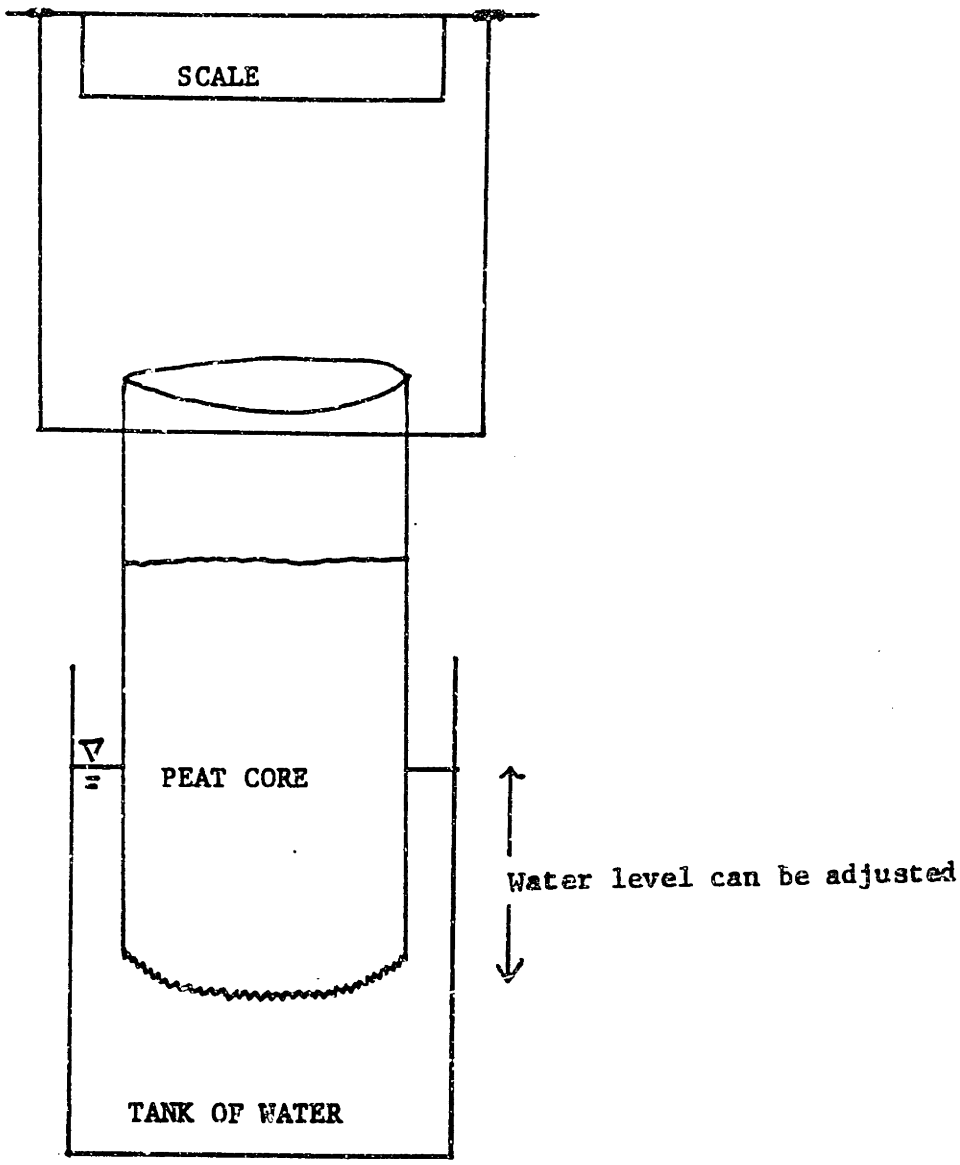

ρ_w = density of water at temperature of measurement

g = acceleration due to gravity

n = porosity

After completing the peat buoyancy experiments, three of the four cores were extruded for examination prior to returning them to the bog. The visibly different sediment horizons were described and approximate thicknesses measured.

RESULTS

The peat mat floats freely in the water as shown in Figures 2-2 and 2-3, where depth to mat versus depth to water are plotted for June 24 to December 10, 1988, and from March 16 to December 8, 1989, respectively. The slope of the regression line is 0.9 cm/cm for both time periods. The r^2 values of 0.97 for 1988 and 0.85 for 1989 show that mat and water levels are very strongly correlated.

From these two years' worth of mat level, water level, and pressure data, four time periods were selected for close study. During these time periods, the mat and water levels were steadily falling; the data are shown in Figures 2-4 through 2-7. It should be noted that depths to mat and water increase as the mat and water are falling, and that 32 cm were added to every water depth to bring it on the same scale as the mat depth. By choosing only time periods in which the mat and water levels were steadily falling, we minimized the potential problem of hysteresis due to friction of the peat against the platform pilings. Hysteresis might

Figure 2–2: Depth to Mat versus Depth to Water, June 24 to December 10, 1988

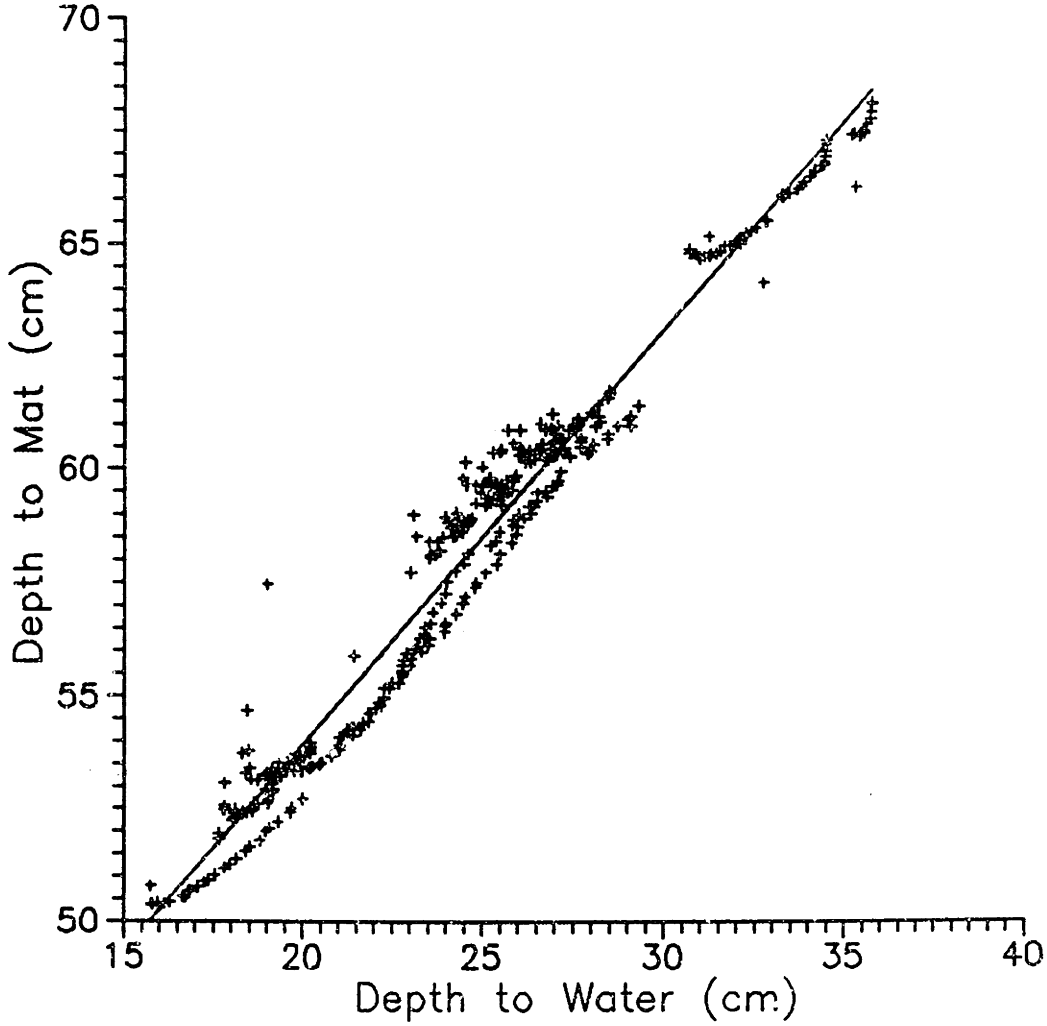

Figure 2–3: Depth to Mat versus Depth to Water, March 16 to December 8, 1989

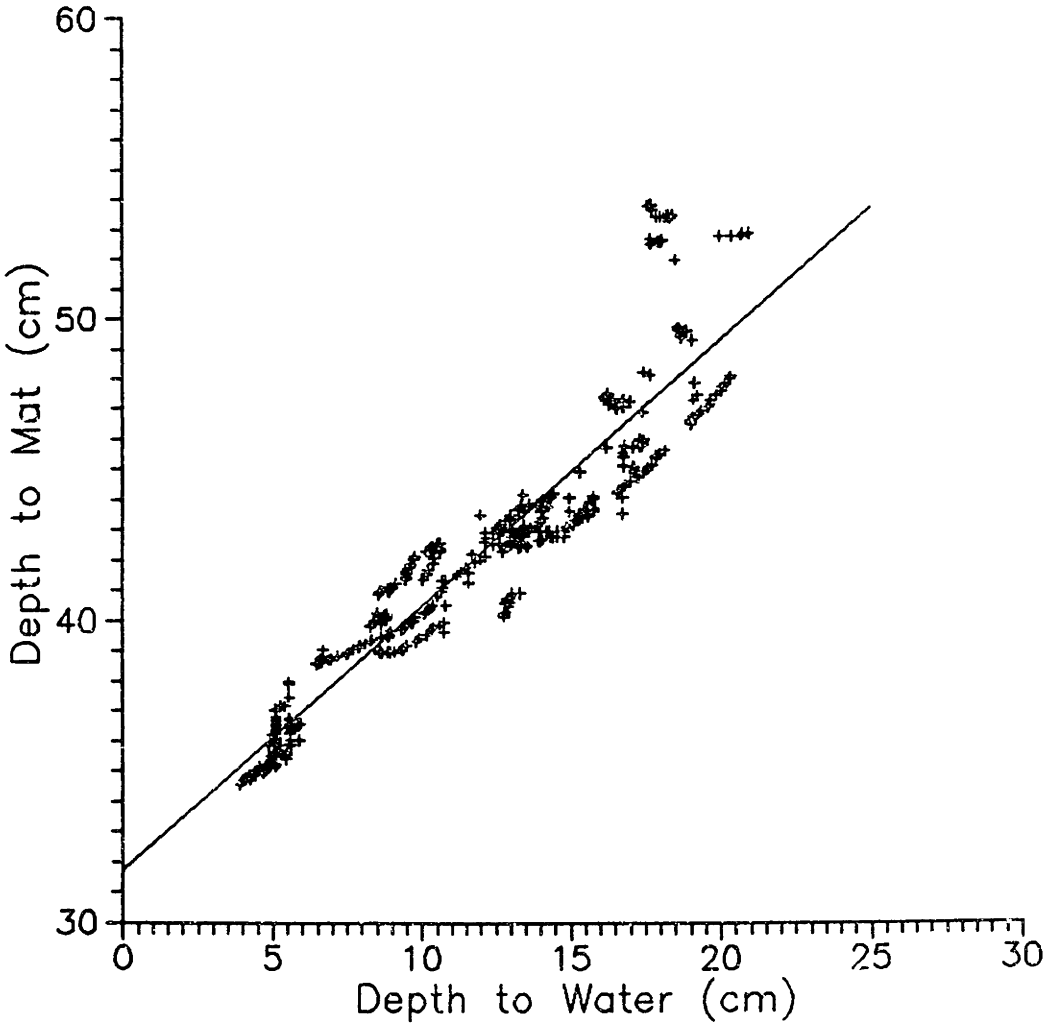

Figure 2–4: Temporal Variations in Mat and Water Heights, 6/29/88 to 7/6/88

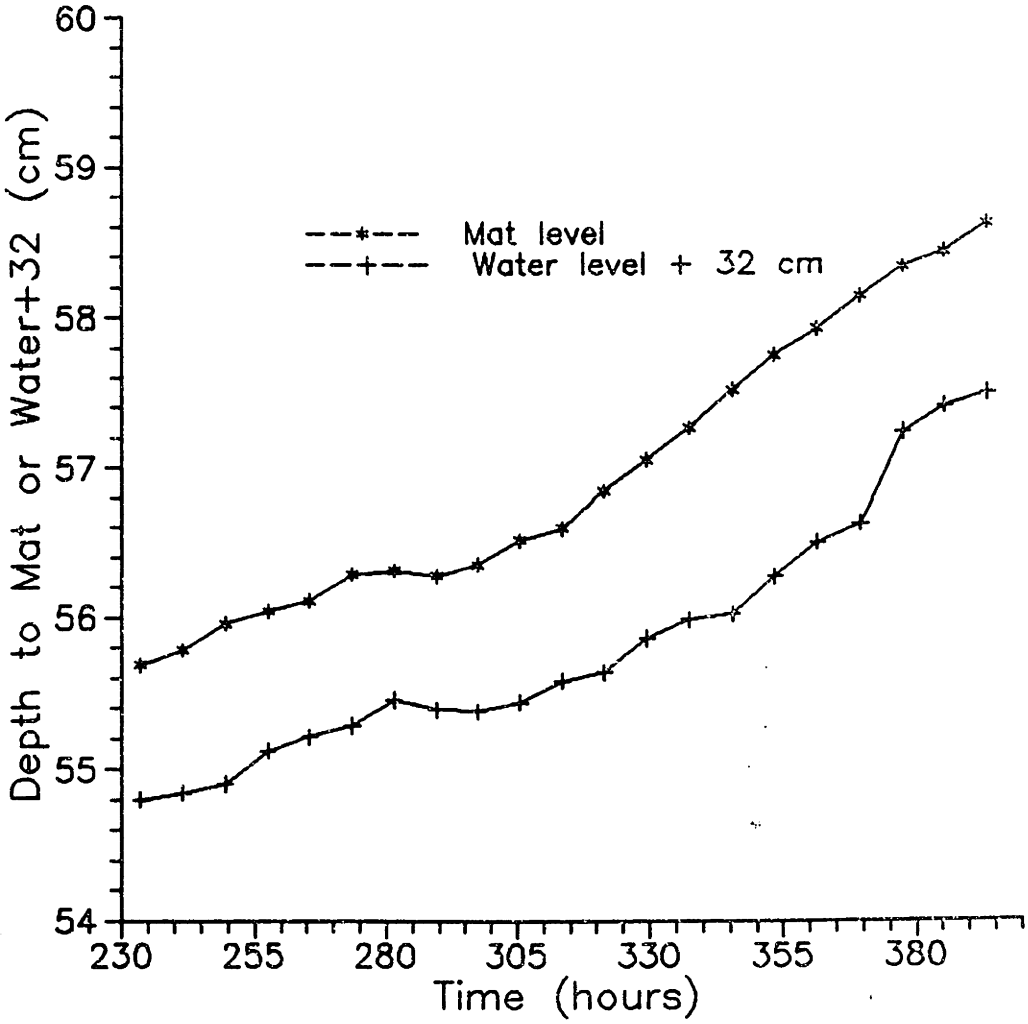

Figure 2–5: Temporal Variations in Mat and Water Heights, 8/11/88 to 8/23/88

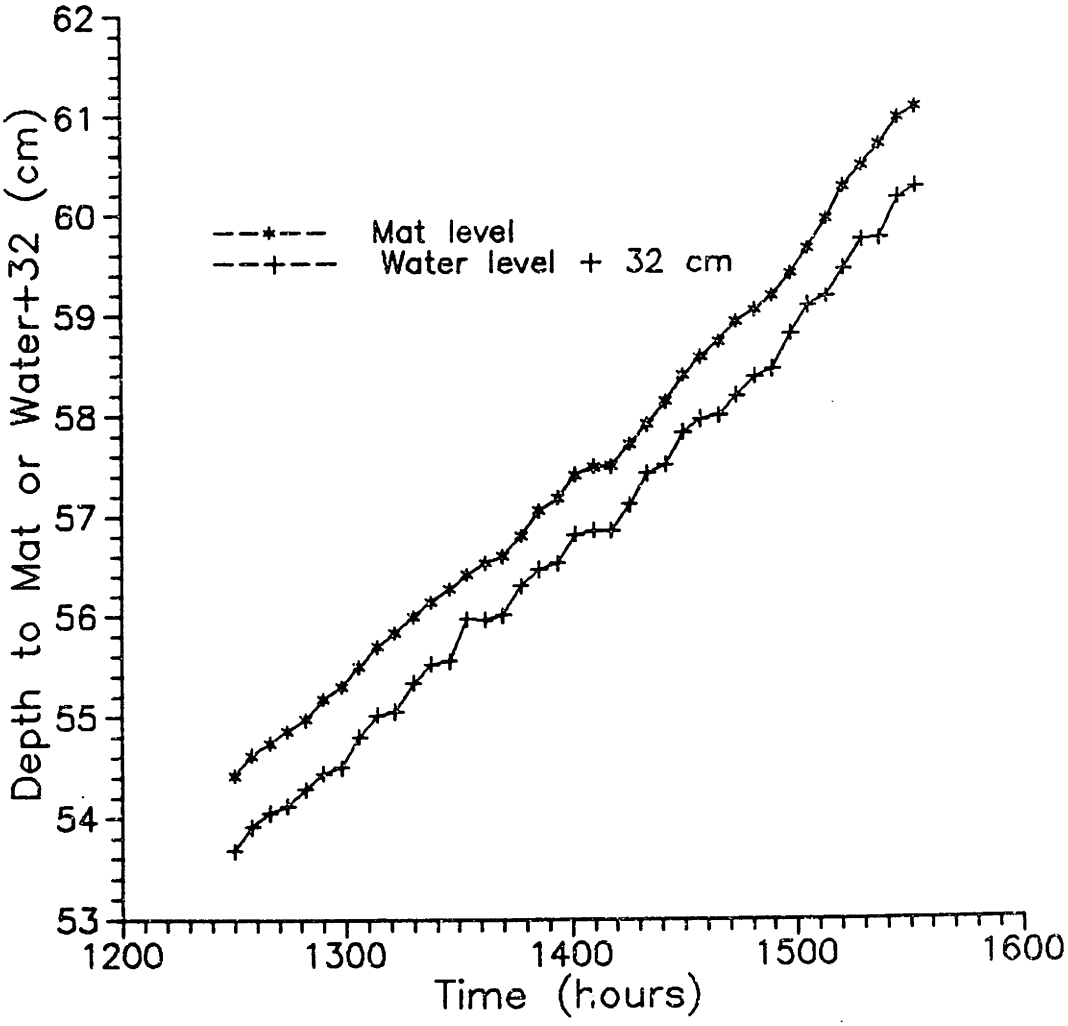

Figure 2–6: Temporal Variations in Mat and Water Heights, 6/23/89 to 6/29/89

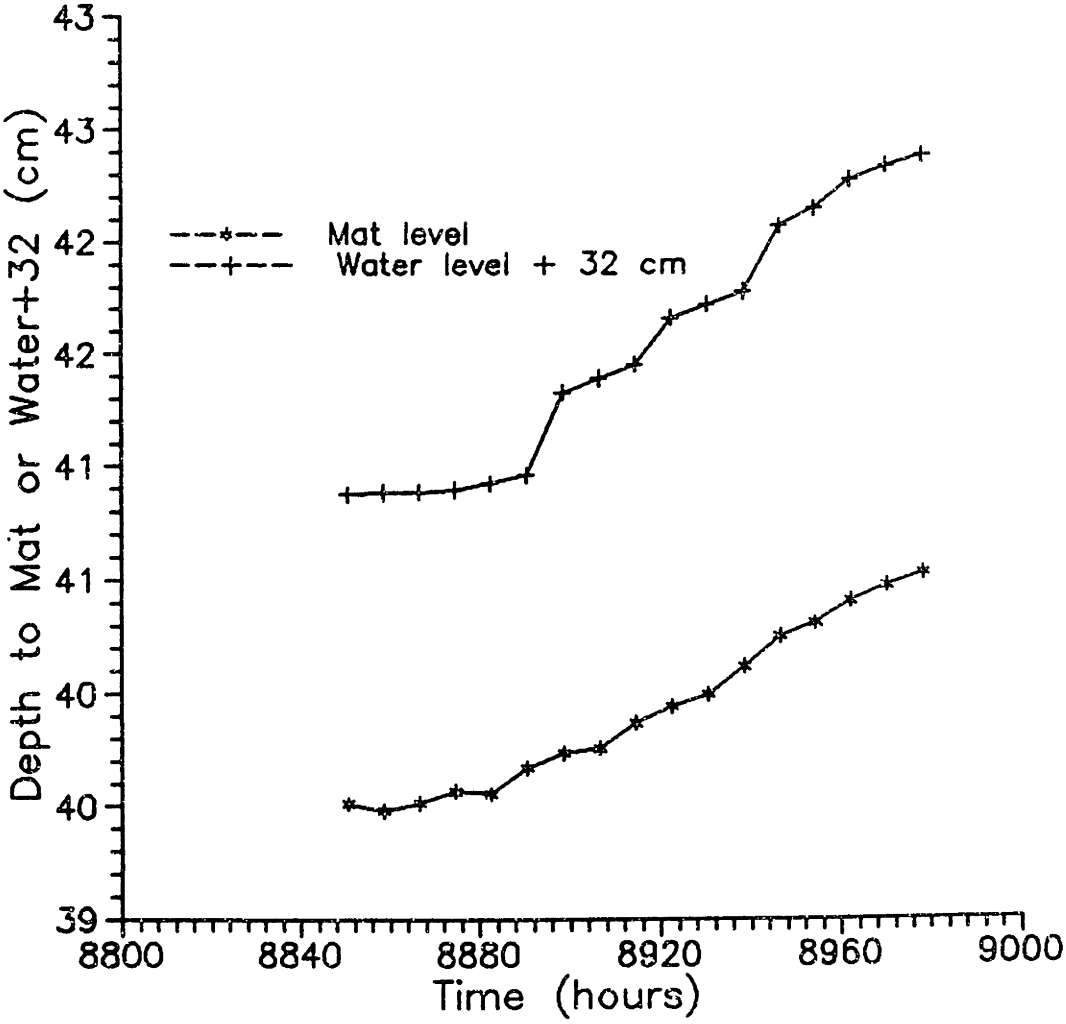

Figure 2–7: Temporal Variations in Mat and Water Heights, 7/29/89 to 8/7/89

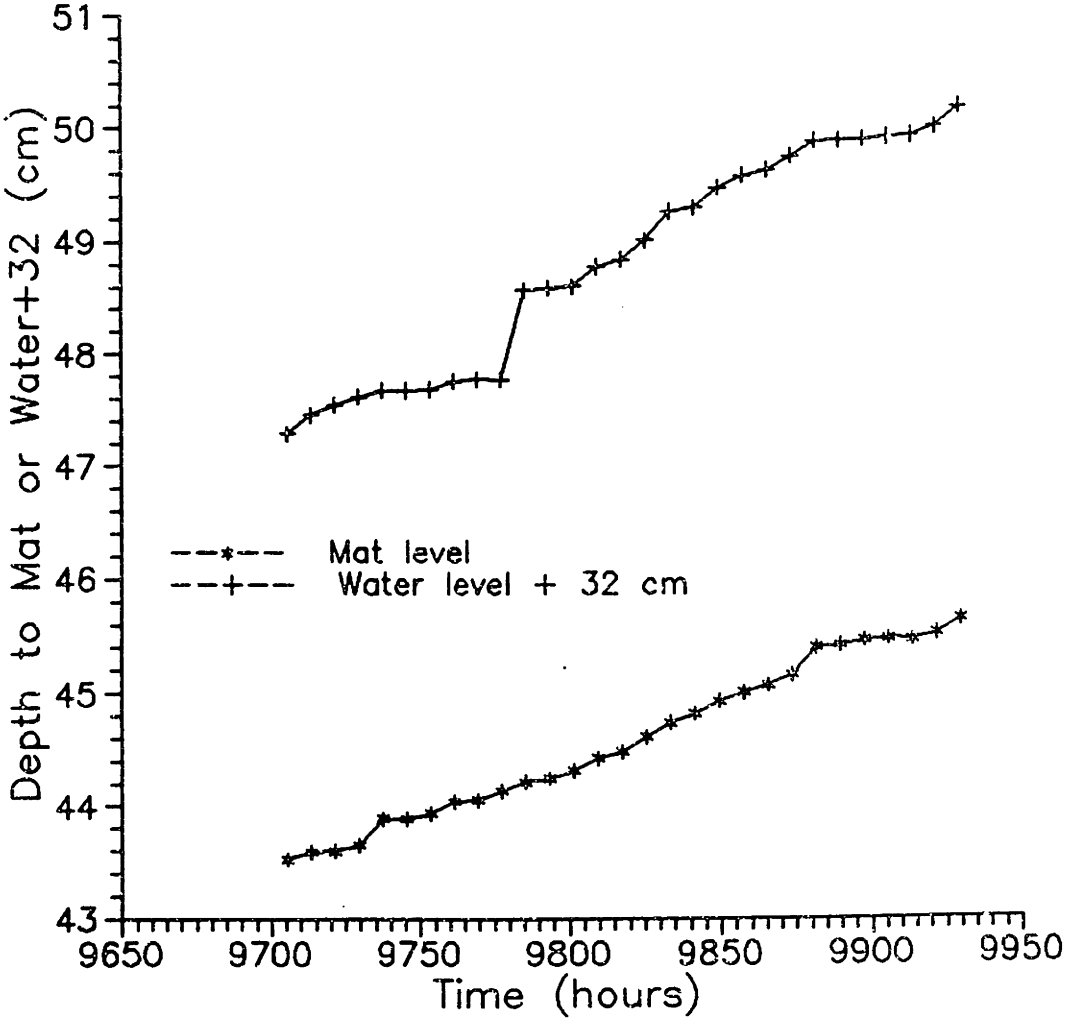

occur if there were periods of rainfall imposed on a general trend of falling mat and water levels, causing the mat level to alternately rise and fall. Friction between the peat mat and the pilings of the rigid platform on which the mat buoyancy recorder is located would then reverse direction, leading to hysteresis. This is minimized if the mat is falling steadily rather than alternately rising and falling due to rainfall events. There were no sufficiently long time periods during which both the mat and water levels steadily rose, so all calculations are based on falling mat and water levels.

To determine if the mat responded to changes in the water level within the digitized 8 hour time period, we looked at the r^2 values for mat level versus water level. We found the correlation between levels worsened if the water level was offset. Thus the mat levels were corrected by subtracting off the water levels occurring at the same time, and the corrected mat levels were then plotted versus pressure, as shown in Figures 2-8 through 2-11. A linear regression was performed, and a student t-test showed the r^2 values for the 4 time periods to be significant at a 95% confidence level.

The regression lines shown in Figures 2-8 through 2-11 indicate that at high pressures, the mat falls more than the water, whereas at low pressures the mat is falling less than the water. The slopes of the regression line vary, however, suggesting that the relationship between mat level and pressure may vary with the absolute height of the mat.

The residuals (observed corrected mat levels minus estimated corrected mat levels) were then plotted versus the rate of change of pressure, to look for

Figure 2–8: Corrected Mat Levels versus Pressure, 6/29/88 to 7/6/88

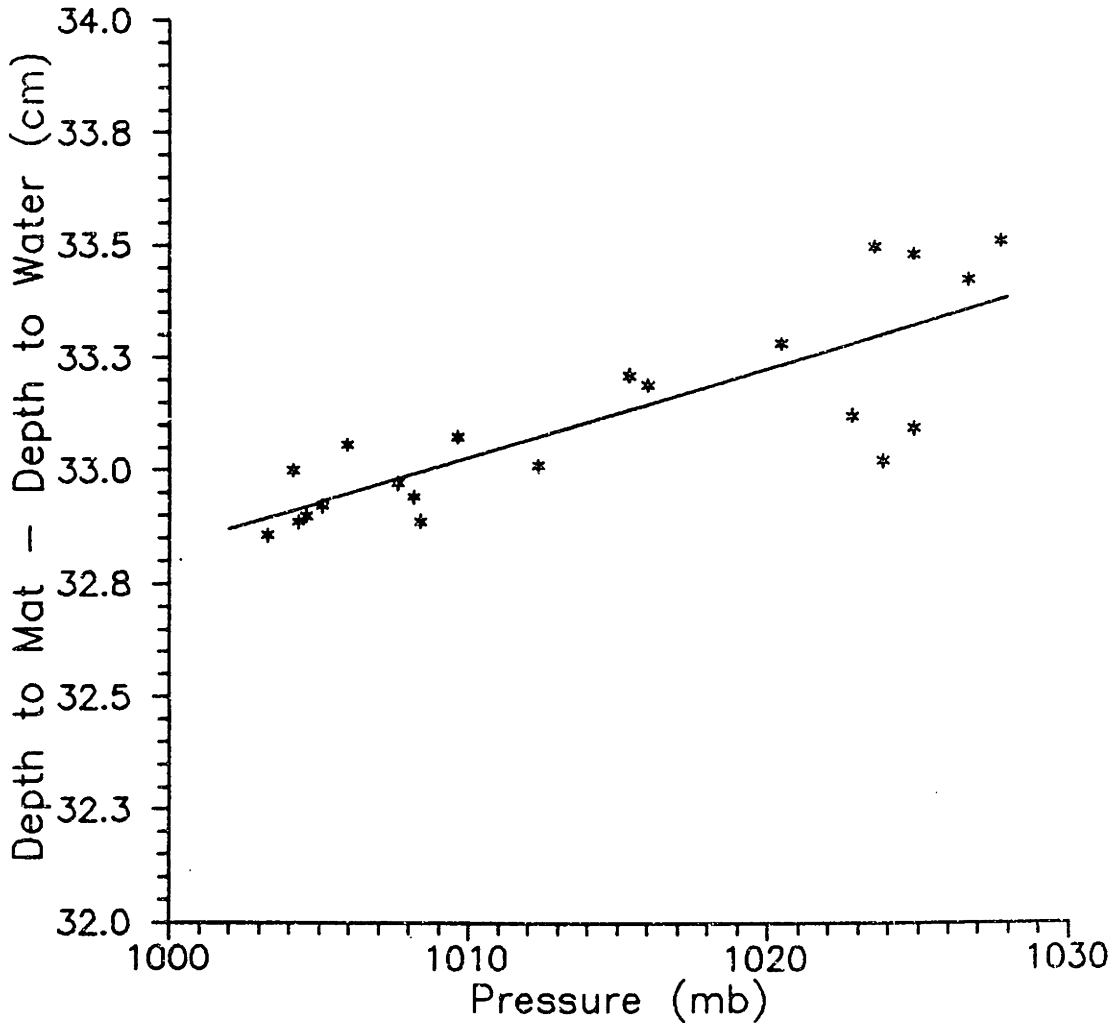

Figure 2–9: Corrected Mat Levels versus Pressure, 8/11/88 to 8/23/88

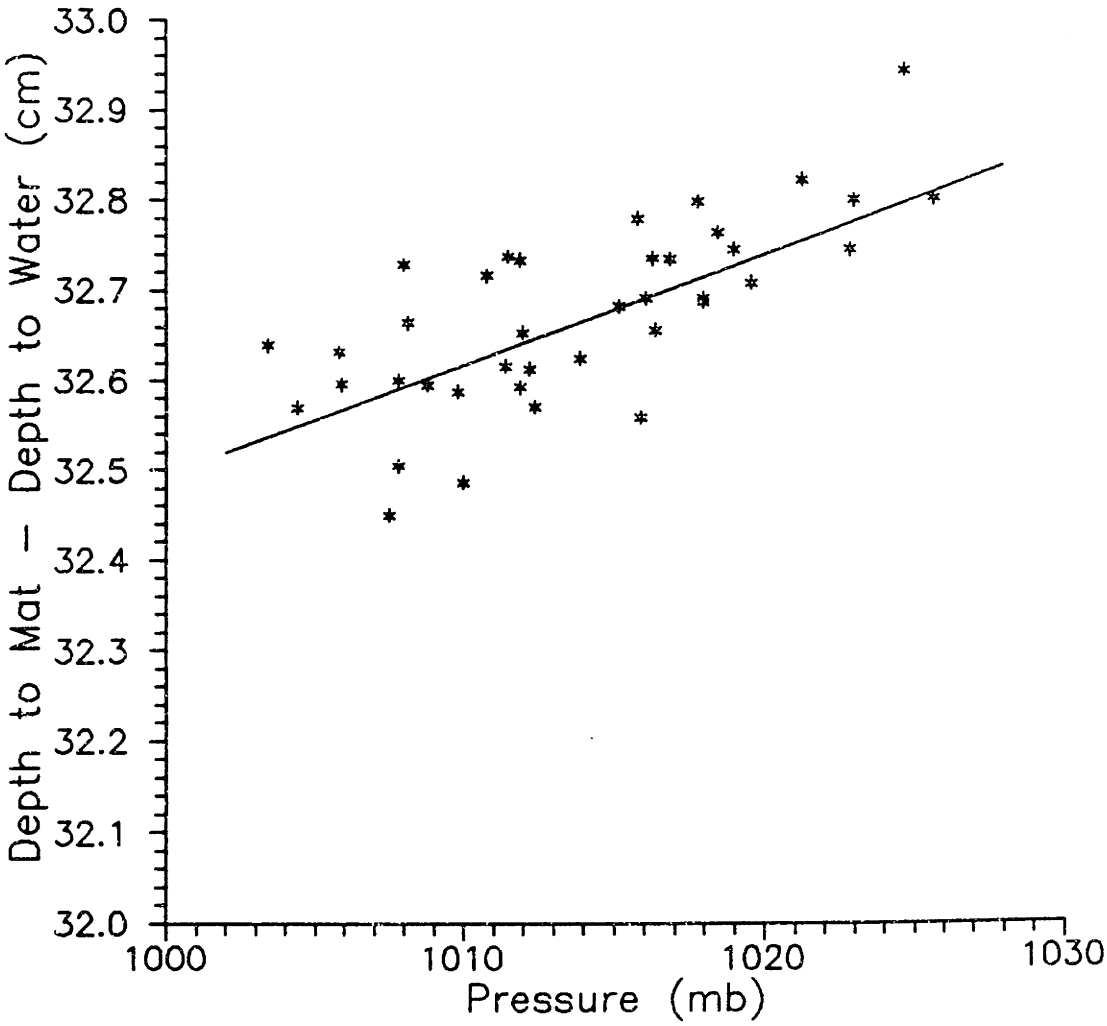

Figure 2–10: Corrected Mat Levels versus Pressure, 6/23/89 to 6/29/89

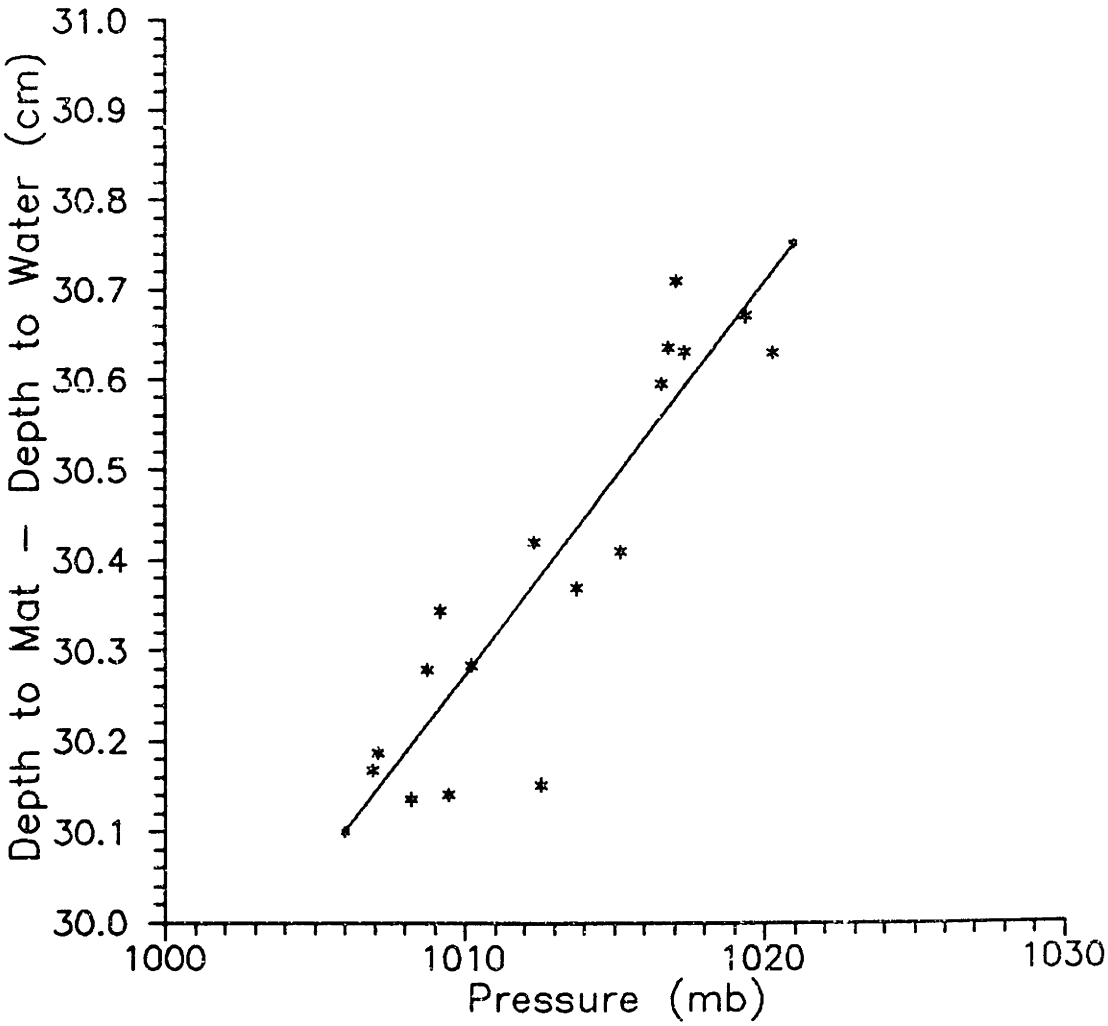

Figure 2–11: Corrected Mat Levels versus Pressure, 7/29/89 to 8/7/89

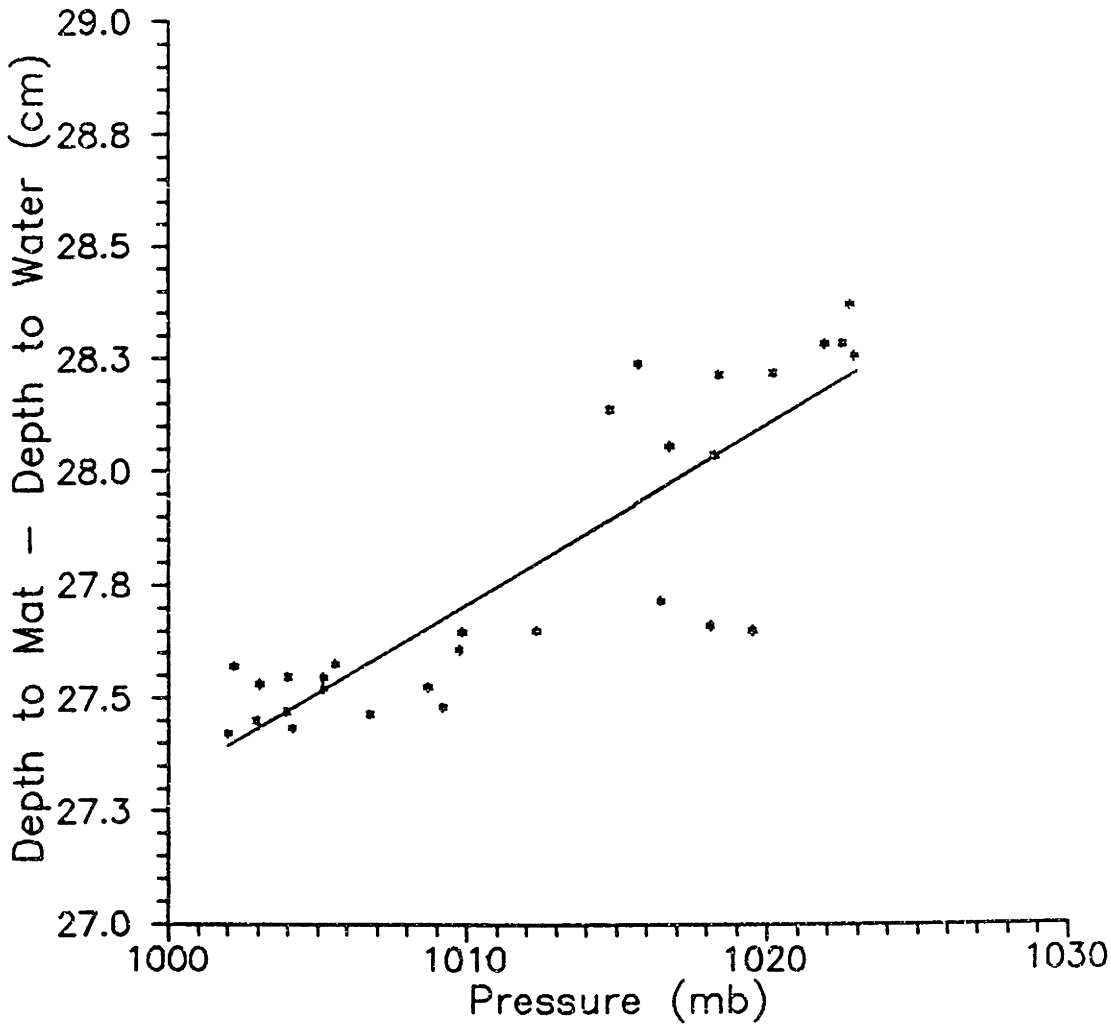

evidence of pressure changes triggering bubble release, but there was no clear-cut trend (see Figures 2-12 through 2-15). The residuals were also plotted versus wind speed, using data from the Worcester (Massachusetts) Municipal Airport, located approximately 47 km southwest of Thoreau's Bog. Again, as Figures 2-16 through 2-19 show, no significant relationship exists.

Data from the peat core buoyancy experiments indicate that from approximately 1 cm below the water table to approximately 1 cm above, porosity ranges from 0.2 to 0.4, with an average value of 0.26. This porosity value is for regions of more compressed and decomposed organic material, as observed in the extruded cores.

Figure 2–12: Corrected Mat Level Residuals versus Pressure Change w.r.t. Time, 6/29/88 to 7/6/88

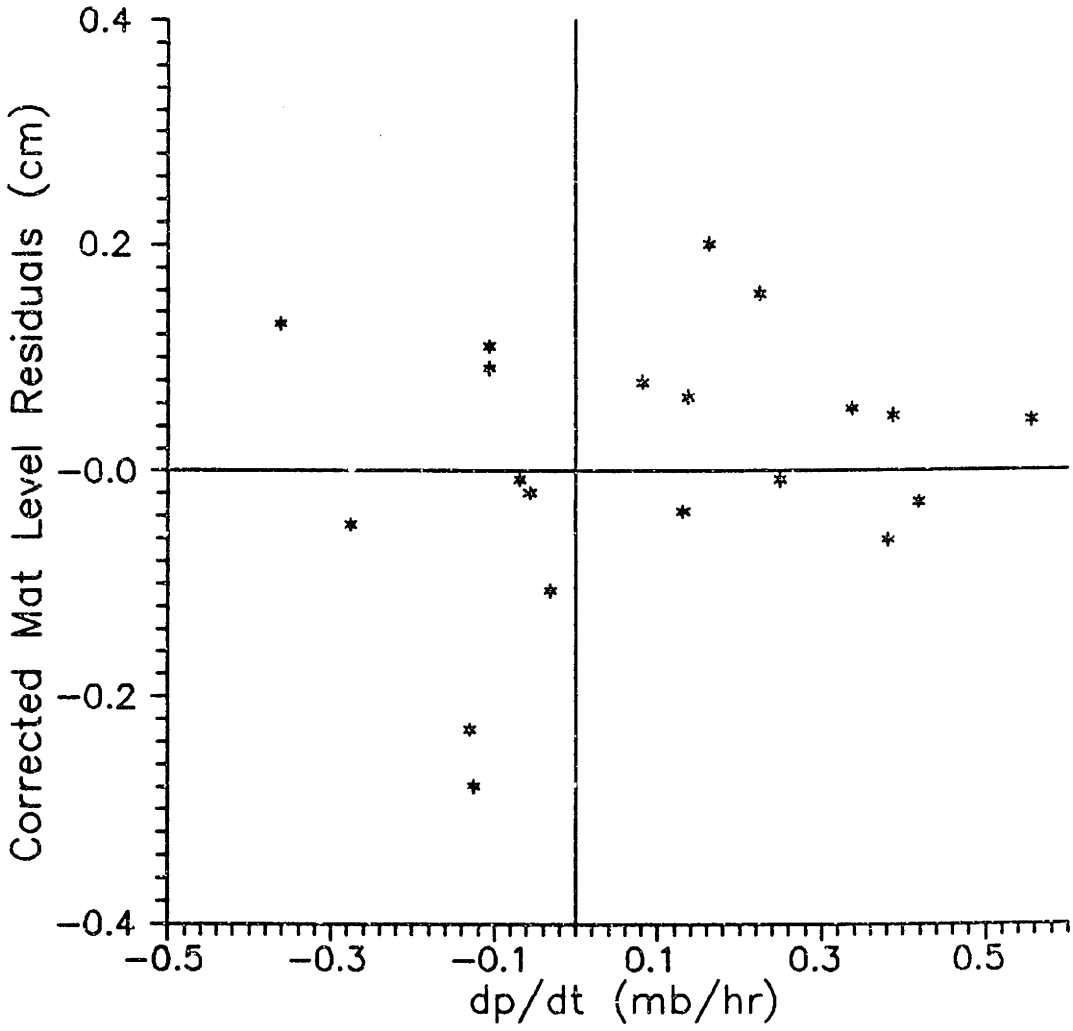

Figure 2–13: Corrected Mat Level Residuals versus Pressure Change w.r.t. Time, 8/11/88 to 8/23/88

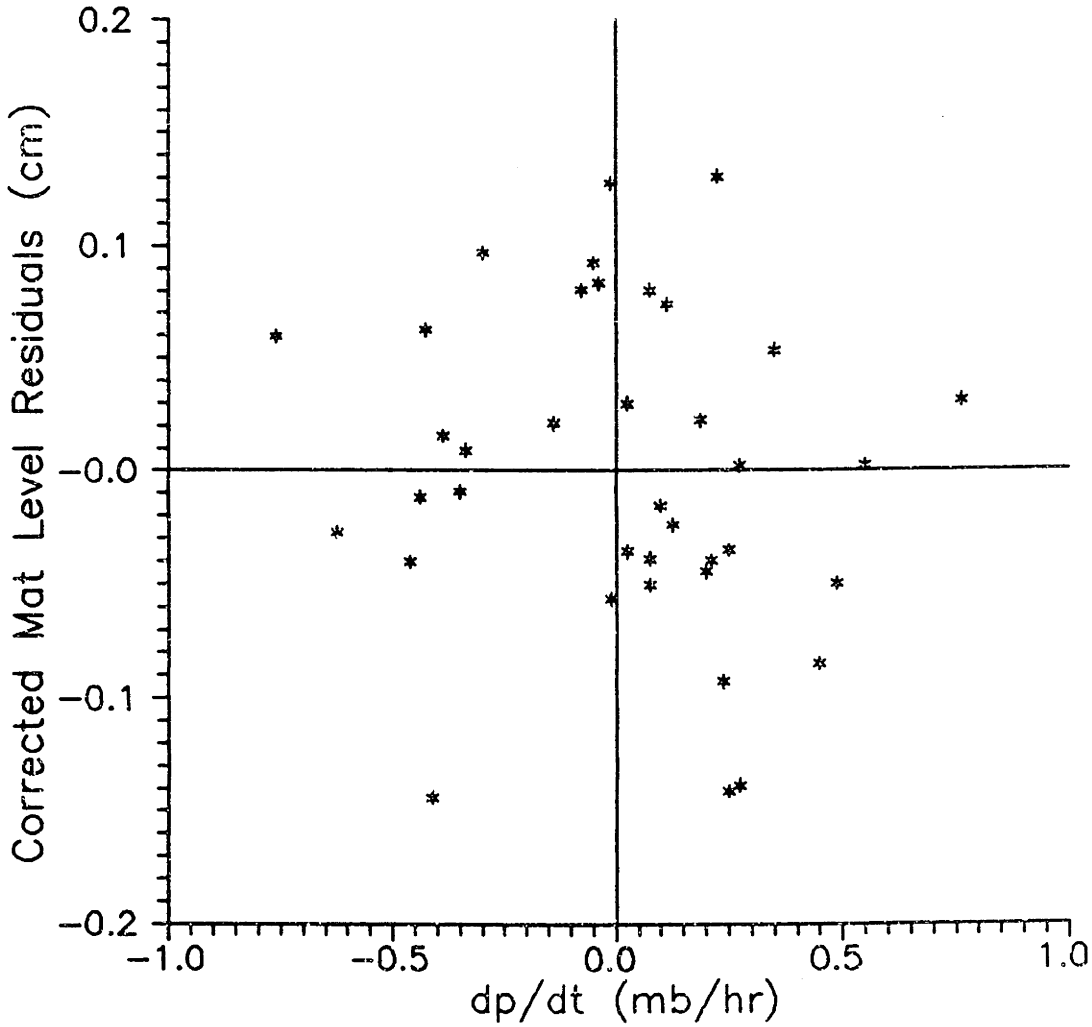

Figure 2–14: Corrected Mat Level Residuals versus Pressure Change w.r.t. Time, 6/23/89 to 6/29/89

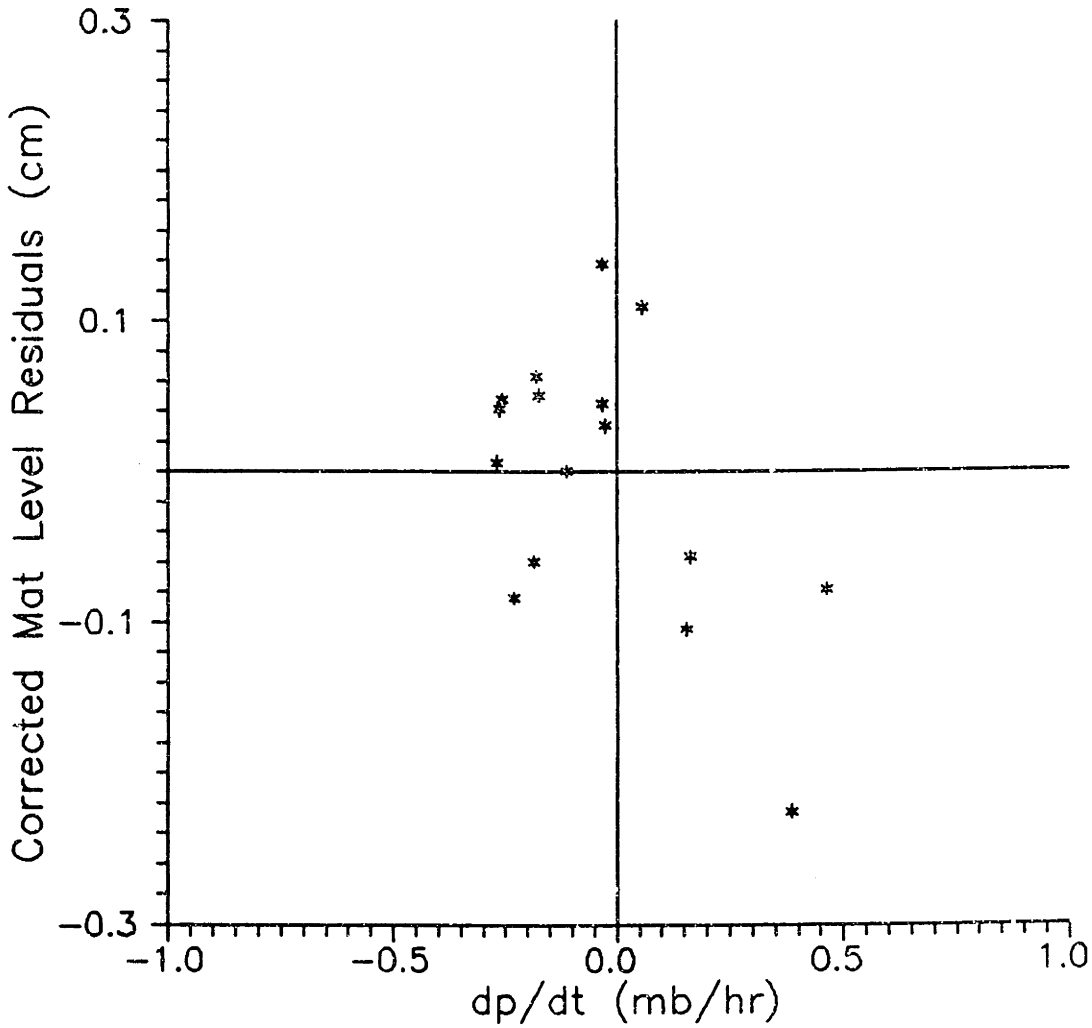

Figure 2–15: Corrected Mat Level Residuals versus Pressure Change w.r.t. Time, 7/29/89 to 8/7/89

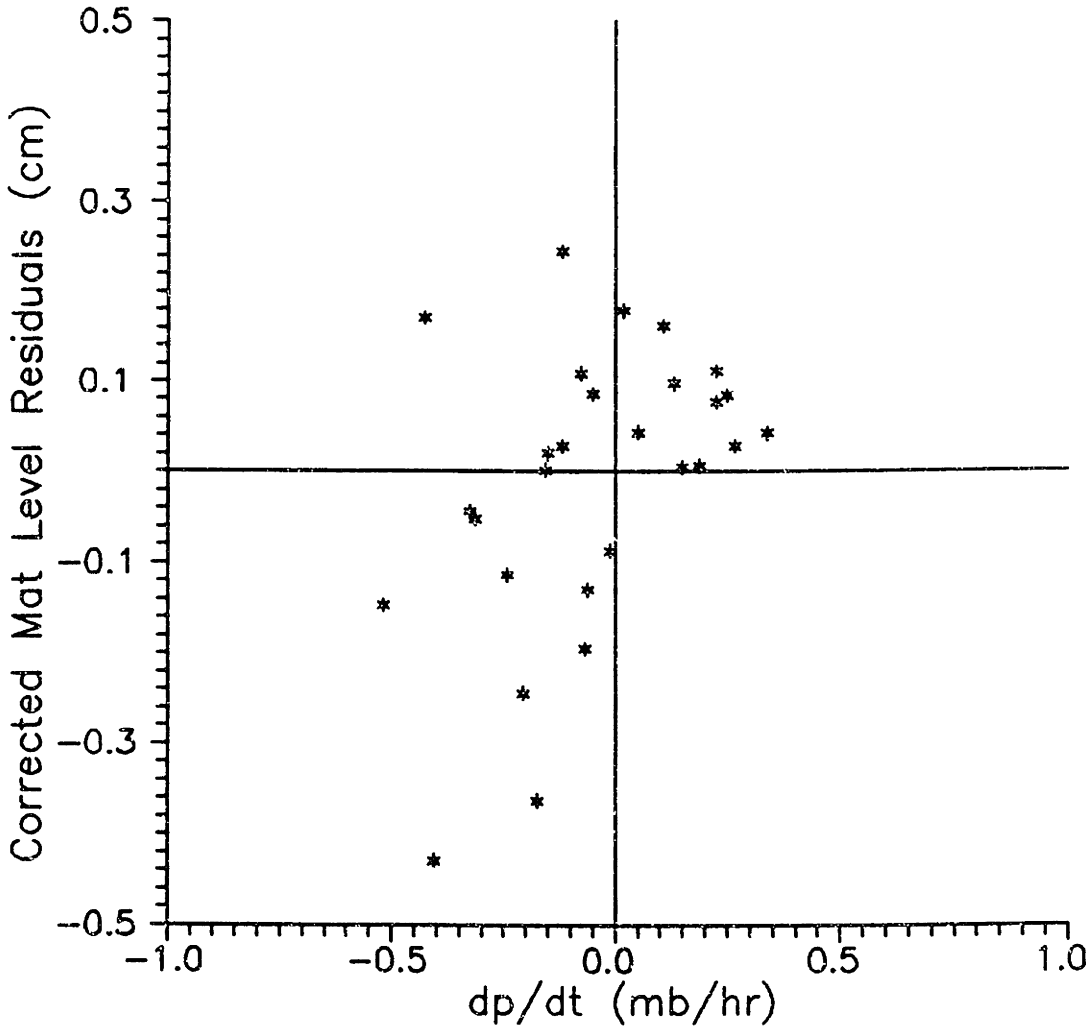

Figure 2–16: Corrected Mat Level Residuals versus Wind Speed, 6/29/88 to 7/6/88

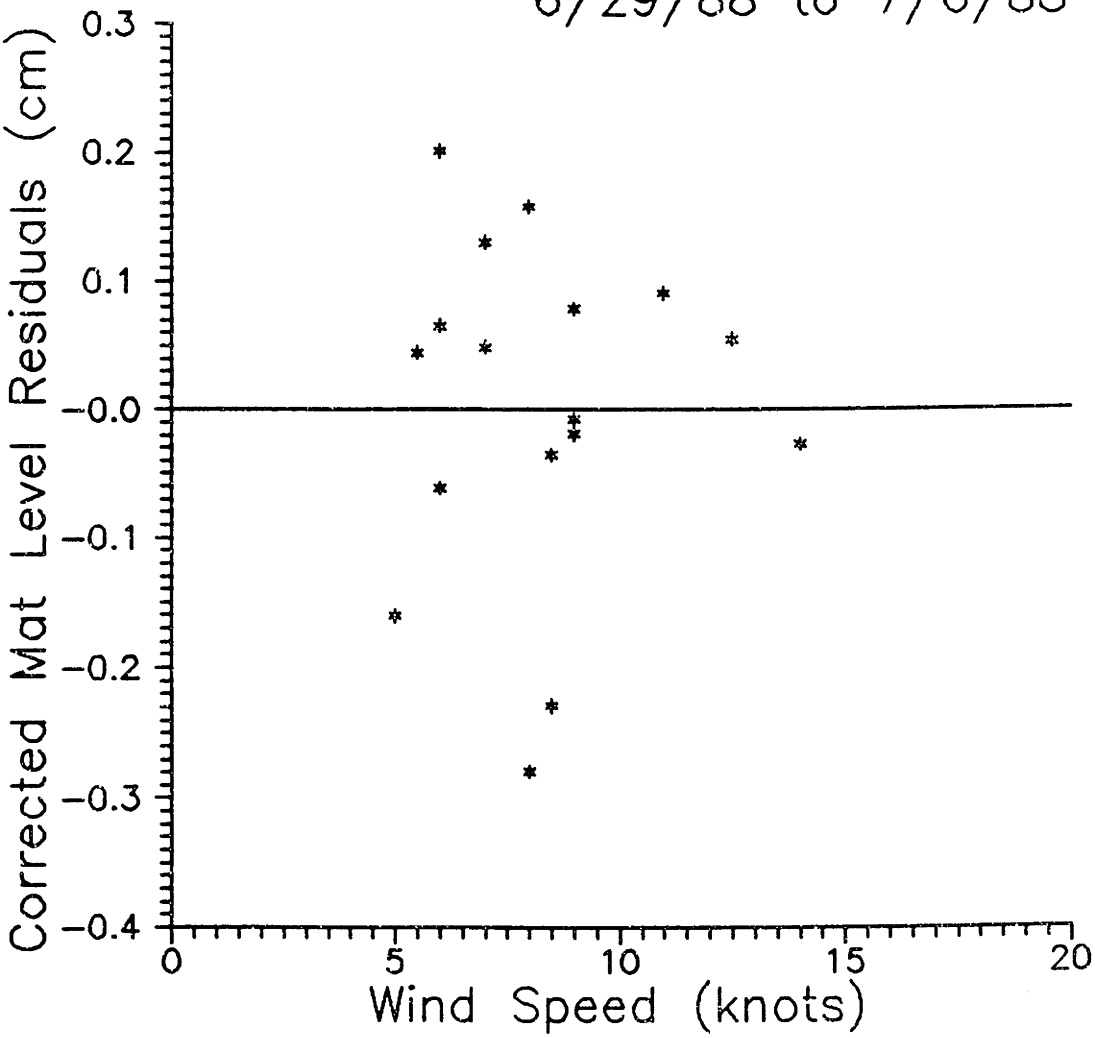

Figure 2–17: Corrected Mat Level Residuals versus Wind Speed, 8/11/88 to 8/23/88

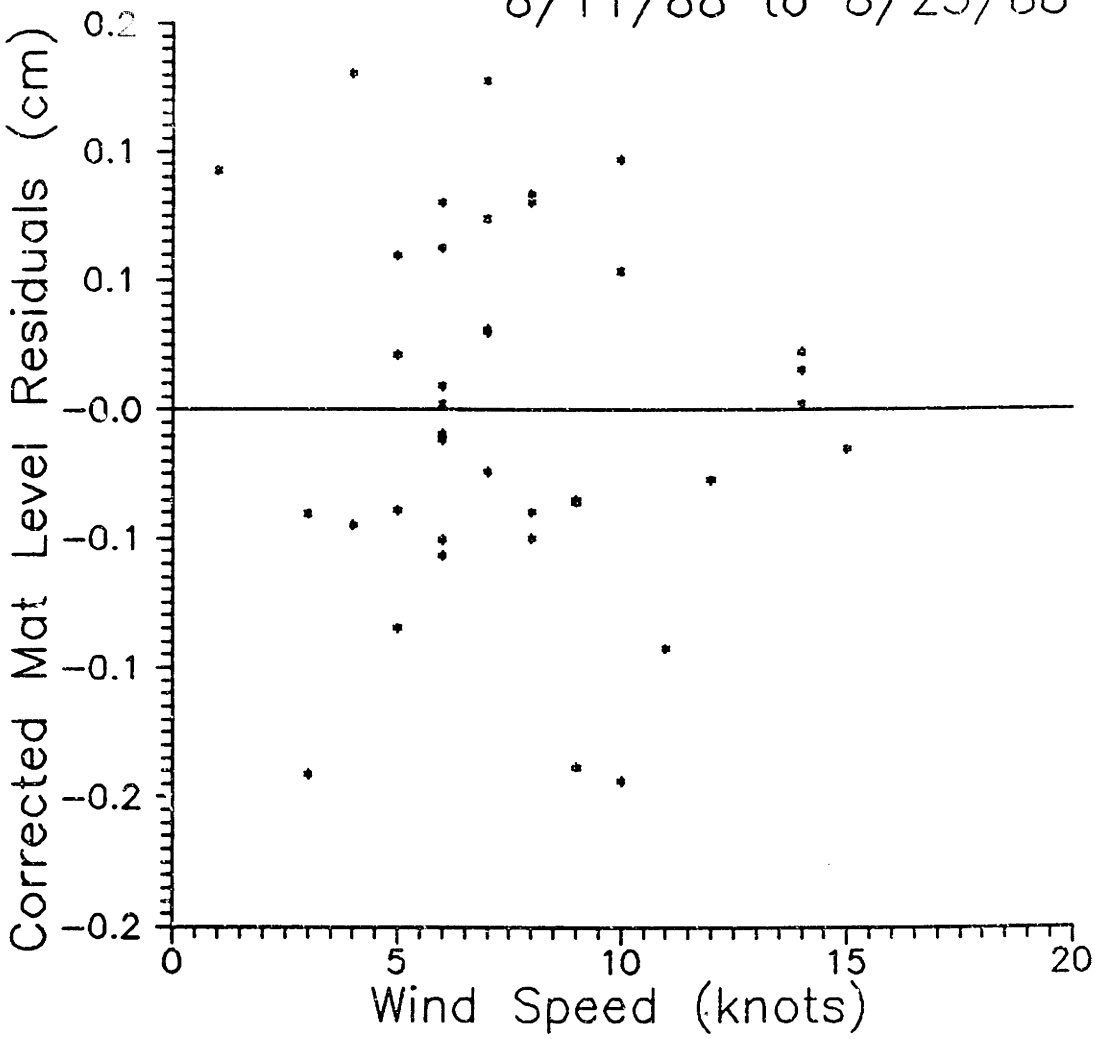

Figure 2–18: Corrected Mat Level Residuals versus Wind Speed, 6/23/89 to 6/29/89

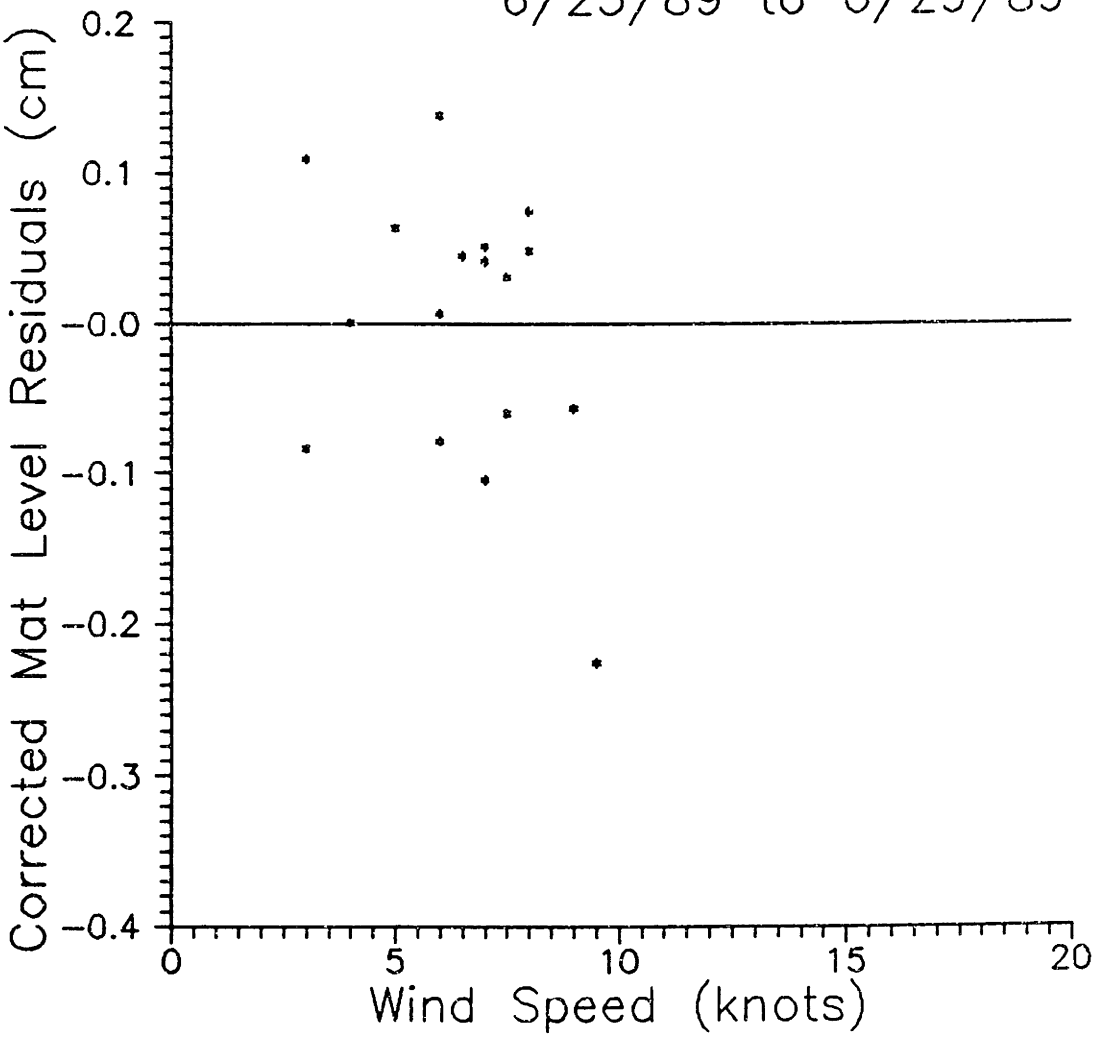

Figure 2–19: Corrected Mat Level Residuals versus Wind Speed, 7/29/89 to 8/7/89

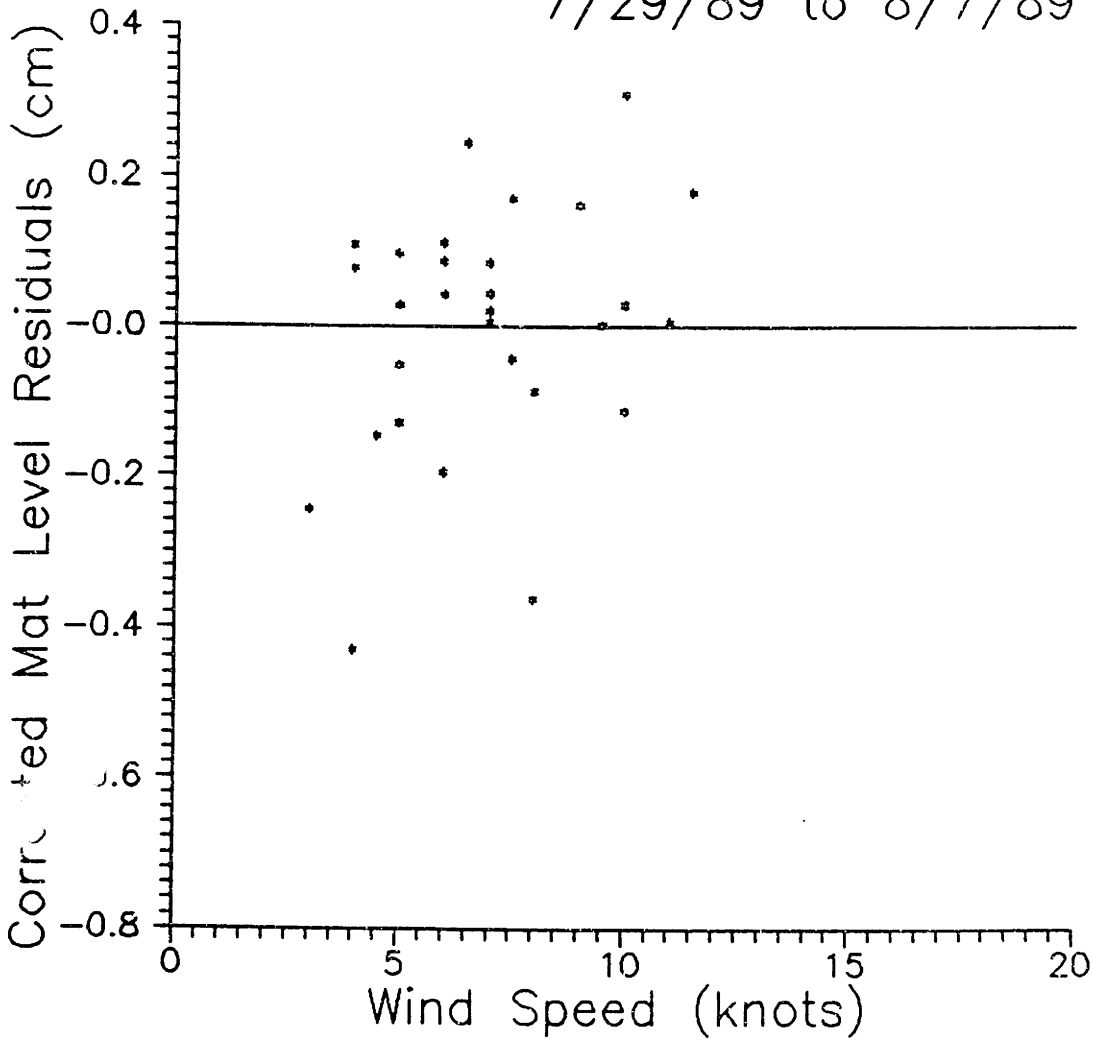

DISCUSSION

There is a statistically significant relationship between the atmospheric pressure and the mat levels corrected for changes in the water level. Consistent with the hypothesis that changes in buoyancy are due to compression or expansion of bubbles entrapped in the mat, at higher pressure, as the mat and water levels fall, the mat falls more than the water. At lower pressures, the gas bubbles in the peat expand, increasing the buoyancy of the mat, and therefore the mat falls less than the water. It should be noted that as the bubbles are alternately compressed and expanded, gases leave or enter the bubble phase according to equilibrium partitioning with porewater concentrations.

As shown in Figures 2-8 through 2-11, the range of corrected mat levels is not more than 1 cm, i.e., the fluctuation in mat level above or below the water table is not more than 1 cm. Because of the similarity in the porosity values measured near the water table in the peat cores taken from different locations in the bog, we are assuming that there are similar porosity conditions at the mat buoyancy recorder. The porosity estimate, in conjunction with the relationship between corrected mat levels and pressure, allows an estimate of bubble volume in the mat to be calculated from the following equations:

$$\Delta F_B = -g\rho_w A\Delta z(1 - n) \qquad (2\text{-}2)$$

$$\Delta F_B = g\rho_w A \Delta V_{bubble} \tag{2-3}$$

where ΔV_{bubble} = change of volume of bubbles present in the peat. Here we are making the assumption that changes in buoyancy due to changes in peat volume are negligible.

Using the ideal gas law, PV = nRT, and differentiating with respect to bubble pressure,

$$\frac{dV_{bubble}}{dP_{bubble}} = \frac{-n_{bubble}RT}{P^2_{bubble}} \tag{2-4}$$

Using a discrete form of the equation,

$$\Delta V_{bubble} = \frac{-n_{bubble}RT}{P^2_{bubble}} \Delta P_{bubble} \tag{2-5}$$

For any given water depth, changes in the pressure of the bubble will be due to changes in the atmospheric pressure, hence $\Delta P_{bubble} = \Delta P_{atm}$. Using a representative depth of 1 m (where hydrostatic pressure is approximately 0.1 atm) and an average atmospheric pressure of 1 atm, $P^2_{bubble} \approx 1.2$ atm^2.

Equating equations 2-2, 2-3, and 2-5, and simplifying:

$$\frac{\Delta z(1 - n)(1.2\ atm^2)}{RT\Delta P_{atm}} = n_{bubble} \qquad (2\text{-}6)$$

Using n = 0.26 from the peat core experiments and an average temperature of 11°C at 1 m depth:

$$\frac{\Delta z}{\Delta P_{atm}} \times \frac{3.8 \times 10^{-2}\ mol \cdot atm}{L} = n_{bubble} \qquad (2\text{-}7)$$

For each of the four time periods, there is a different relationship between change in corrected mat level and change in pressure. Table 2-1, below, has a summary of these calculations.

Table 2-1: Bubble Volume Calculations.

DATE	SLOPE (cm/mb)	r^2	% bubbles	DEPTH TO MAT (cm)
6/29-7/6/88	0.020	0.67	8%	55.7 - 58.6
8/11-8/23/88	0.013	0.52	5%	54.4 - 61.0
6/23-6/29/89	0.042	0.81	17.5%	39.5 - 40.5
7/29-8/7/89	0.039	0.75	16%	43.5 - 45.6

For the time period 6/29/88 through 7/6/88, the slope of the regression line is 0.020 cm/mb or 20 cm/atm.

$$\left(\frac{10^4 cm^2}{1m^2}\right)\left(\frac{20cm}{atm}\right)\left(\frac{3.8 \times 10^{-2}\ mole \cdot atm}{L}\right)\left(\frac{1L}{1000\ cm^3}\right) = \frac{7.6\ mol}{m^2} \quad (2\text{-}8)$$

Again, using the ideal gas law, per 1 m^2 of bog,

$$V_{bubble} = \frac{(7.6\ mol)}{(1.1\ atm)}\left(0.08206\frac{L \cdot atm}{mol\ K}\right)(284\ K) = \frac{161\ L}{m^2} \quad (2\text{-}9)$$

For an approximate mat thickness of 2 m, this corresponds to bubbles filling 8% of the peat mat volume. As shown in Table 2-1, for the periods studied, this percentage ranges from 5% to 17.5%.

The residuals from the four time periods were plotted versus changes in pressure and versus wind speed to determine if such meteorological changes triggered bubble release, but no significant trend was found. The scatter around each of the four regression lines, however, indicates that there are other forces besides atmospheric pressure regulating the release of bubbles. Such forces could include site-specific wind events, changes in temperature, physical disturbance by wildlife, or fluctuations in CH_4 production.

REFERENCES

Army, T.P. 1987. Production and transport of biogenic volatiles from a freshwater, floating-mat bog. Ph.D. Thesis, Massachusetts Institute of Technology, 325 pp.

Bartlett, K.B., P.M. Crill, D.I. Sebacher, R.C. Harriss, J.O. Wilson, and J.M. Melack. 1988. Methane flux from the Central Amazonian floodplain. Journal of Geophysical Research, 93(D2): 1571-1582.

Chanton, J.P. and C.S. Martens. 1988. Seasonal variations in ebullitive flux and carbon isotopic composition of methane in a tidal freshwater estuary. Global Biogeochemical Cycles, 2(3): 289-298.

Devol, A.H., J.E. Richey, W.A. Clark, S.L. King, and L.A. Martinelli. 1988. Methane emissions to the troposphere from the Amazon floodplain. Journal of Geophysical Research, 93(D2): 1583-1592.

Martens, C.S., G.W. Kipphut, and J. Val Klump. 1980. Sediment-water chemical exchange in the coastal zone traced by *in situ* radon-222 flux measurements. Science, 208: 285-288.

CHAPTER 3

The Unsaturated Zone

INTRODUCTION

Northern peatlands are a major source of atmospheric methane (CH_4), contributing about 25% (as much as 60% by some estimates) of the global flux to the atmosphere (Wahlen et al., 1989; Matthews and Fung, 1987; Harriss et al., 1985; Crill et al., 1988). Numerous direct measurements of fluxes of CH_4 out of peatlands have been made using flux chamber methods (see Table 3-1). While the data have established the importance of the peatland source, they typically exhibit great variability, perhaps due to spatial heterogeneity, seasonality of CH_4 production resulting from fluctuations in temperature and hydrology, and/or disturbance to the CH_4 release process by the measurement technique. Projections of future CH_4 fluxes under altered climatic conditions are difficult to make based on efflux data alone, since gas releases involve the interaction of several chemical, physical, and biological processes (e.g., microbial production, reoxidation, diffusion, and ebullition). Understanding the interactions of these processes as they control methane release is essential to allow forecasting of methane evolution rates from northern peatlands under future conditions of temperature and moisture.

One potential control of methane release to the atmosphere is CH_4 oxidation (Coleman et al. 1981; Cicerone and Oremland, 1988; Chanton et al., 1989). Reoxidation occurs when methane, produced anaerobically, reaches near-surface sediment where favored electron acceptors such as oxygen are present. This is most likely to occur in the unsaturated, aerated zone of peatlands

Table 3-1: Methane Fluxes from Northern Peatlands, Measured Using Flux Chambers.

CH_4 FLUX	LOCATION	REFERENCE
4.33 ± 0.8 mol/m^2·yr	Alaska coastal tundra	Sebacher et al., 1986
0.07 ± 0.07	Alaska coastal tundra	Sebacher et al., 1986
1.77 ± 0.32	Alaska coastal tundra	Sebacher et al., 1986
0.41 - 19.76	Minnesota open bog	Crill et al.,1988
0.75 - 10.68	Minnesota peatland	Harriss et al., 1985

(part of the acrotelm, the upper layer of less humified peat) and/or in the uppermost layers of water-saturated peat. Previous studies in a Danish wetland and an Appalachian Mountain peatland have suggested that reoxidation can diminish the atmospheric flux of methane by greater than 90% (King, 1990; Yavitt et al., 1988). Clear trends of decreased CH_4 efflux with lowered water tables have been reported by Sebacher et al. (1986) and Harriss et al. (1982).

It is not clear whether reoxidation is more important in the uppermost water-saturated sediment or in the unsaturated sediment. In Sphagnum peatlands, the porosity of peat typically increases dramatically in the several centimeters near the surface; this tends to decrease the residence time of methane and therefore may limit reoxidation rates in this zone. A few centimeters deeper in the unsaturated peat profile, lower porosity will tend to increase the residence time of CH_4 due to greater resistance to transport. In saturated sediment, oxygen availability decreases rapidly with depth, thus restricting the depth to which methane oxidation using oxygen as the electron acceptor can occur. But with lower diffusion coefficients in water, methane residence times in saturated sediment will be much longer than in unsaturated sediment (unless methane passes this peat layer by ebullition). Understanding the roles of the unsaturated zone and the upper, oxygenated layer of the saturated zone is essential to understanding the overall process of methane emission.

This chapter describes a study of the dynamics of CH_4 in the unsaturated zone of a sphagnum peatland. This zone is a final barrier to CH_4 escape (even if bubbling dominates in the saturated zone), and profiles of CH_4 in this zone convey

information on both rates of vertical CH_4 transport and rates of CH_4 reoxidation in unsaturated peat. Moreover, since CH_4 profiles can be obtained with little site disturbance, their analysis results in net atmospheric CH_4 flux measurements which seem unlikely to be affected by bubble release triggered by disturbance or by alteration of boundary conditions. Effective diffusion coefficients for the unsaturated zone are based on peat porosity measurements and results of the propane tracer test. In conjunction with the CH_4 profiles, they allow actual CH_4 fluxes to the atmosphere to be calculated.

MATERIALS AND METHODS

Site

Thoreau's Bog, located in Concord, Massachusetts, is a Sphagnum bog typical of northern peatlands with respect to vegetation (Hemond, 1980) and porewater chemistry (Gorham et al., 1985; Hemond, 1980). The vegetation is dominated by Sphagnum spp. and ericaceous shrubs; the porewater is acidic and chemically dominated by humic substances. All peatlands are supported in part by the buoyancy of the organic sediment with its associated gas-filled voids; at Thoreau's Bog much of the sediment is fully supported by buoyancy, making it a classical floating-mat bog. The water table typically lies 12-15 cm below the surface of the Sphagnum moss.

CH_4 Profiles

In order to obtain profiles of CH_4 concentrations in the unsaturated zone (approximately the upper 15 cm of sediment), gas samples from the unsaturated zone were taken in wetted glass Popper (R) syringes fitted with 3-way Luer lok(R) valves. A 3 mm O.D. stainless steel hypodermic needle, with 10 closely spaced holes drilled in the bottom and the end crimped shut, was fitted to the valve. The needle and valve were flushed with approximately 5 ml of gas at the desired sampling depth, and then a 10 ml gas sample was obtained. The depth interval from which gas was drawn at each sampling point was therefore about 3 cm, depending on porosity. The unsaturated zone was sampled at 3 cm depth intervals, from the surface to the water table. Syringes were held by an observer located on a fixed platform, constructed of open mesh expanded metal on a rigid frame supported by PVC-encased iron pipes sunk into the mineral soil beneath the bog. Compression of the bog surface by the presence of the observer was thereby eliminated, allowing undisturbed profiles of methane in peat near the platform to be obtained.

Wide areal coverage of the bog surface was achieved by holding the syringes vertically by a clamp at the end of a 1.8 meter long stainless steel rod. A second clamp was used to compress a spring between the plunger and the barrel of the syringe. When the sampling holes in the needle were positioned at the desired depth in the peat, the second clamp was pulled off remotely by a string, thereby releasing the spring and causing a gas sample to be pulled into the syringe. The volume of air present in the needle and valve before sampling was

accounted for during sample analysis. The background CH_4 concentration in that volume was measured by taking air samples above the bog surface. At two stations, after the unsaturated zone was sampled remotely, the observer approached the sampling station on foot and sampled directly by hand, providing a disturbed-site comparison.

The gas samples were analyzed using a Perkin-Elmer gas chromatograph with a flame ionization detector (Model 3920 B) and a 1.8 m by 0.2 cm I.D. glass column containing Super Q, coupled to a Hewlett Packard Integrator (Model HP3394A). Standards were made from a 525 ppm methane in helium standard, Certified Master Gas, Scott Specialty Gases. Error of reproducibility associated with the standards, which were analyzed before, during, and after the samples, was usually less than 1%.

Peat Porosity

Air-filled porosity as a function of depth was determined for four 12.7 cm diameter peat cores. The experimental set-up is shown in Figure 3-1. For each porosity measurement, water was added to the tank to a given level, and the core was allowed to equilibrate so that the water level in the core was the same as the water level in the tank. The weight of the peat core at that water level was recorded; the water level was then lowered, the core allowed to re-equilibrate, and a new weight recorded. It was assumed that any changes in the weight of water held above the water table by capillary forces were small compared to changes in the buoyant force.

Figure 3-1: Peat Porosity Experiment

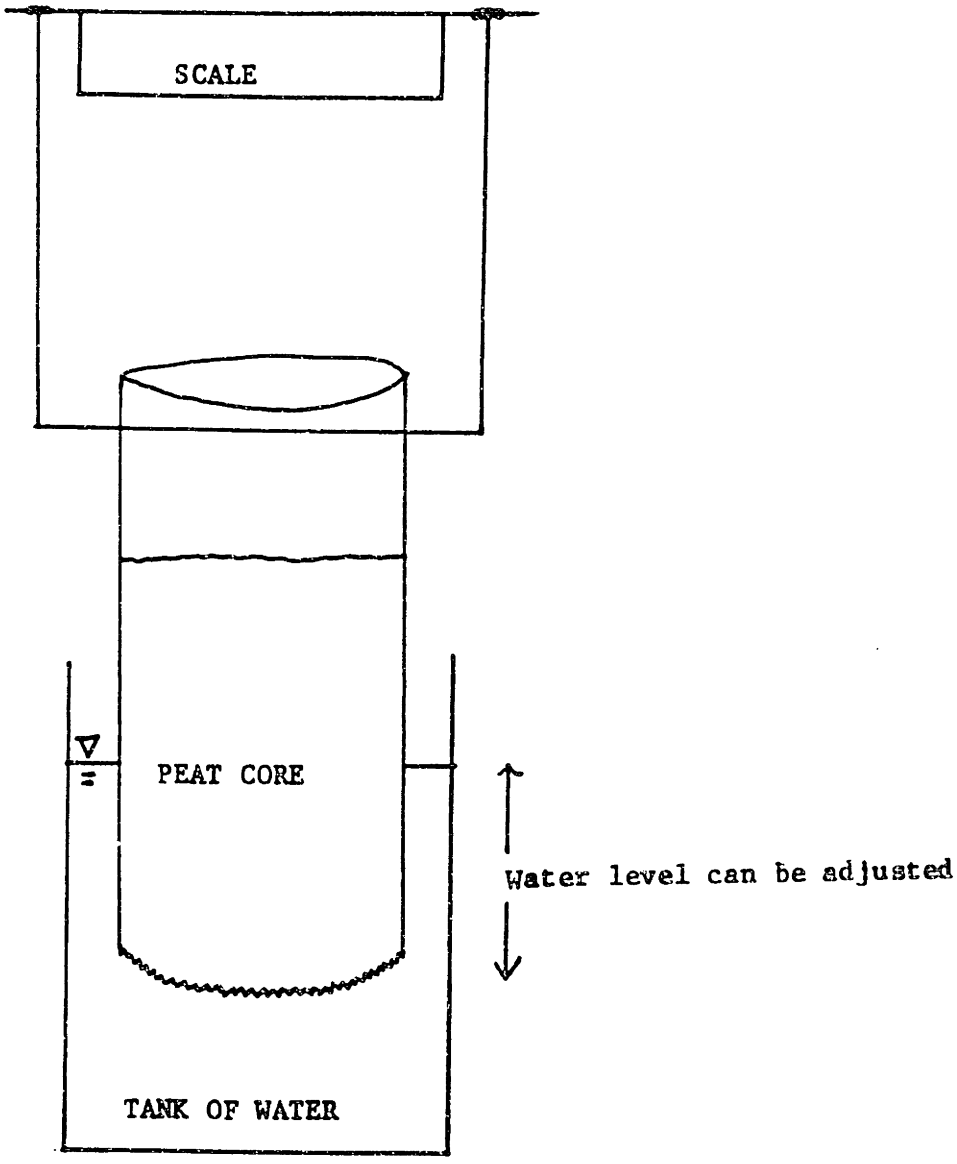

By using the changes in the buoyant force (as measured by the scale) and the changes in the water level in the tank, the air-filled porosity, n, was calculated for each depth increment using the following relationship:

$$n = 1 - \frac{\Delta F_B}{\Delta z \, g \cdot A \cdot \rho_w} \qquad (3\text{-}1)$$

where:

F_B = buoyant force $[M \cdot L]/T^2$

z = depth of core submerged [L]

A = cross sectional area of core $[L^2]$

ρ_w = density of water at temperature of measurement $[M/L^3]$

g = acceleration due to gravity $[L/T^2]$

n = air-filled porosity

Propane Tracer Test

A tracer experiment using propane gas (C_3H_8) was conducted as an alternative means to estimate effective diffusion coefficients in the peat. The experiment was set up in an undisturbed peat site which could be sampled by an observer located on the fixed platform. In order to approximate a plane source of C_3H_8, 33 cm lengths of Silastic(R) (dimethyl silicone) tubing, which is highly permeable to C_3H_8, were laid approximately 5 cm apart and approximately 1 cm above the water table in an area of peat 33 cm by 20 cm. The tubing has a 2 mm O.D. and 0.24 mm thick walls. The tubing was emplaced by threading a $^1/_4$" O.D.

stainless steel tube through the peat directly above the water table, and then pulling the Silastic(R) tubing through the stainless steel tubing, which was subsequently removed. The lengths of the tubing were connected in series with short lengths of $^1/_{16}$" O.D. stainless steel tubing. A 1 L propane cylinder with a regulator and flow valve was connected to one end of the Silastic(R) tubing; C_3H_8 flowed through the tubing at an entrance pressure of approximately 10 kPa and the C_3H_8 was flared at the other end of the tubing. Maintaining a flame throughout the experiment insured that C_3H_8 flow through the tubing was continuous, and prevented C_3H_8 from dispersing back over the site, thereby modifying the concentration gradient.

Gas samples were taken an hour after the C_3H_8 began flowing through the tubing, at 2.4 cm depth intervals. It was determined experimentally in the field, and theoretically, that an hour was sufficient time to establish steady state conditions. Samples were taken in glass Popper(R) syringes fitted with 3-way Luer Lok(R) valves attached to the previously described 3 mm O.D. stainless steel hypodermic needle. The needle and valve were flushed with approximately 1 ml of gas at the desired sampling depth, and then a 5 ml gas sample was obtained. The depth interval from which gas was drawn at each sampling point was therefore about 2.3 cm, depending on porosity. The gas samples were analyzed for both methane and propane using a Perkin-Elmer gas chromatograph, as previously described. Propane standards were made using the same cylinder of propane used in the field experiment.

Laboratory experiments were conducted to establish the flux of C_3H_8 out of

the tubing into a sealed, air-filled vessel under 2 different temperatures and 2 different moisture regimes. The experiment was run at 9.7°C under dry gas conditions and at 19°C under dry and water vapor saturated gas conditions. The C_3H_8 flux out of the Silastic(R) tubing was not significantly different under any of the conditions.

RESULTS

Methane profiles obtained in the unsaturated zone are shown in Figures 3-2 through 3-8. Methane concentration is expressed as a partial pressure in atmospheres; depth in centimeters refers to the distance below the top of the Sphagnum moss.

Figures 3-2 and 3-3 show methane profiles at stations UZ-P1 through UZ-P5 and UZ-P7 through UZ-P13; these profiles were obtained by a worker sitting on the fixed platform on three days, July 13, July 30, and August 2, 1990. The CH_4 concentration for each 3 cm depth sampling interval is plotted at the middle of the interval. At stations UZ-P7 and UZ-P8, duplicates were taken; the error bars are shown on the figure. When the water table lies below the 12 - 15 cm sampling interval, there tends to be an approximately one order of magnitude range in methane concentrations below the 6 - 9 cm sampling interval (plotted at 7.5 cm). When the water table lies at a shallower depth, the approximately one order of magnitude range in methane concentrations occurs beneath the 3 - 6 cm depth interval (plotted at 4.5 cm). The greatest spatial heterogeneity is found

Figure 3-2: Unsaturated Zone Profiles Taken from Platform

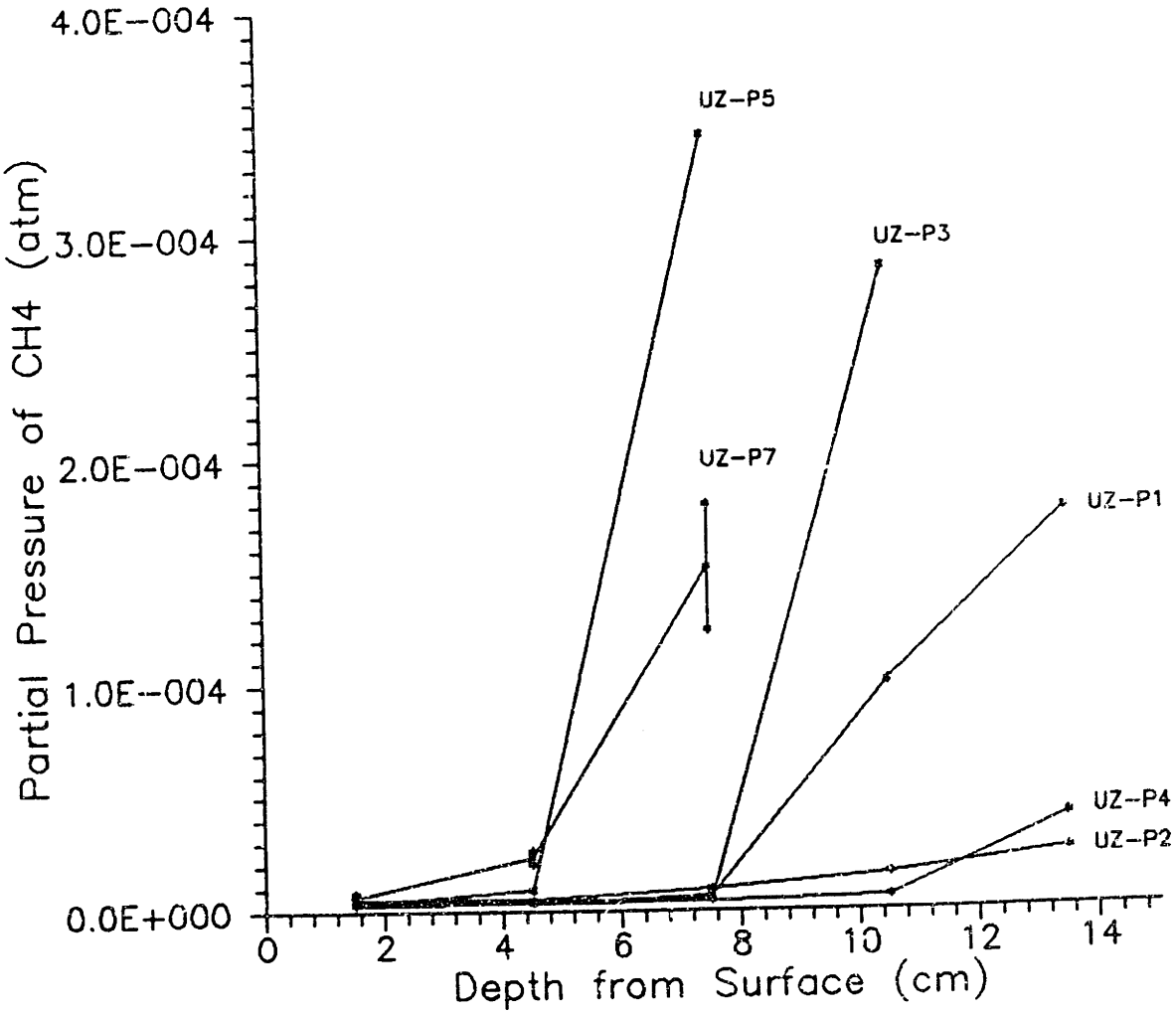

Figure 3-3: Unsaturated Zone Profiles Taken from Platform

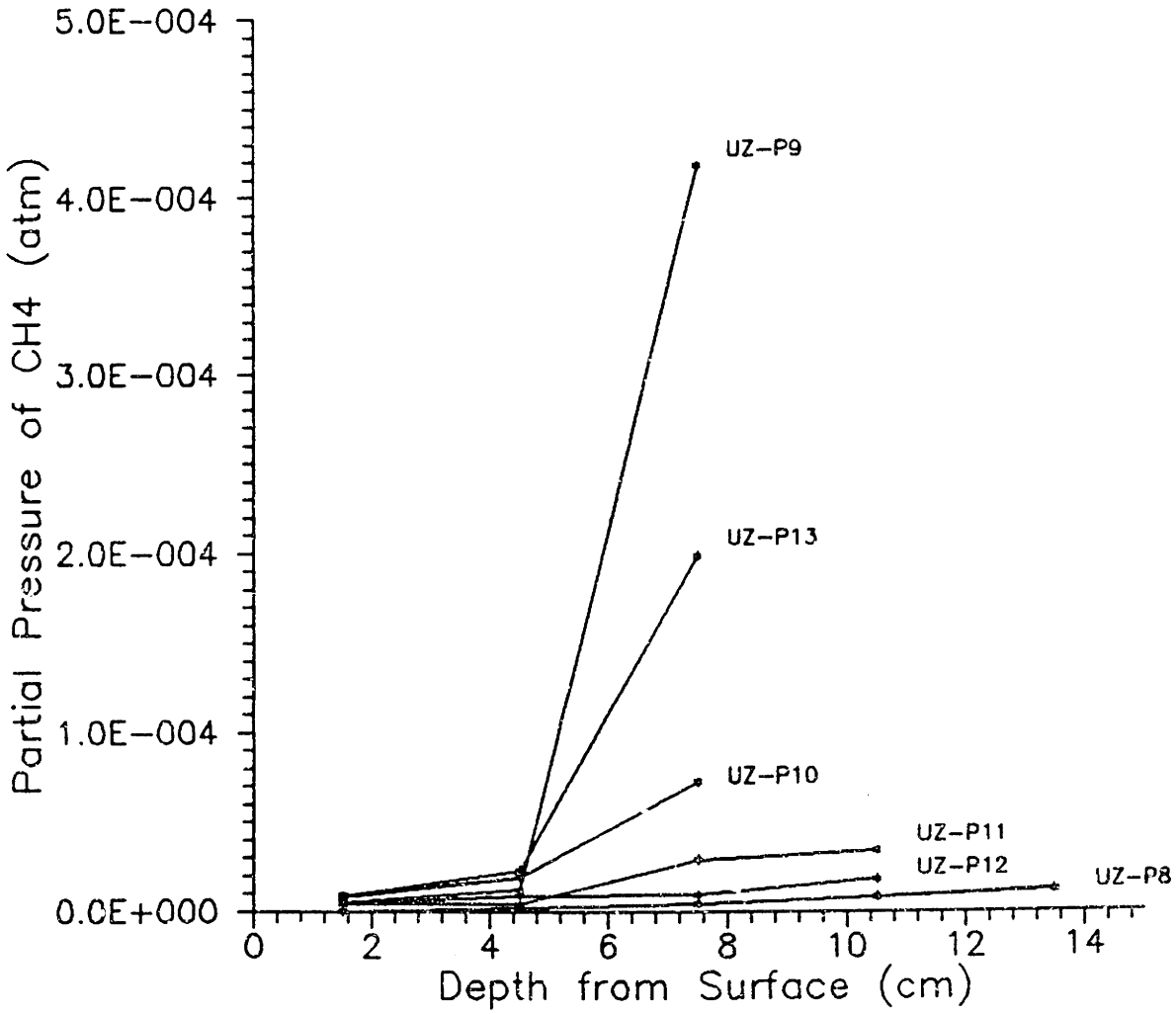

Figure 3-4: Unsaturated Zone Profiles Taken Remotely

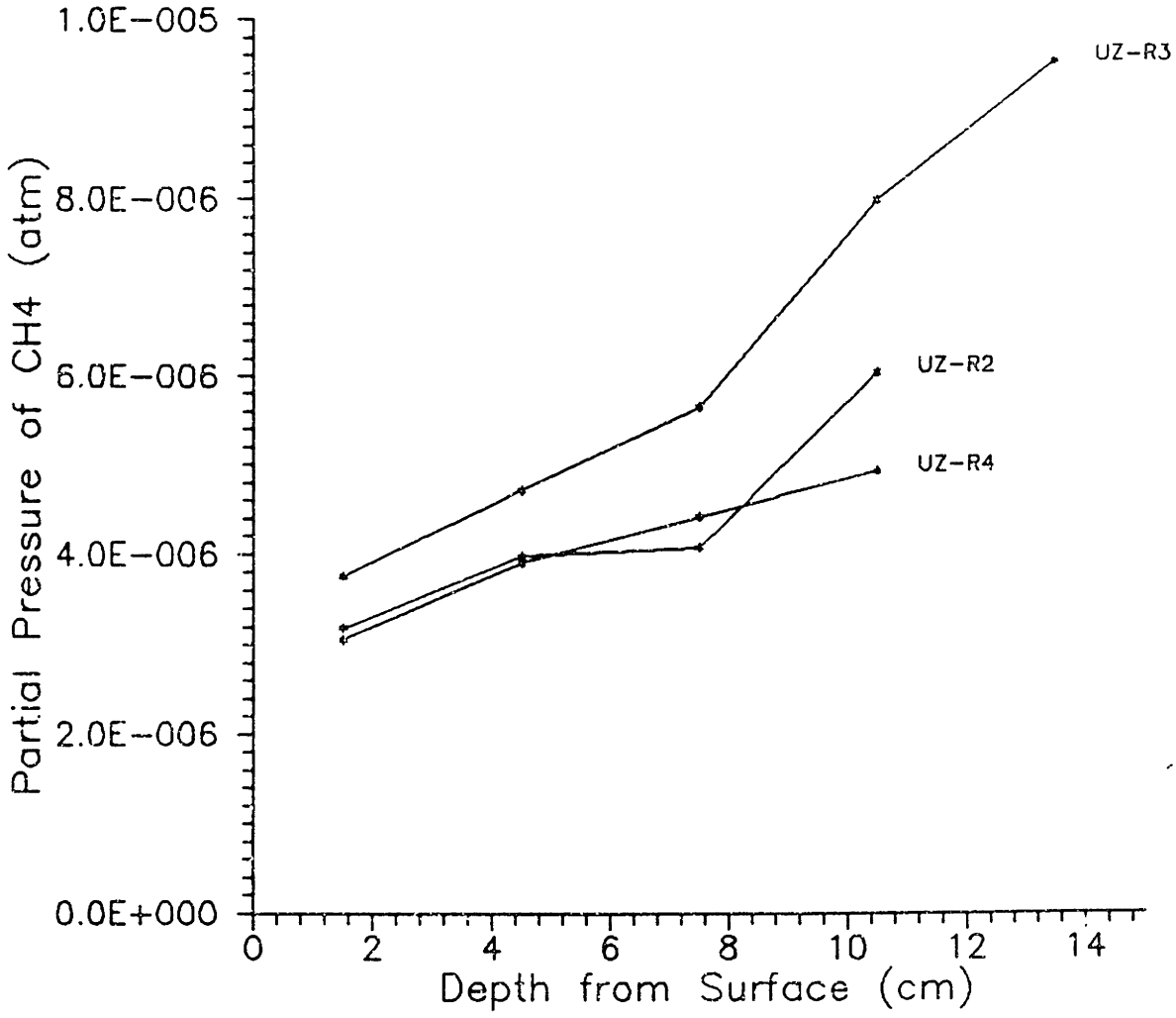

Figure 3–5: Undisturbed and Disturbed Unsaturated Zone Profiles

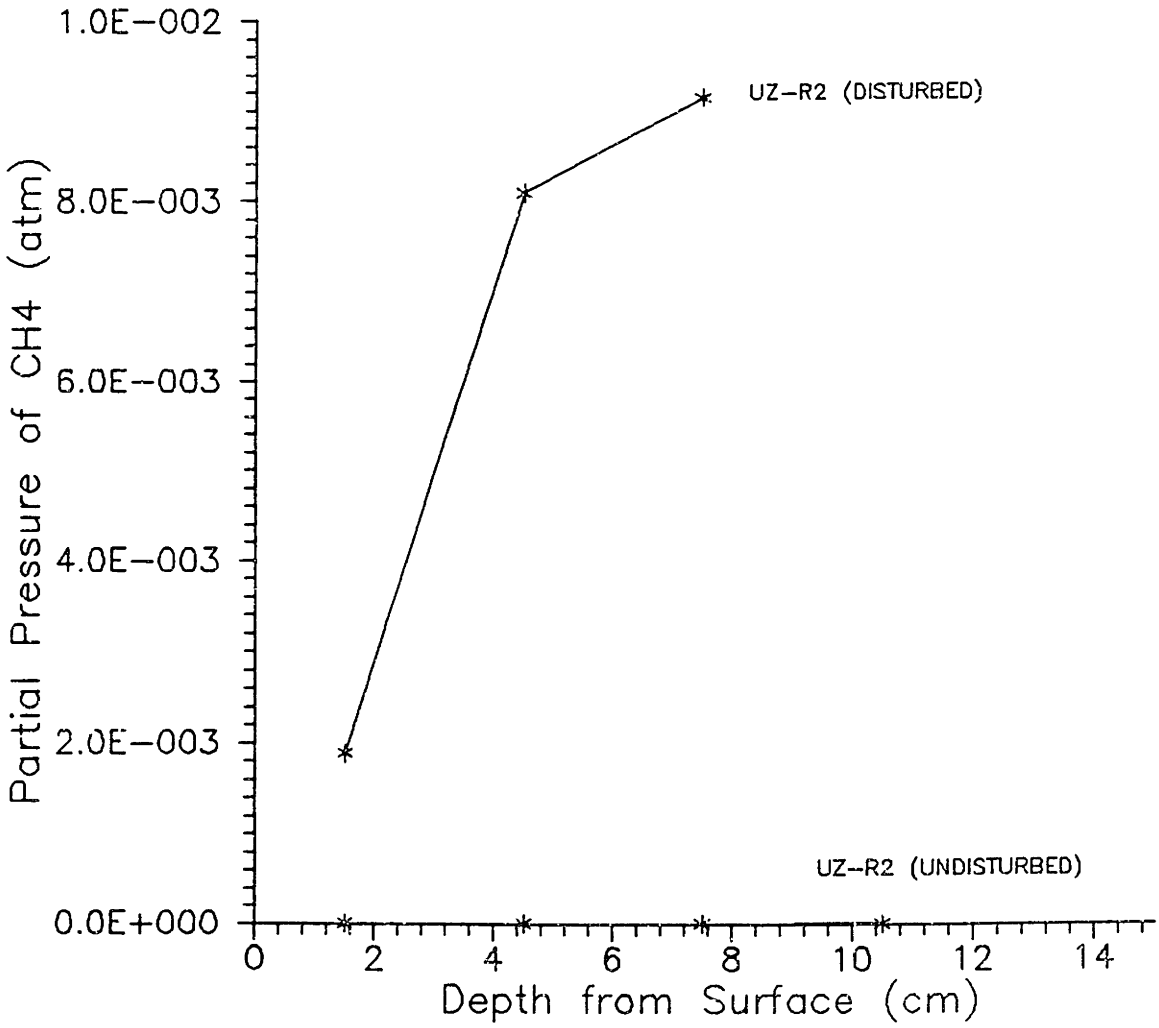

Figure 3-6: Unsaturated Zone Profiles Taken Remotely

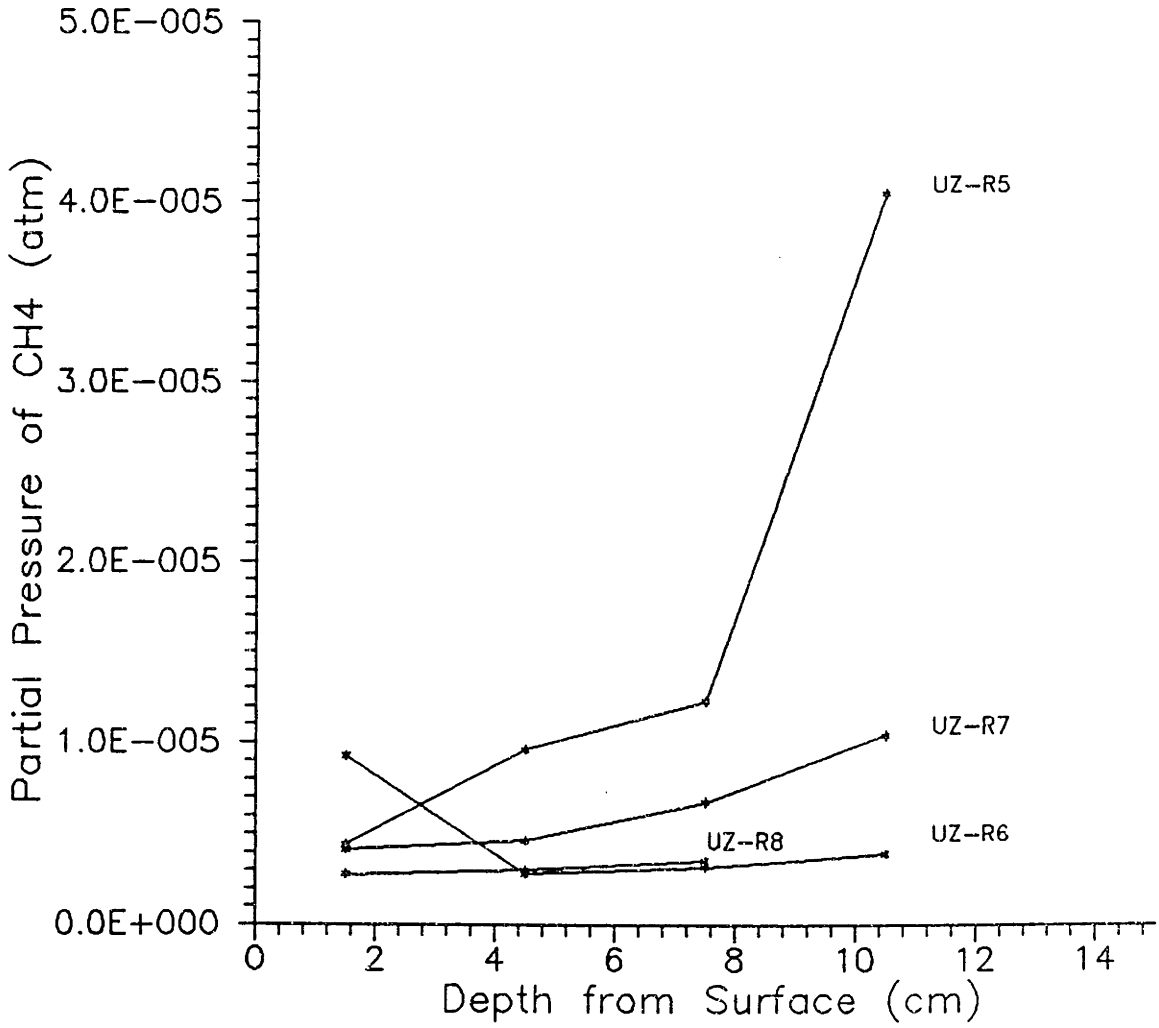

Figure 3-7: Unsaturated Zone Profiles Taken Remotely and from Platform

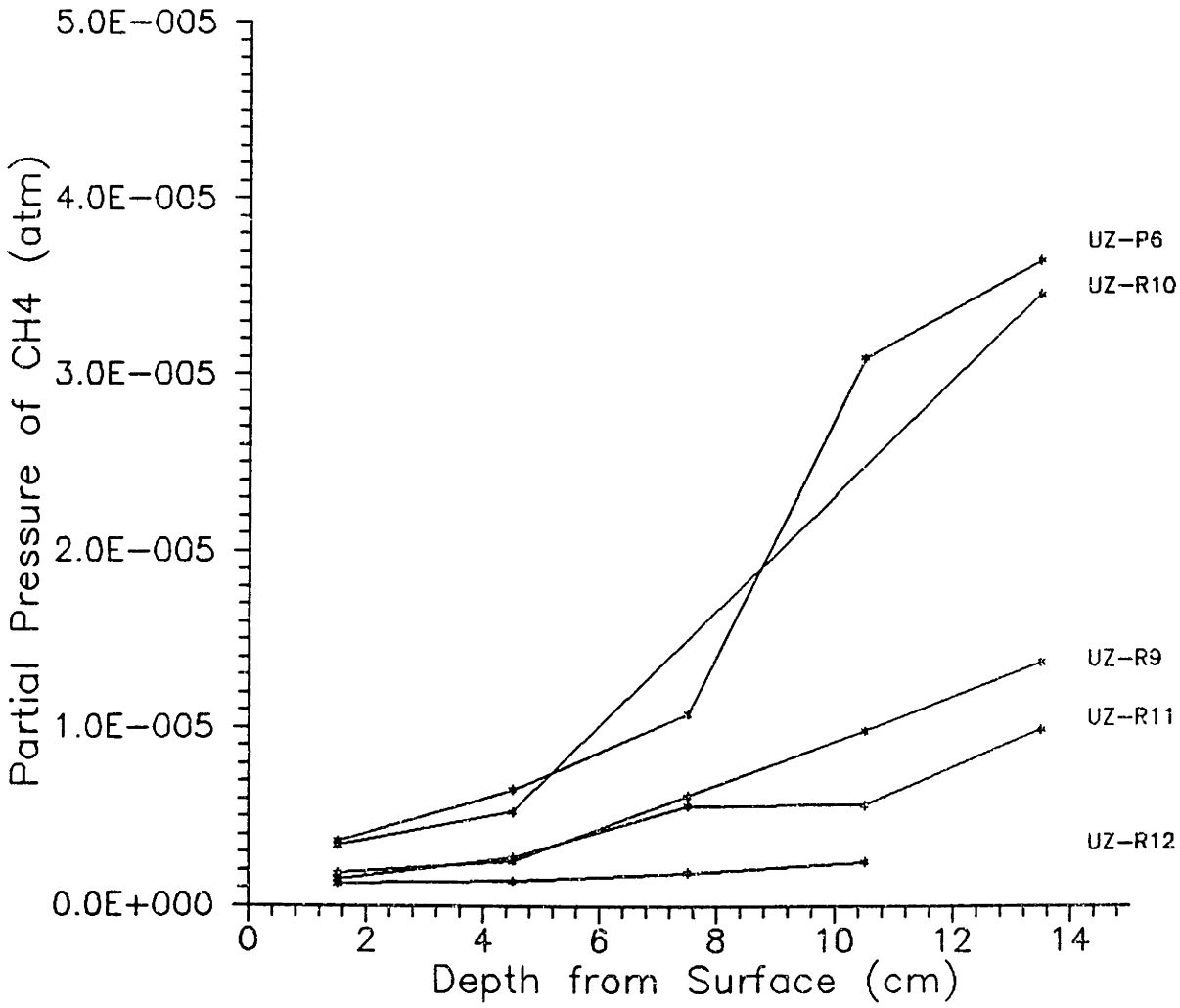

Figure 3-8: Unsaturated Zone Profiles Taken Remotely

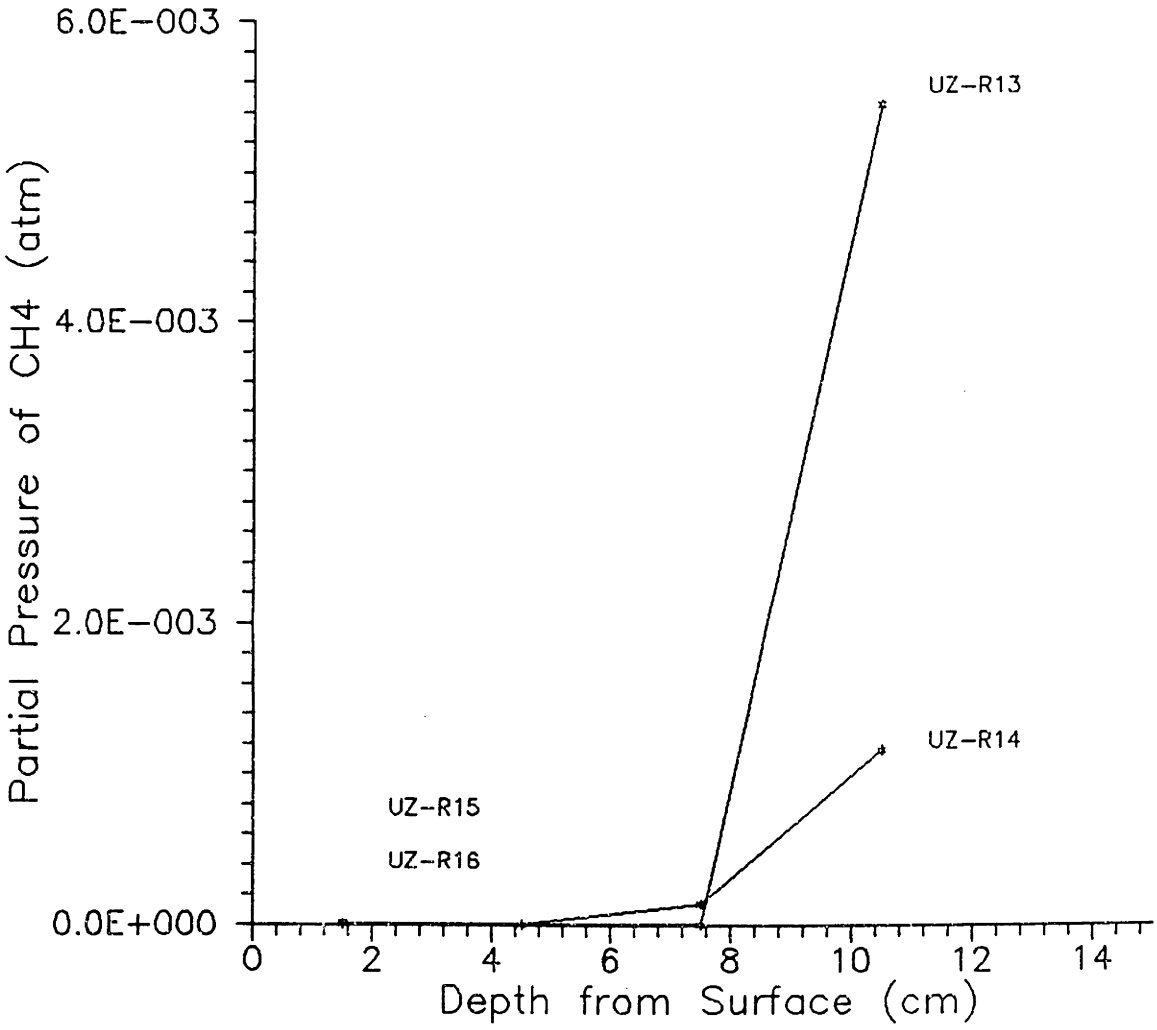

closest to the water table.

Figure 3-4 shows profiles obtained using the 1.8 m remote sampling rod at stations UZ-R1 through UZ-R4 in the bog on August 9, 1990. These profiles were taken at sites spanning a transect approximately 20 m long. Two of the profiles show a sharp increase in methane concentration below the 6-9 cm sampling range. When the stations UZ-R2 and UZ-R4 were approached on foot and sampled by hand, the profile of station UZ-R2 showed approximately a thousand-fold increase in methane concentrations at all depths, whereas the profile of station UZ-R4 showed only a 2-fold increase in methane concentrations. The thousand-fold increase at station UZ-R2 is shown in Figure 3-5.

Figure 3-6 shows four profiles obtained using the remote sampling rod on August 15, 1990. Two of the four profiles (UZ-R5 and UZ-R7) show the sharp increase in methane concentration below the 6-9 cm sampling interval, as before.

Figure 3-7 shows five profiles obtained August 23, 1990. One profile (UZ-P6) was obtained by hand from the rigid platform, one by operating the remote sampling rod from the platform (UZ-R9), and the other three by using the remote sampling rod in a rectangular area approximately 9 meters by 4 meters in the vicinity of the rigid platform. Profiles from stations UZ-P6 and UZ-R10 show the sharp increase in concentration below the 6-9 cm interval, as before. Profiles from the other three stations have lower CH_4 concentrations at depth and are all fairly linear.

Figure 3-8 shows four profiles obtained on September 7, 1990 using the remote sampling rod. The stations spanned a transect approximately 8 m long.

The profiles of stations UZ-R13, UZ-R14, and UZ-R15 show the sharp increase in CH_4 concentration below the 6 - 9 cm interval.

Several flux box measurements were made at two permanently-installed chambers located near the fixed platform, chamber P and chamber OP. The chambers are located approximately 1.2 m apart. On July 13, 1990, a CH_4 flux of 1.7×10^{-12} mol·cm^{-2}·s^{-1} was measured at chamber P and a CH_4 flux of 7.5×10^{-12} mol·cm^{-2}·s^{-1} was measured at chamber OP. Both measurements were made by an observer located on the fixed platform. On August 7, 1990 a CH_4 flux of 1.6×10^{-11} mol·cm^{-2}·s^{-1} was measured at chamber P -- an order of magnitude higher than on July 13 -- whereas at chamber OP the flux remained about the same, at 3.5×10^{-12} mol·cm^{-2}·s^{-1}. Chamber OP was then approached on foot and a CH_4 flux of 1.6×10^{-10} mol·cm^{-2}·s^{-1} was measured, two orders of magnitude greater than the undisturbed measurement (see Figure 3-9).

Data from the peat core buoyancy experiments indicate that from the surface of the peat down to approximately 5.5 cm (in the region of live moss), porosity values range from 0.4 to 0.7. Because peat compression during sampling is most difficult to avoid in the upper, loose layer of live moss, this range of porosity is considered a minimum value. Below 5.5 cm porosity ranges from 0.1 to 0.4, and is typically about 0.2.

The results of the propane tracer tests are shown in Figures 3-10. Five C_3H_8 profiles were taken on two days, October 11, 1990 and November 16, 1990. The propane partial pressures at each depth were averaged and two concentration gradients were calculated based on the sharpest change in slope on

Figure 3-9: Flux Box Experiment, Disturbed Sampling after 30 min.

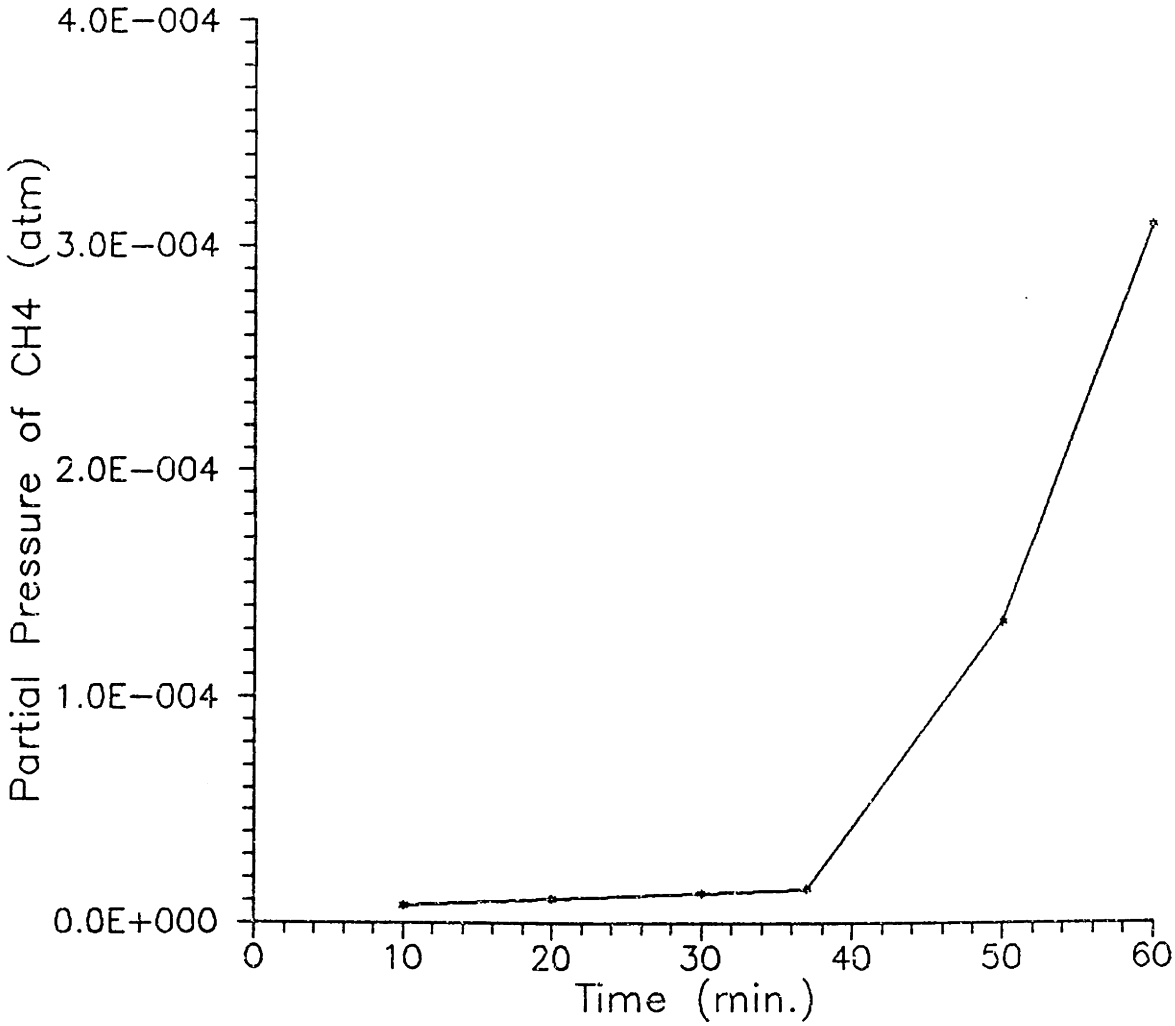

Figure 3–10: Propane Tracer Tests, 10/11/90 and 11/16/90

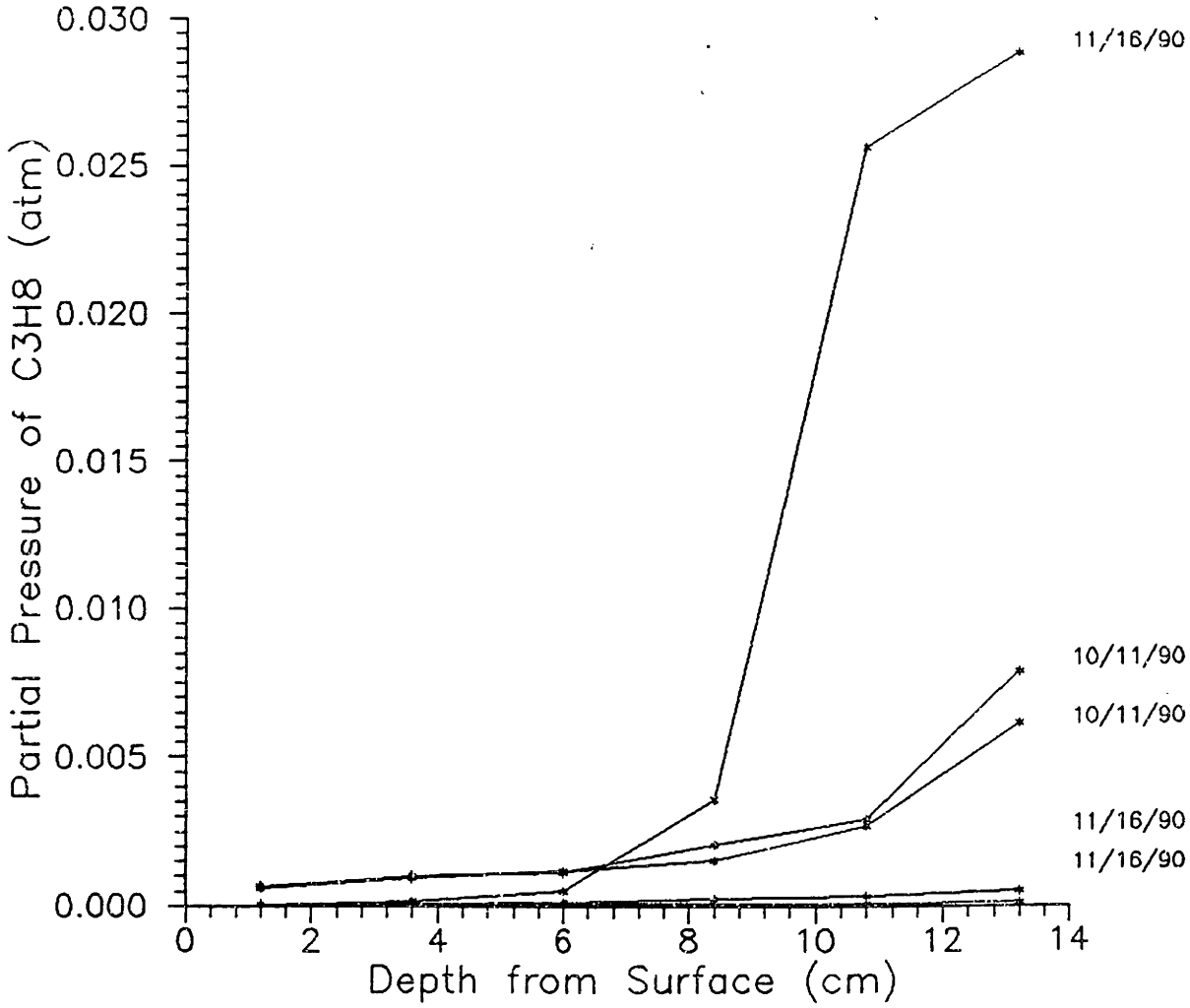

the graph, which occurred at approximately an 8.4 cm depth. Laboratory experiments indicated the flux of C_3H_8 out of the silastic tubing into air to be 3.2 x 10^{-8} mol·s^{-1} per cm length of tubing, or 7.3 x 10^{-9} mol·cm^{-2}·s^{-1} in the field plot area.

Seven CH_4 profiles taken in the propane tracer test plot on October 25, November 1, and November 16, 1990 are shown in Figure 3-11. These seven profiles were obtained before propane began flowing through the silastic tubing for the tracer test. It is interesting to note that on this scale, temporal variability is greater than spatial variability; the differences in CH_4 partial pressures are greater from day to day than from location to location on any given day. These profiles can also be compared to profiles at stations UZ-P6 and UZ-R9, taken on August 23, 1990 and shown in Figure 3-7. These stations are located near the propane tracer test plot and have CH_4 concentrations approximately 1 order of magnitude higher than those found in the plot two months later.

DISCUSSION

CH_4 Flux to the Unsaturated Zone

The CH_4 flux estimates below are based on measured CH_4 gradients averaged over all stations sampled in July, August, and September 1990. The estimates are based on two different diffusion coefficients, one derived from the peat core experiments and one derived from the propane tracer test experiments. CH_4 flux estimates from the propane tracer test site in October and November of

Figure 3–11: Methane Profiles from Propane Tracer Tests, 10/25/90, 11/1/90, and 11/16/90

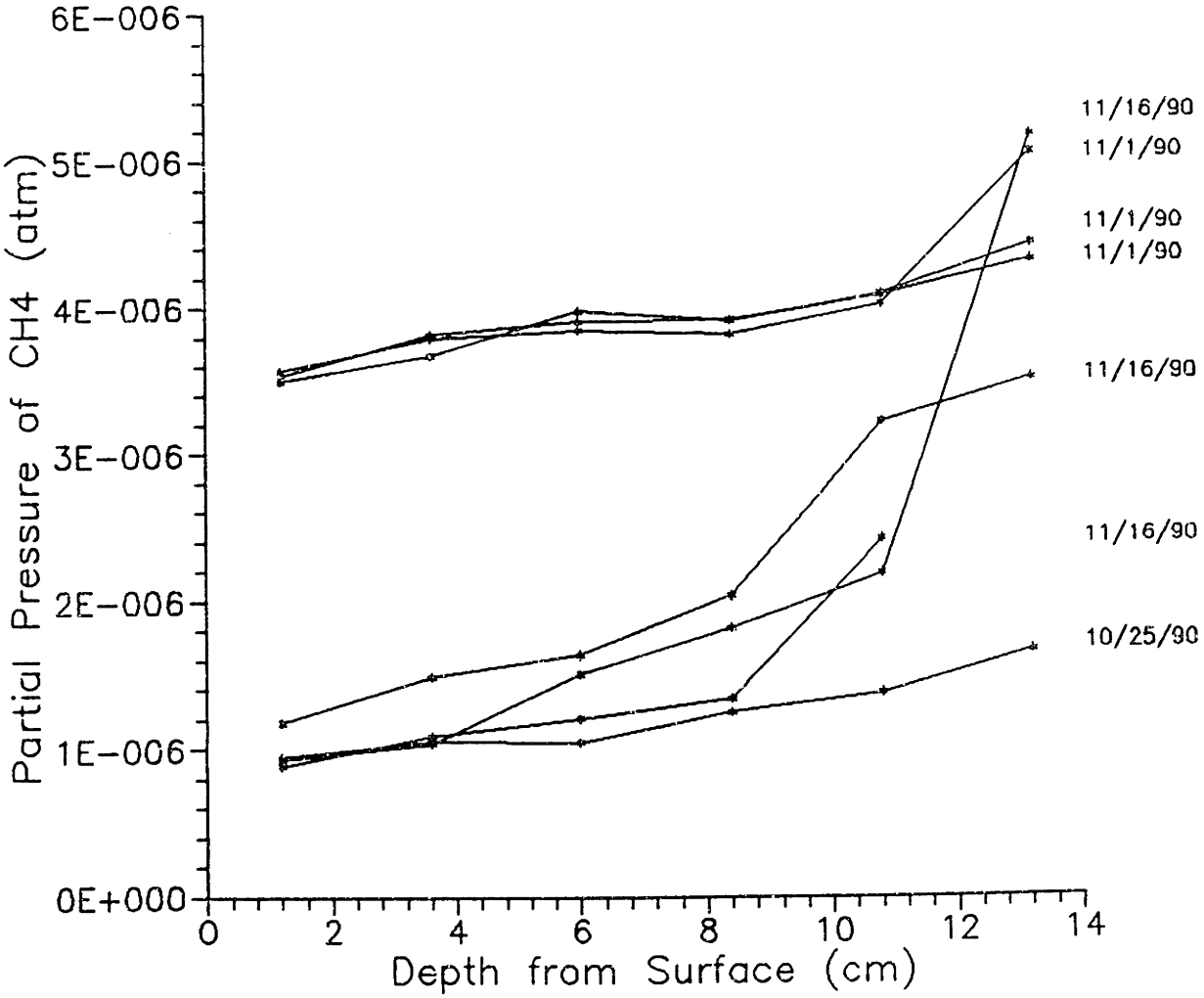

1990 are also made based on the average CH_4 gradient in that plot. See Table 3-2 for a summary of all the flux calculations.

An approximate molecular diffusion coefficient, D, for CH_4 in air is taken as 0.24 $cm^2 \cdot sec^{-1}$ (from value for water vapor at 8°C in Weast, 1988). For the 6 to 12 cm depth interval, measured peat porosity, n, is 0.2, and a tortuosity factor, Ω, of 2 is assumed. The effective molecular diffusion coefficient D^* is then:

$$D^* \approx \frac{Dn}{\Omega} \approx 0.024\ cm^2 \cdot sec^{-1} \qquad (3\text{-}2)$$

The mean CH_4 gradient, dc/dz, for the depth interval 6 to 12 cm is 1.5 x 10^{-5} $atm \cdot cm^{-1}$, or 6.3 x 10^{-10} $mol \cdot cm^{-4}$ (at 15°C). Following Fick's Law, the CH_4 flux, J, at this depth is:

$$J = D^* \, dc/dz \approx 1.5 \times 10^{-11}\ mol \cdot cm^{-2} \cdot s^{-1} \qquad (3\text{-}3)$$

Assuming that the CH_4 efflux occurs at this rate for 6 months of the year, the corresponding annual flux is 2.4 moles $CH_4 \cdot m^{-2} \cdot yr^{-1}$. This value is comparable to a value of ebullition flux in the saturated zone of Thoreau's Bog estimated at 3 $moles \cdot m^{-2} \cdot yr^{-1}$ on the basis of a bubble stripping analysis (Hemond et al., 1987). It is premature to claim, however, that all of the CH_4 produced in the bog necessarily reaches the unsaturated zone; this CH_4 flux value is only approximate, with confidence limits poorly quantified due to a lack of a full year's data.

The maximum C_3H_8 flux out of Silastic(R) tubing into air was measured to

Table 3-2: Methane Fluxes in the Unsaturated Zone.

DEPTH	DATA	D[cm^2/s]	CALCULATED FLUX mol/[m^2-yr]
0 - 6 cm	July, Aug., Sept. 1990	0.17	0.8
6 - 12 cm	July, Aug., Sept. 1990	0.024	2.4
0 - 6 cm	July, Aug., Sept. 1990	0.20	1.0
6 - 12 cm	July, Aug., Sept. 1990	0.023	2.3
0 - 7.2 cm	October, November 1990	0.17	0.01
7.2 - 14.4 cm	October, November 1990	0.024	0.05
0 - 7.2 cm	October, November 1990	0.20	0.01
7.2 - 14.4 cm	October, November 1990	0.023	0.05

be 7.3 x 10^{-9} mol·cm^{-2}·s^{-1}. In the peat, however, much of the tubing is occluded by wet peat, greatly decreasing the C_3H_8 flux in the areas of occlusion. An estimate of the fraction of tubing area not blocked by wet peat is given by the peat porosity. Since the porosity estimate near the water table is about 0.2, the actual flux of C_3H_8 in situ is taken as 1.5 x 10^{-9} mol·cm^{-2}·s^{-1}. Diffusion of C_3H_8 through water and peat surrounding the tubing is considered to be negligible by comparison. Based on this flux and the measured C_3H_8 gradients, an effective molecular diffusion coefficient of 0.023 cm^2·s^{-1} is calculated. Repeating the above calculation, the annual average flux is 2.3 mole CH_4·m^{-2}·yr^{-1}.

The mean CH_4 gradient for the depth interval 7.2 cm to 14.4 cm in the propane tracer test plot is 3.0 $_{\times}$ 10^{-7} atm·cm^{-1} or 1.3 $_{\times}$ 10^{-11} mol·cm^{-4}. Using D^* = 0.024 cm^2·sec^{-1}, the annual CH_4 flux is 0.05 mol·m^{-2}·yr^{-1}. It is expected that the estimated CH_4 flux from the propane tracer test plot is much lower than the previous estimated bog-wide CH_4 flux because these measurements were made in late October and November when temperatures at depth, where CH_4 is produced, were lower. In July, August, and September the average temperature at depth was 14°C, whereas in October and November it was 10°C.

Methane Reoxidation Rate

In a diffusive environment where the effective molecular diffusion coefficient is homogeneous, the sink strength for a biogeochemical can be calculated from the divergence of the chemical gradient. At steady-state, in one dimension z, mass conservation is:

$$D^* \frac{d^2c}{dz^2} = -r \qquad (3\text{-}4)$$

where r is the sink (or source) strength. This is manifest, for example, in the association of a concave-upward chemical profile (if depth is plotted horizontally) with an environment in which the chemical is consumed (i.e., an oxygen profile in an organic sediment).

The CH_4 profiles seen in Thoreau's Bog are generally concave upward. In the upper layers of the Sphagnum peat, however, the changes in porosity with depth suggest an increasing D^* near the surface. Near the surface, in fact, stalks of Sphagnum are arranged in a columnar geometry, suggesting not only higher porosity but lower tortuosity for vertical transport. At a few centimeters depth the stalks begin to collapse and assume a more horizontal arrangement, causing porosity to decrease and tortuosity to increase. Romanov (1968) also invokes this change in geometry in explaining the rapid decrease in hydraulic conductivity with depth in relatively unhumified, upper-profile Sphagnum peats.

Rather than invoke Eq. 3-4 with a constant D^*, we can estimate reoxidation rates by estimating the methane flux in the depth interval 0 to 9 cm, and comparing it with the flux for the 6 to 12 cm interval. This is really just a discretized application of a more general version of Eq. 3-4, where D^* varies with depth z:

$$\frac{d}{dz}\left(D^* \frac{dc}{dz}\right) = -r \qquad (3\text{-}5)$$

For the upper peat, between 0 and 6 cm, we let n = 0.7, and Ω = 1; thus D^e becomes 0.17 cm^2/sec. The corresponding mean gradient is 3.2 x 10^{-11} $mol \cdot cm^{-4}$ and the calculated CH_4 flux is 5.4 x 10^{-12} $mol \cdot cm^{-2} \cdot sec^{-1}$, or 0.8 $moles \cdot m^{-2} \cdot yr^{-1}$. This result suggests that (i) the actual CH_4 efflux from Thoreau's Bog to the atmosphere is closer to 0.8 $mol \cdot m^{-2} \cdot yr^{-1}$ than 2.4 $mol \cdot m^{-2} \cdot yr^{-1}$, the value calculated for the 6 to 12 cm depth interval, and (ii) reoxidation in the unsaturated zone amounts to 1.6 $mol \cdot m^{-2} \cdot yr^{-1}$, a large fraction of the total CH_4 production in the bog. The upward concavity of the CH_4 profiles does not seem to be attributable only to variability of peat porosity with depth.

From the propane tracer test, an effective molecular diffusion coefficient of 0.20 $cm^2 \cdot sec^{-1}$ was measured for the 0 to 9.6 cm depth interval. Repeating the above calculation, the annual CH_4 flux is 1.0 $mol \cdot m^{-2} \cdot yr^{-1}$. Again, it is inferred that a significant fraction of total CH_4 production is being reoxidized.

In the propane tracer test plot, the mean CH_4 gradient for the depth interval 0 to 7.2 cm is 7.08 $_{\times}$ 10^{-8} $atm \cdot cm^{-1}$ or 3 $_{\times}$ 10^{-12} $mol \cdot cm^{-4}$.

Using D^e = 0.024 $cm^2 \cdot sec^{-1}$, the annual flux is 0.01 $mol \cdot m^{-2} \cdot yr^{-1}$. See Table 3-2 for a summary of all the flux calculations. Although the absolute fluxes from the propane tracer test site are lower, as expected, the fraction of CH_4 oxidized remains significant.

It is evident from inspection of the figures that much higher reoxidation rates occur at those stations which have the higher CH_4 concentrations in the 9

-15 cm intervals. The cause of the horizontal variability itself cannot be determined without information on the processes occurring in the underlying saturated zone, although we suspect that the observed CH_4 profiles are evidence that ebullition is, at least in part, focused into discrete tubes and fissures which deposit methane non-uniformly into the unsaturated zone.

Disturbance of Sampling Site

Figure 3-5 shows the CH_4 profile at station UZ-R2, before and after the station was approached on foot by an observer. A dramatic 1000-fold change occurred, evidence of the triggering of bubble release by the observer and of the need for avoiding disturbance when making subsurface measurements in peatlands (this is also true for hydrologic measurements; e.g., Hemond, 1982). At another station (UZ-R4), only a 2-fold change in methane concentrations occurred. A flux chamber experiment conducted from the rigid platform, first sampling without disturbance of the peat surface and later walking up to the chamber to withdraw gas samples, shows a 100-fold change (Fig. 3-9). The fact that the largest relative change in CH_4 profile concentrations occurred at the station having higher undisturbed CH_4 concentrations (see Fig. 3-4) also supports the hypothesis that high CH_4 concentrations in the unsaturated zone are associated with bubbling from CH_4 efflux tubes and fissures. The structure, origins, and controls of such hypothesized bubble fissures remain to be elucidated.

REFERENCES

Chanton, J.P., P.M. Crill, K.B. Bartlett, and C.S. Martens. 1989. Amazon capims (grassmats): A source of C-13 enriched methane to the troposphere. Geophys. Res. Lett. 16: 799-802.

Cicerone, R.J., and R.S. Oremland. 1988. Biogeochemical aspects of atmospheric methane. Global Biogeochemical Cycles 2(4): 299-327.

Coleman, D.D., J.B. Risatte, and M. Schoell. 1981. Fractionation of carbon and hydrogen isotopes by methane oxidizing bacteria. Geochim. Cosmo. Acta, 45: 1033-1037.

Crill, P.M., K.B. Bartlett, R.C. Harriss, E. Gorham, E.S. Verry, D.I. Sebacher, L. Madzar, and W. Sanner. 1988. Methane flux from Minnesota peatlands. Global Biogeochemical Cycles, 2(4): 371-384.

Gorham, E., S.J. Eisenreich, J. Ford, and M.V. Santelmann. 1985. The chemistry of bog waters. In: Chemical Processes in Lakes. Werner Stumm (Ed.), John Wiley and Sons, Inc., pp. 339-363.

Harriss, R.C., D.I. Sebacher, and F.P. Day, Jr. 1982. Methane flux in the Great Dismal Swamp. Nature 297: 673-674.

Harriss, R.C., E. Gorham, D.I. Sebacher, K.B. Barlett, and P.A. Flebbe. 1985. Methane flux from northern peatlands. Nature 315: 652-654.

Hemond, H.F. 1980. Biogeochemistry of Thoreau's Bog, Concord, Massachusetts. Ecological Monographs, 50(4): 507-526.

Hemond, H.F. 1982. A low-cost mulitichannel recording piezometer system for wetland research. Water Resources Res., 18: 182-186.

Hemond, H.F., T.P. Army, W.K. Nuttle, and D.G. Chen. 1987. Element cycling in wetlands: Interactions with physical mass transport. In: R. Hites and S. Eisenreich (Eds.), Sources and Fates of Aquatic Pollutants, American Chemical Society Advances in Chemistry Series, pp. 519-537.

King, G.M. 1990. Regulation by light of methane emissions from a wetland. Nature 345: 513-515.

Matthews, E., and I. Fung. 1987. Methane emission from natural wetlands: Global distribution, area, and environmental characteristics of sources. Global Biogeochemical Cycles, 1(1): 61-86.

Romanov, V.V. 1968. Hydrophysics of Bogs (translated from Russian), Israel Program for Scientific Translations.

Sebacher, D.I., R.C. Harriss, K.B. Bartlett, S.M. Sebacher, and S.S. Grice. 1986. Atmospheric methane sources: Alaskan tundra bogs, an Alpine fen, and a subarctic Boreal marsh. Tellus 38B: 1-10.

Wahlen, M., N. Tanaka, R. Henry, B. Deck, J. Zeglen, J.S. Vogel, J. Southon, A. Shemesh, R. Fairbanks, and W. Broecker. 1989. Carbon-14 in methane sources and in atmospheric methane: the contribution from fossil carbon. Science 245: 286-290.

Weast, R.C. 1988. [Editor in Chief], Handbook of Chemistry and Physics, First Student Edition, CRC Press, Inc., Boca Raton, Florida.

Yavitt, J.B., G.E. Lang, and D.M. Downey. 1988. Potential methane production and methane oxidation rates in peatland ecosystems of the Appalachian Mountains, United States. Global Biogeochemical Cycles, 2(3): 253- 268.

APPENDIX A

Molar Concentrations of N_2, CH_4, and CO_2 in Well Porewaters

Day 1 = January 3, 1990

DAYS	P-0.99'	D-2.25'	C-2.2'	NITROGEN AC-2.25'	A-2.25'	G-2.25'	P-2.25'	2 ft avg
1		3.06E-04	3.53E-04	3.36E-04		7.67E-04		4.40E-04
12		2.59E-04	4.10E-04	4.18E-04	5.51E-04	4.53E-04		4.18E-04
33		3.24E-04	4.26E-04	3.92E-04	4.79E-04	3.86E-04		4.01E-04
50	4.63E-04	3.23E-04	3.90E-04	3.51E-04	4.09E-04	6.05E-04	1.33E-04	3.68E-04
66		4.92E-04	7.59E-04	4.87E-04		8.36E-04		6.44E-04
80		3.79E-04	2.46E-04	6.12E-04	7.83E-04			5.05E-04
100				4.18E-04	7.56E-04	8.65E-04		6.79E-04
116	6.62E-04	3.41E-04	3.97E-04	3.06E-04	3.74E-04	6.66E-04		4.17E-04
129	7.96E-04	4.56E-04	4.32E-04	5.52E-04	4.48E-04		1.03E-04	3.98E-04
143	4.10E-04		4.47E-04	3.75E-04	4.09E-04	6.13E-04	2.31E-04	4.15E-04
157		3.48E-04	2.12E-04	4.41E-04	3.62E-04		1.73E-04	3.07E-04
168		3.84E-04	3.24E-04		3.71E-04	5.10E-04	1.70E-04	3.52E-04
182		7.51E-05			1.98E-04	3.63E-04		2.12E-04
196	1.56E-04	3.49E-04	2.03E-04	5.58E-04	3.41E-04	3.61E-04	9.36E-05	3.18E-04
213	4.83E-05	8.29E-05	2.93E-04	3.47E-04	1.59E-04	5.85E-04	1.44E-04	2.68E-04
226	1.79E-04	7.95E-04	1.74E-04	6.88E-05	2.50E-05	3.46E-04	3.30E-05	2.40E-04
240	1.09E-04	1.03E-04	2.03E-04	6.31E-05	1.56E-04	1.76E-04		1.40E-04
254	1.27E-04	1.39E-04	2.25E-04	2.56E-04	4.27E-04	4.64E-04	2.22E-05	2.56E-04
268	2.55E-05	1.28E-04	1.76E-04	1.85E-04	3.64E-04	3.47E-04	8.24E-05	2.14E-04
287	3.95E-04	1.72E-04	2.89E-04	7.15E-05	1.88E-04	1.81E-04		1.80E-04
301	2.14E-04		2.10E-04	1.41E-04	9.24E-05	2.14E-04		1.64E-04
315	4.36E-04	1.52E-04	5.06E-04	3.60E-04	8.50E-04	5.06E-04	1.52E-04	4.21E-04
331		7.33E-05	3.35E-04	1.30E-04	2.24E-04	3.12E-04		2.15E-04
352	3.20E-04	2.68E-04	1.07E-04	9.72E-05	2.57E-04	2.77E-04	2.72E-04	2.13E-04

DAYS	D-3.04'	C-3.02'	AC-3.02'	A-3.0'	NITROGEN G-3.02'	P-3.0'	3 ft avg
1		5.59E-04	3.95E-04		4.70E-04		4.75E-04
12	3.83E-04	4.25E-04	2.90E-04	6.04E-04			4.25E-04
33	2.95E-04	6.46E-04	4.12E-04	6.53E-04	5.10E-04		5.03E-04
50	4.04E-04	5.15E-04	4.36E-04	5.25E-04	5.83E-04	1.92E-04	4.42E-04
66	3.81E-04	8.75E-04	5.20E-04		8.95E-04	1.74E-04	5.69E-04
80	4.79E-04	4.98E-04	4.82E-04	9.48E-04	7.75E-04	7.19E-04	6.50E-04
100	4.67E-04	8.85E-04	5.61E-04	9.27E-04	9.81E-04	2.33E-04	6.76E-04
116	4.03E-04	6.15E-04	6.09E-04	7.79E-04	7.20E-04		6.25E-04
129	3.44E-04	7.05E-04		6.61E-04	4.50E-04		5.40E-04
143		6.62E-04	7.23E-04		5.75E-04	3.49E-04	5.77E-04
157	4.19E-04	6.90E-04	5.68E-04	7.56E-04		3.21E-04	5.51E-04
168		6.35E-04		4.56E-04	5.14E-04	2.82E-04	4.72E-04
182	3.21E-04		4.58E-04	8.18E-04	4.36E-04	3.48E-05	4.13E-04
196	8.37E-04			8.04E-04	7.29E-04	7.66E-05	6.12E-04
213	2.92E-04	5.00E-04		7.27E-04		4.04E-05	3.90E-04
226	1.31E-04	2.99E-04		1.38E-04	4.23E-04	3.84E-05	2.06E-04
240	1.24E-04	2.02E-04	1.36E-04	1.96E-04		1.02E-04	1.52E-04
254	5.62E-05	2.55E-04	1.87E-04	3.03E-04	2.45E-04	7.14E-05	1.86E-04
268	1.57E-04	4.34E-04	2.57E-04		5.44E-04		3.48E-04
287	2.52E-04	3.93E-04	1.72E-04	2.21E-04	2.90E-04	8.53E-05	2.36E-04
301	2.88E-04	2.92E-04	3.07E-04	3.56E-04	3.66E-04		3.22E-04
315		3.92E-04	5.08E-04	5.79E-04	7.57E-04	5.01E-04	5.48E-04
331	7.32E-05	1.78E-04	2.36E-04	1.80E-04	6.96E-04		2.73E-04
352	1.63E-04	1.92E-04	9.61E-05		4.74E-04		2.31E-04

DAYS	NITROGEN							
	D-4.5'	C-4.66'	A-4.27'	G-4.66'	P-4.16'	4 ft avg	A-5.15'	A-6.69'
1	3.16E-04	2.62E-04	4.43E-04	4.06E-04		3.57E-04	3.03E-04	
12	3.80E-04	4.25E-04	3.97E-04	4.19E-04		4.05E-04		
33	3.27E-04	4.69E-04				3.98E-04	2.66E-04	
50	4.09E-04				2.98E-04	3.54E-04	3.74E-04	
66	5.85E-04	7.73E-04	5.06E-04			6.21E-04	4.16E-04	
80	4.98E-04		7.81E-04			6.39E-04	4.70E-04	
100	3.83E-04	5.98E-04	6.61E-04		3.10E-04	4.88E-04	4.33E-04	
116	4.15E-04	5.25E-04	8.35E-04	9.18E-04	2.27E-04	5.84E-04	3.66E-04	
129	5.61E-04	7.23E-04	4.51E-04	6.48E-04	2.14E-04	5.19E-04	3.50E-04	
143	4.50E-04	4.91E-04	5.93E-04	6.84E-04		5.55E-04		
157	4.32E-04	7.46E-04		4.66E-04	1.92E-04	4.59E-04	4.79E-04	
168	4.58E-04	6.85E-04	4.56E-04	6.47E-04	7.11E-04	5.92E-04	4.80E-04	
182	1.88E-04	4.69E-04	3.40E-04	3.08E-04	7.24E-05	2.75E-04	2.94E-04	2.15E-04
196	3.71E-04	6.44E-04	4.75E-04	4.10E-04	6.19E-04	5.04E-04	3.64E-04	
213	2.68E-04	4.25E-04	3.44E-04	4.92E-04	1.02E-04	3.26E-04		9.40E-04
226	2.57E-04	2.89E-04	1.55E-04	2.28E-04	1.87E-05	1.90E-04		
240	2.08E-04	3.96E-04	2.34E-04	1.46E-04	2.41E-04	2.45E-04	2.27E-04	
254	1.43E-04		2.86E-04		6.16E-05	1.64E-04	4.22E-04	
268	1.71E-04	3.10E-04	1.58E-04	1.95E-04	8.45E-04	3.36E-04	1.73E-04	2.84E-04
287	2.40E-04	3.83E-04	4.97E-04			3.73E-04	2.61E-04	3.21E-04
301	1.03E-04	3.15E-04		1.85E-04		2.01E-04	5.00E-04	
315	4.04E-04	6.65E-04	8.10E-04	5.75E-04	3.08E-04	5.52E-04	6.33E-04	
331	3.83E-05	1.39E-04	2.58E-04	1.85E-04	4.50E-05	1.33E-04	1.40E-04	1.24E-04
352	1.17E-04	1.70E-04	1.88E-04	1.35E-04		1.52E-04	7.59E-05	1.89E-04

				METHANE				
DAYS	P-0.99'	D-2.25'	C-2.2'	AC-2.25'	A-2.25'	G-2.25'	P-2.25'	2 ft avg
1		9.20E-04	1.33E-03	7.51E-04		3.81E-04		8.46E-04
12		7.19E-04	1.21E-03	8.54E-04	6.03E-04	3.21E-04		7.42E-04
33		7.16E-04	1.21E-03	6.96E-04	4.54E-04			7.69E-04
50	1.31E-03	6.53E-04	1.32E-03	5.35E-04	3.87E-04	4.13E-05	1.26E-03	6.98E-04
66		8.76E-04	2.20E-03	8.36E-04	7.63E-04	9.20E-05		9.54E-04
80		7.01E-04	1.42E-03	7.09E-04	3.94E-04			8.05E-04
100		9.05E-04	1.34E-03	6.69E-04	2.97E-04			8.02E-04
116	9.09E-04	5.70E-04	1.13E-03	5.00E-04	2.62E-04			6.16E-04
129	9.77E-04	5.80E-04	1.14E-03	5.27E-04	2.08E-04		9.66E-04	6.85E-04
143	4.27E-04	1.65E-03	1.15E-03	5.33E-04	2.78E-04	5.09E-05	9.10E-04	7.61E-04
157	1.73E-03	3.95E-04	9.80E-04	4.18E-04	2.06E-04	1.62E-06	9.41E-04	4.90E-04
168	3.33E-03	4.60E-04	9.87E-04	3.35E-04	2.91E-04	2.38E-04	9.63E-04	5.46E-04
182	2.50E-03	3.12E-04	1.05E-03	5.10E-04	2.19E-04	1.16E-04	6.90E-04	4.82E-04
196	6.33E-04	5.24E-04	9.48E-04	4.78E-04	3.43E-04	3.72E-04	9.90E-04	6.09E-04
213	3.02E-04	3.44E-04	8.70E-04	2.94E-04	2.97E-04	2.64E-04	6.28E-04	4.49E-04
226	5.13E-04	5.85E-04	6.73E-04	3.85E-04	2.16E-04	1.74E-04	5.21E-04	4.26E-04
240	5.93E-04	6.61E-04	8.59E-04	4.70E-04	3.86E-04	1.53E-04	9.24E-04	5.75E-04
254	6.42E-04	5.94E-04	7.68E-04	4.72E-04	3.95E-04	5.17E-04	9.54E-04	6.17E-04
268	5.81E-04	4.60E-04	7.73E-04	3.69E-04	2.28E-04	3.60E-04	7.34E-04	4.87E-04
287	2.71E-04	4.11E-04	8.38E-04	3.08E-04	2.32E-04		1.01E-03	5.61E-04
301	2.69E-04	5.39E-04	7.76E-04	4.20E-04	1.95E-04		6.11E-04	5.08E-04
315	3.56E-04	5.78E-04	9.48E-04	3.85E-04	3.64E-04		7.69E-04	6.09E-04
331		5.53E-04	1.01E-03	4.09E-04	3.51E-04		9.64E-04	6.58E-04
352	2.02E-04	7.16E-04	1.04E-03	4.09E-04	2.88E-04		7.66E-04	6.44E-04

METHANE

DAYS	D-3.04'	C-3.02'	AC-3.02'	A-3.0'	G-3.02'	P-3.0'	3 ft avg
1	1.59E-03	8.24E-04	7.33E-04	7.20E-04	4.60E-04		8.65E-04
12	8.32E-04	7.36E-04	6.40E-04	8.71E-04	4.84E-04		7.13E-04
33	7.21E-04	9.33E-04	6.95E-04	7.00E-04			7.62E-04
50	6.14E-04	8.47E-04	6.94E-04	6.24E-04	1.00E-04	1.04E-03	6.53E-04
66	8.46E-04	1.63E-03	8.14E-04		1.60E-04	1.28E-03	9.45E-04
80	7.15E-04	1.17E-03	7.74E-04	3.96E-04		1.43E-03	8.98E-04
100	8.50E-04	1.15E-03	7.58E-04	3.20E-04	1.16E-04	1.32E-03	7.54E-04
116	7.13E-04	8.99E-04	4.34E-04	2.77E-04	1.25E-04	1.28E-03	6.22E-04
129	6.11E-04	1.14E-03	5.52E-04	1.67E-04		1.23E-03	7.40E-04
143	5.34E-04	1.03E-03	5.52E-04	2.34E-04	8.75E-05	1.11E-03	5.92E-04
157	5.59E-04	6.21E-04	3.48E-04	1.81E-04	9.20E-05	1.11E-03	4.85E-04
168	5.73E-04	6.39E-04	3.78E-04	1.83E-04	3.68E-04	7.91E-04	4.89E-04
182	4.43E-04	7.40E-04	4.42E-04	1.79E-04	1.72E-04	7.39E-04	4.53E-04
196	6.70E-04	8.23E-04	4.83E-04	4.03E-04	5.02E-04	1.05E-03	6.55E-04
213	5.23E-04	6.43E-04	2.20E-04	5.53E-04	2.44E-04	7.60E-04	4.91E-04
226	5.33E-04	6.99E-04	3.96E-04	2.57E-04	2.09E-04	5.50E-04	4.41E-04
240	5.36E-04	7.57E-04	4.05E-04	3.40E-04	2.29E-04	1.04E-03	5.52E-04
254	3.83E-04	6.93E-04	3.80E-04	3.53E-04	3.43E-04	9.87E-04	5.23E-04
268	4.50E-04	7.98E-04	2.68E-04	2.26E-04	4.42E-04	6.71E-04	4.76E-04
287	5.45E-04	8.20E-04	3.51E-04	2.50E-04	4.88E-05	6.65E-04	4.47E-04
301	4.64E-04	7.50E-04	3.77E-04	3.19E-04	1.93E-05	7.80E-04	4.52E-04
315	5.39E-04	9.23E-04	3.86E-04	3.38E-04		8.68E-04	6.11E-04
331	4.90E-04	9.61E-04	5.03E-04	4.27E-04	1.20E-04	8.46E-04	5.58E-04
352	6.26E-04	9.63E-04	3.98E-04	3.83E-04		1.33E-03	7.41E-04

DAYS	METHANE D-4.5'	C-4.66'	A-4.27'	G-4.66'	P-4.16'	4 ft avg	A-5.15'	A-6.69'
1	5.92E-04	5.30E-04	9.75E-04	7.56E-04		7.13E-04	7.66E-04	
12	5.57E-04	6.49E-04	8.27E-04	6.63E-04		6.74E-04	7.04E-04	
33	5.17E-04	5.29E-04				5.23E-04	6.69E-04	
50	6.37E-04				1.12E-03	8.77E-04	6.86E-04	
66	7.83E-04	6.49E-04	7.05E-04			7.13E-04	6.81E-04	
80	7.38E-04	4.90E-04	6.31E-04		1.26E-03	7.80E-04	8.60E-04	
100	7.51E-04	5.98E-04	7.35E-04		1.38E-03	8.66E-04	7.29E-04	
116	6.32E-04	4.80E-04	6.41E-04	4.13E-04	1.24E-03	6.81E-04	6.03E-04	
129	7.05E-04	6.32E-04	5.36E-04	2.00E-04	9.51E-04	6.05E-04	6.73E-04	
143	5.98E-04	4.33E-04	6.19E-04	3.03E-04	1.15E-03	6.21E-04	7.16E-04	
157	5.39E-04	3.77E-04	6.88E-04	4.80E-04	1.09E-03	6.35E-04	6.57E-04	
168	5.40E-04	3.75E-04	5.09E-04	5.60E-04	1.07E-03	6.10E-04	5.61E-04	
182	4.50E-04	2.97E-04	4.57E-04	4.07E-04	8.86E-04	4.99E-04	5.00E-04	4.70E-04
196	6.35E-04	5.65E-04	7.48E-04	7.07E-04	1.16E-03	7.63E-04	6.92E-04	9.06E-04
213	5.11E-04	4.56E-04	5.68E-04	4.61E-04	6.85E-04	5.36E-04	4.57E-04	4.95E-04
226	5.78E-04	3.98E-04	4.16E-04	6.22E-04	1.08E-03	6.19E-04	5.59E-04	7.22E-04
240	5.86E-04	4.40E-04	6.60E-04	6.45E-04	9.57E-04	6.58E-04	6.42E-04	8.78E-04
254	5.36E-04	4.99E-04	6.03E-04	6.47E-04	1.10E-03	6.76E-04	7.59E-04	
268	4.35E-04	4.97E-04	3.89E-04	5.39E-04	7.76E-04	5.27E-04	5.12E-04	5.96E-04
287	4.17E-04	3.92E-04	4.14E-04	4.08E-04	5.56E-04	4.37E-04	5.48E-04	5.63E-04
301	3.62E-04	3.34E-04	3.88E-04	4.37E-04	5.78E-04	4.20E-04	4.06E-04	6.05E-04
315	4.56E-04	3.74E-04	4.26E-04	3.41E-04	5.98E-04	4.39E-04	3.66E-04	5.10E-04
331	4.10E-04	3.99E-04	5.76E-04	3.65E-04	8.06E-04	5.11E-04	4.49E-04	5.13E-04
352	4.91E-04	4.50E-04	5.34E-04	3.90E-04	8.78E-04	5.49E-04	5.11E-04	4.69E-04

CARBON DIOXIDE

DAYS	P-0.99'	D-2.25'	C-2.2'	AC-2.25'	A-2.25'	G-2.25'	P-2.25'	2 ft avg
1		2.46E-03	3.89E-03	2.55E-03		1.31E-03		2.55E-03
12		2.17E-03	3.72E-03	2.87E-03	2.26E-03	1.28E-03		2.46E-03
33		1.97E-03	3.75E-03	2.44E-03	1.85E-03			2.50E-03
50	3.97E-03	1.90E-03	3.95E-03	2.01E-03	1.75E-03	1.04E-03	3.89E-03	2.42E-03
66		2.17E-03	4.36E-03	2.52E-03	2.01E-03	1.26E-03		2.46E-03
80		1.59E-03	3.96E-03	1.85E-03	1.39E-03			2.20E-03
100	1.07E-03	2.03E-03	3.27E-03	1.99E-03	1.31E-03	8.46E-04		1.89E-03
116	1.91E-03	1.58E-03	3.27E-03	1.59E-03	1.27E-03	1.06E-03		1.75E-03
129	1.23E-03	1.71E-03	2.77E-03	1.88E-03	1.57E-03	9.31E-04	3.05E-03	1.99E-03
143	1.80E-03	1.58E-03	2.64E-03	1.80E-03	1.45E-03	6.31E-04	2.72E-03	1.80E-03
157	1.92E-03	1.41E-03	2.72E-03	1.74E-03	1.54E-03	7.11E-04	3.07E-03	1.87E-03
168	2.98E-03	1.71E-03	2.93E-03	1.38E-03	1.68E-03	1.39E-03	3.31E-03	2.07E-03
182	2.32E-03	1.37E-03	3.01E-03	2.10E-03	1.53E-03	1.07E-03	2.59E-03	1.95E-03
196	3.40E-03	2.02E-03	3.13E-03	1.80E-03	1.87E-03	1.77E-03	3.72E-03	2.38E-03
213	1.95E-03	1.85E-03	3.26E-03	1.55E-03	1.94E-03	1.48E-03	2.82E-03	2.15E-03
226	2.26E-03	1.85E-03	3.38E-03	1.95E-03	1.70E-03	9.24E-04	2.25E-03	2.01E-03
240	2.49E-03	2.63E-03	3.91E-03	2.62E-03	2.71E-03	9.17E-04	3.50E-03	2.71E-03
254	3.07E-03	2.58E-03	3.72E-03	2.32E-03	2.53E-03	1.84E-03	3.80E-03	2.80E-03
268	2.76E-03	2.26E-03	3.90E-03	2.10E-03	2.00E-03	1.57E-03	3.17E-03	2.50E-03
287	1.02E-03	2.04E-03	4.17E-03	2.06E-03	2.16E-03	5.04E-04	3.47E-03	2.40E-03
301	1.14E-03	2.27E-03	3.97E-03	2.63E-03	1.76E-03	5.00E-04	2.86E-03	2.33E-03
315	1.28E-03	2.32E-03	3.90E-03	2.23E-03	2.24E-03	5.94E-04	3.27E-03	2.43E-03
331		2.11E-03	3.72E-03	1.92E-03	2.07E-03	7.05E-04	3.40E-03	2.32E-03
352	9.74E-04	2.25E-03	3.42E-03	2.02E-03	1.71E-03	6.10E-04	2.91E-03	2.15E-03

CARBON DIOXIDE

DAYS	D-3.04'	C-3.02'	AC-3.02'	A-3.0'	G-3.02'	P-3.0'	3 ft avg
1	2.19E-03	2.46E-03	2.44E-03	2.39E-03	1.59E-03		2.21E-03
12	2.61E-03	2.51E-03	2.42E-03	2.51E-03	1.77E-03		2.36E-03
33	2.33E-03	2.85E-03	2.45E-03	1.90E-03			2.38E-03
50	2.05E-03	2.83E-03	2.43E-03	1.84E-03	1.21E-03	3.57E-03	2.32E-03
66	2.53E-03	3.56E-03	2.51E-03		1.52E-03	3.64E-03	2.75E-03
80	2.02E-03	3.39E-03	2.23E-03	1.06E-03		3.87E-03	2.51E-03
100	2.25E-03	3.02E-03	2.11E-03	1.18E-03	1.16E-03	3.92E-03	2.27E-03
116	2.18E-03	2.60E-03	1.53E-03	1.17E-03	1.24E-03	3.17E-03	1.98E-03
129	2.14E-03	3.35E-03	1.96E-03	1.15E-03	9.63E-04	2.84E-03	2.07E-03
143	1.72E-03	2.73E-03	1.76E-03	1.21E-03	9.19E-04	2.71E-03	1.84E-03
157	2.01E-03	2.21E-03	1.59E-03	1.46E-03	1.16E-03	3.01E-03	1.91E-03
168	1.88E-03	2.19E-03	1.57E-03	1.28E-03	1.70E-03	2.74E-03	1.89E-03
182	1.71E-03	2.53E-03	1.72E-03	1.30E-03	1.27E-03	2.44E-03	1.83E-03
196	2.24E-03	2.46E-03	1.65E-03	1.91E-03	1.97E-03	3.63E-03	2.31E-03
213	2.05E-03	2.30E-03	1.32E-03	1.86E-03	1.36E-03	2.95E-03	1.98E-03
226	2.05E-03	2.20E-03	1.50E-03	1.65E-03	1.05E-03	2.23E-03	1.78E-03
240	2.13E-03	2.39E-03	1.87E-03	2.01E-03	1.13E-03	3.36E-03	2.15E-03
254	1.78E-03	2.37E-03	1.93E-03	1.97E-03	1.49E-03	3.49E-03	2.17E-03
268	2.06E-03	2.55E-03	1.60E-03	1.54E-03	1.77E-03	2.79E-03	2.05E-03
287	2.32E-03	3.03E-03	2.14E-03	1.68E-03	5.90E-04	2.57E-03	2.05E-03
301	2.17E-03	3.21E-03	2.16E-03	1.90E-03	5.97E-04	2.86E-03	2.15E-03
315	2.43E-03	3.44E-03	1.88E-03	1.87E-03	5.56E-04	2.82E-03	2.16E-03
331	2.01E-03	3.60E-03	1.94E-03	2.00E-03	9.05E-04	2.79E-03	2.21E-03
352	2.43E-03	3.52E-03	1.85E-03	1.74E-03	7.11E-04	2.80E-03	2.17E-03

CARBON DIOXIDE

DAYS	D-4.5'	C-4.66'	A-4.27'	G-4.66'	P-4.16'	4 ft avg	A-5.15'	A-6.69'
1	1.96E-03	2.03E-03	1.98E-03	2.55E-03		2.13E-03	2.53E-03	
12	1.99E-03	2.37E-03	2.63E-03	2.35E-03		2.33E-03	2.24E-03	
33	1.78E-03	2.07E-03				1.92E-03	2.41E-03	
50	2.06E-03				3.38E-03	2.72E-03	2.48E-03	
66	2.21E-03	2.15E-03	2.21E-03			2.19E-03	2.38E-03	
80	1.98E-03	1.62E-03	1.86E-03		3.18E-03	2.16E-03	2.60E-03	
100	2.28E-03	2.02E-03	2.18E-03		3.49E-03	2.49E-03	2.41E-03	
116	1.79E-03	1.68E-03	1.74E-03	1.78E-03	3.14E-03	2.03E-03	2.12E-03	
129	2.07E-03	2.20E-03	1.89E-03	1.39E-03	2.81E-03	2.07E-03	2.41E-03	
143	1.75E-03	1.44E-03	1.89E-03	1.37E-03	3.09E-03	1.91E-03	2.31E-03	
157	1.83E-03	1.60E-03	1.87E-03	2.01E-03	3.20E-03	2.10E-03	2.43E-03	
168	1.78E-03	1.50E-03	1.78E-03	2.12E-03	3.15E-03	2.07E-03	2.11E-03	
182	1.63E-03	1.16E-03	1.64E-03	1.80E-03	2.73E-03	1.79E-03	2.02E-03	1.82E-03
196	2.03E-03	1.94E-03	2.33E-03	2.34E-03	3.32E-03	2.39E-03	2.42E-03	2.53E-03
213	1.69E-03	1.70E-03	2.11E-03	1.99E-03	2.59E-03	2.02E-03	1.94E-03	1.96E-03
226	1.86E-03	1.50E-03	1.56E-03	2.25E-03	3.30E-03	2.09E-03	2.08E-03	1.98E-03
240	1.99E-03	1.63E-03	2.27E-03	2.36E-03	3.31E-03	2.31E-03	2.25E-03	2.43E-03
254	1.93E-03	1.93E-03	2.19E-03	2.39E-03	3.72E-03	2.43E-03	2.53E-03	
268	1.70E-03	1.93E-03	1.65E-03	2.23E-03	3.20E-03	2.14E-03	2.11E-03	2.26E-03
287	1.57E-03	1.66E-03	1.46E-03	1.72E-03	2.25E-03	1.73E-03	2.13E-03	2.16E-03
301	1.62E-03	1.61E-03	1.76E-03	1.88E-03	2.38E-03	1.85E-03	1.96E-03	1.79E-03
315	1.78E-03	1.75E-03	1.73E-03	1.61E-03	2.55E-03	1.88E-03	1.69E-03	2.01E-03
331	1.57E-03	1.74E-03	2.09E-03	1.46E-03	3.04E-03	1.98E-03	1.79E-03	1.97E-03
352	1.83E-03	2.18E-03	2.13E-03	1.73E-03	3.22E-03	2.22E-03	2.12E-03	1.98E-03

APPENDIX B

Temperatures of Well Porewaters

Day 1 = January 3, 1990

DAYS	TEMPERATURE (centigrade) P-0.99'	D-2.25'	C-2.2'	AC-2.25'	A-2.25'	G-2.25'	P-2.25'	2 ft avg
1		2.8	1.3	2.4	3.1	2.4		5.202
12		1.7	1.9	2.0	1.9	2.6		3.657
33		1.4	1.4	1.8	1.2	0.8		2.528
50		1.7	1.3	1.6	1.6	1.7		1.911
66		1.6	1.1	1.2	1.2	1.5		1.86
80		1.4	1.1	1.4	1.9	1.0		2.378
100	2.4	2.4	1.9	2.7	3.2	2.9	1.8	3.423
116	4.5	5.6	4.9	5.1	6.4	5.9	2.6	4.903
129	8.1	7.5	7.8	7.2	9.1	8.7	5.0	6.691
143	8.7	8.4	9.1	8.5	9.6	9.4	7.4	8.6327
157	12.7	10.4	10.8	10.3	11.8	10.1	9.4	10.562
168	14.7	11.5	12.0	11.2	12.7	10.0	10.8	12.311
182	15.5	13.0	14.1	13.1	15.1	13.8	12.7	13.731
196		13.7	14.2	13.4	14.8	12.4		14.698
213	18.4	15.4	16.3	15.4	16.6	14.9	15.8	15.13
226	18.7	16.6	18.0	17.1	19.1	18.3	16.6	14.99
240	18.6	16.2	17.7	16.7	18.0	17.3	16.3	14.288
254	16.9	15.3	16.3	15.6	16.2	15.4	15.6	13.087
268	13.6	13.8	14.6	13.9	14.6	13.9	14.1	11.488
287	15.4	14.2	15.3	14.4	16.0	16.5	13.9	9.631
301	9.7	12.1	12.8	12.3	12.4	11.7	12.3	7.6745
315	7.6	9.6	9.8	10.0	9.6	8.3	10.1	5.787
331	6.6	7.2	7.6		7.4	7.6	7.8	4.132
352	3.9	5.5	5.0	6.3	4.8	4.8	5.7	2.851

					TEMPERATURE (centigrade)		
DAYS	D-3.04'	C-3.02'	AC-3.02'	A-3.0'	G-3.02'	P-3.0'	3 ft avg
1	3.6	3.6	4.4	4.2	4.6		6.321
12	2.8	3.9	3.8	3.7	3.9		4.946
33	2.3	2.6	3.3	2.0	1.2		3.818
50	2.3	2.6	2.8	2.4	2.6	2.3	3.034
66	2.0	1.8	2.2	1.8	2.1	2.2	2.662
80	1.7	1.4	2.1	1.9	1.4	1.9	2.734
100	2.7	1.9	2.7	3.4	3.4	2.6	3.244
116	4.2	3.4	4.1	5.0	5.3	2.8	4.147
129	5.7	6.1	5.2	7.0	7.4	4.1	5.367
143	6.8	7.2	6.9	8.1	8.4	6.3	6.797
157	7.9	8.1	7.9	9.2	8.5	7.6	8.3151
168	8.7	8.8	8.6	9.7	8.5	8.7	9.79
182	10.0	11.0	10.1	11.8	11.4	10.4	11.095
196	10.8	10.9	10.8	12.2	10.5		12.118
213	12.3	12.9	12.3	13.4	12.4	13.1	12.77
226	13.4	15.1	14.1	16.4	16.1	14.2	12.996
240	13.8	15.5	14.6	15.6	15.4	14.6	12.775
254	13.7	14.3	14.0	14.6	13.9	14.3	12.127
268	13.1	13.7	13.3	14.0	13.2	13.8	11.109
287	12.9	14.2	13.2	14.2	15.3	12.9	9.806
301	12.4	13.6	12.8	13.2	12.7	12.7	8.3323
315	10.7	11.4	10.8	11.1	10.0	11.1	6.814
331	9.2	9.4		9.1	8.9	6.4	5.382
352	7.6	7.3	7.8	7.1	6.4	7.4	4.16

DAYS	TEMPERATURE (centigrade) D-4.5′	C-4.66′	A-4.27′	G-4.66′	P-4.16′	4 ft avg	A-5.15′	A-6.69′
1	6.2	3.2	5.6	6.8		7.4967	7.4	
12	5.4	5.6	5.2	7.1		6.396	6.7	
33	4.6	3.8				5.405	5.9	
50	4.4				3.9	4.608	5.2	
66	4.1	2.8	4.0			4.075	5.1	
80	3.6	2.2	3.6		3.3	3.85	4.5	
100	3.4	2.2	4.1	4.6	3.6	3.954	4.9	5.8
116	3.9	3.1	4.9	5.6	3.6	4.377	5.4	5.8
129	4.8	5.0	5.8	6.3	4.0	5.083	5.6	
143	5.7	5.7	6.9	7.2	5.5	6.011	6.2	5.9
157	6.4	6.5	7.8	7.3	6.6	7.0818	6.9	6.4
168	7.1	7.1	8.2	7.6	7.4	8.2024	7.2	6.6
182	8.1	8.8	9.4	9.1	8.7	9.277	7.9	7.1
196	9.0	9.2	10.1	9.0		10.21[illegible]	8.8	7.8
213	10.1	10.8	11.3	10.3	10.9	10.927	9.5	8.4
226	11.3	12.7	13.6	13.2	12.1	11.362	11.3	9.7
240	12.0	13.7	13.6	12.8	12.9	11.478	11.7	10.2
254	12.2	12.7	12.9	12.3	12.7	11.265	11.5	10.3
268	12.1	12.4	12.9	12.1	12.9	10.743	11.7	10.6
287	12.0	13.8	12.8	13.6	12.3	9.955	11.8	11.3
301	12.0	13.4	12.9	12.5	12.3	8.969	12.1	11.1
315	10.8	11.9	11.0	10.8	11.3	7.8715	11.2	10.7
331	9.6	9.8	10.1	9.9	9.7	6.7556	10.5	10.4
352	8.7	8.3	8.4	8.3	8.6	5.718	9.2	9.5

APPENDIX C

Partial Pressures of Porewater Gases

Day 1 = January 3, 1990

DAYS	PARTIAL PRESSURES 2 FT CH4	2 FT N2	2 FT CO2	2 FT H2O	SUM 2 FT
1	0.384715	0.472188	0.040170	0.007167	0.904242
12	0.323297	0.432274	0.036541	0.006965	0.799078
33	0.324186	0.403686	0.035594	0.006623	0.770091
50	0.289048	0.365033	0.033670	0.006768	0.694520
66	0.394124	0.637023	0.034168	0.006623	1.071940
80	0.337982	0.506124	0.031086	0.006671	0.881865
100	0.346907	0.698478	0.027828	0.007218	1.080432
116	0.277772	0.443866	0.027251	0.008669	0.757560
129	0.324525	0.441564	0.032987	0.010300	0.809377
143	0.379468	0.480591	0.032071	0.011101	0.903233
157	0.256724	0.370370	0.035459	0.012528	0.675083
168	0.298151	0.439492	0.041637	0.013301	0.792582
182	0.272615	0.272595	0.041033	0.015368	0.601613
196	0.351946	0.415678	0.051878	0.015469	0.834972
213	0.262187	0.354116	0.047476	0.017711	0.681493
226	0.247601	0.316116	0.044143	0.019857	0.627718
240	0.329327	0.181925	0.058268	0.019240	0.588762
254	0.343347	0.324083	0.057780	0.017599	0.742811
268	0.261164	0.262807	0.048981	0.015875	0.588829
287	0.286805	0.213283	0.044155	0.016826	0.561071
301	0.247060	0.186360	0.040092	0.014116	0.487629
315	0.281505	0.457515	0.038955	0.011796	0.789772
331	0.290377	0.224507	0.035063	0.010230	0.560178
352	0.273966	0.216142	0.031026	0.008791	0.529926

DAYS	PARTIAL PRESSURES 3 FT CH4	3 FT N2	3 FT CO2	3 FT H2O	SUM 3 FT
1	0.405568	0.522231	0.036253	0.008084	0.972137
12	0.321823	0.453370	0.036820	0.007859	0.819874
33	0.333467	0.522457	0.035560	0.007116	0.898601
50	0.279185	0.450600	0.033672	0.007218	0.770676
66	0.399775	0.574344	0.039335	0.006965	1.020421
80	0.380555	0.657566	0.036047	0.006817	1.080987
100	0.324294	0.691819	0.033212	0.007375	1.056700
116	0.274561	0.654036	0.029924	0.008084	0.966607
129	0.338344	0.581406	0.032685	0.009164	0.961599
143	0.281065	0.641895	0.030682	0.010091	0.963734
157	0.239711	0.633309	0.033527	0.010730	0.917279
168	0.251027	0.559546	0.035044	0.011176	0.856795
182	0.240130	0.503986	0.035328	0.012781	0.792226
196	0.356260	0.761149	0.046228	0.012952	1.176591
213	0.271027	0.491116	0.040387	0.014490	0.817021
226	0.244742	0.260564	0.036655	0.016718	0.558680
240	0.304878	0.191640	0.043904	0.016718	0.557141
254	0.284696	0.231681	0.043455	0.015875	0.575708
268	0.252741	0.424053	0.039703	0.015268	0.731766
287	0.229460	0.279552	0.038017	0.015569	0.562599
301	0.223434	0.370115	0.037836	0.014681	0.646067
315	0.290315	0.609059	0.036070	0.012781	0.948227
331	0.255165	0.293608	0.034950	0.011026	0.594751
352	0.327196	0.242040	0.032889	0.010091	0.612217

DAYS	PARTIAL PRESSURES 4 FT CH4	4 FT N2	4 FT CO2	4 FT H2O	SUM 4 FT
1	0.345277	0.402664	0.036370	0.008852	0.793165
12	0.316744	0.446624	0.038325	0.009101	0.810796
33	0.239206	0.429127	0.030458	0.008140	0.706933
50	0.392533	0.373981	0.041809	0.008140	0.816465
66	0.314045	0.648850	0.032992	0.007803	1.003692
80	0.341627	0.663886	0.032307	0.007586	1.045407
100	0.380325	0.508020	0.037404	0.007803	0.933554
116	0.302813	0.613960	0.030913	0.008140	0.955828
129	0.274223	0.555304	0.032465	0.008730	0.870724
143	0.288865	0.605694	0.030898	0.009356	0.934815
157	0.304005	0.513621	0.035372	0.009818	0.862816
168	0.300986	0.678542	0.036171	0.010230	1.025930
182	0.253172	0.323259	0.032626	0.011176	0.620234
196	0.396096	0.603161	0.044922	0.011560	1.055740
213	0.283414	0.396209	0.038803	0.012696	0.731124
226	0.330371	0.232371	0.040843	0.014396	0.617982
240	0.352268	0.301063	0.045313	0.014777	0.713423
254	0.360352	0.200235	0.047274	0.014396	0.622258
268	0.277363	0.406510	0.040918	0.014302	0.739095
287	0.225642	0.444291	0.032234	0.014681	0.716850
301	0.211106	0.234535	0.033276	0.014396	0.493314
315	0.214615	0.629062	0.032601	0.013126	0.889405
331	0.242689	0.147871	0.032943	0.011955	0.435459
352	0.253097	0.165340	0.035530	0.010951	0.464919

APPENDIX D

Mat, Water, Pressure, and Wind Data for Four Selected Periods

6/29/88 - 7/6/88

time (hrs)	mat (cm)	water (cm)	pressure (mb)	mat-water	wind (knots)
233.5	55.689	22.801	1008.4	32.888	
241.5	55.789	22.847	1008.15	32.942	
249.5	55.962	22.906	1005.95	33.056	
257.5	56.044	23.122	1005.1	32.922	
265.5	56.113	23.214	1004.55	32.899	9
273.5	56.288	23.288	1004.1	33	11
281.5	56.314	23.457	1003.25	32.857	8.5
289.5	56.277	23.391	1004.3	32.886	14
297.5	56.353	23.381	1007.65	32.972	9
305.5	56.516	23.442	1009.65	33.074	12.5
313.5	56.596	23.585	1012.35	33.011	6
321.5	56.85	23.639	1015.4	33.211	9
329.5	57.056	23.866	1016.05	33.19	5.5
337.5	57.268	23.986	1020.5	33.282	7
345.5	57.519	24.024	1023.6	33.495	6
353.5	57.749	24.272	1024.9	33.477	8
361.5	57.922	24.501	1026.7	33.421	6
369.5	58.133	24.626	1027.8	33.507	7
377.5	58.326	25.235	1024.9	33.091	8.5
385.5	58.426	25.406	1023.85	33.02	8
393.5	58.612	25.493	1022.85	33.119	5

8/11/88 - 8/23/88

time (hrs)	mat (cm)	water (cm)	pressure (mb)	mat-water	wind (knots)
1250.0	54.42	21.675	1019	32.745	9
1258.0	54.621	21.913	1019.6	32.708	5
1266.0	54.742	22.051	1016.1	32.691	6
1274.0	54.858	22.123	1016.3	32.735	7
1282.0	54.976	22.289	1018	32.687	8
1290.0	55.176	22.442	1016.9	32.734	5
1298.0	55.3	22.502	1017.8	32.798	7
1306.0	55.493	22.802	1018	32.691	9
1314.0	55.696	23.014	1015.2	32.682	6
1322.0	55.83	23.051	1015.8	32.779	6
1330.0	55.992	23.336	1016.4	32.656	6
1338.0	56.141	23.525	1011.4	32.616	12
1346.0	56.272	23.556	1010.8	32.716	8
1354.0	56.419	23.969	1007.5	32.45	10
1362.0	56.532	23.962	1004.4	32.57	14
1370.0	56.602	24.006	1005.9	32.596	14
1378.0	56.807	24.302	1007.8	32.505	11
1386.0	57.054	24.466	1009.8	32.588	9
1394.0	57.183	24.53	1012	32.653	6
1402.0	57.409	24.816	1011.9	32.593	6
1410.0	57.489	24.857	1005.8	32.632	5
1418.0	57.497	24.858	1003.4	32.639	10
1426.0	57.715	25.115	1007.8	32.6	14
1434.0	57.908	25.421	1010	32.487	9
1442.0	58.134	25.509	1013.9	32.625	8
1450.0	58.391	25.832	1015.9	32.559	3
1458.0	58.573	25.96	1012.2	32.613	3
1466.0	58.727	25.994	1011.9	32.733	8
1474.0	58.928	26.191	1011.5	32.737	1
1482.0	59.041	26.377	1008.1	32.664	6
1490.0	59.18	26.452	1008	32.728	7
1498.0	59.401	26.806	1008.8	32.595	15

8/11/88 - 8/23/88

time (hrs)	mat (cm)	water (cm)	pressure (mb)	mat-water	wind (knots)
1506.0	59.65	27.079	1012.4	32.571	5
1514.0	59.94	27.176	1018.5	32.764	7
1522.0	60.266	27.444	1021.3	32.822	10
1530.0	60.476	27.732	1022.9	32.744	4
1538.0	60.687	27.745	1024.7	32.942	4
1546.0	60.951	28.151	1025.7	32.8	7
1554.0	61.057	28.258	1023	32.799	6

6/23/89 - 6/29/89

time (hrs)	mat (cm)	water (cm)	pressure (mb)	mat-water	wind (knots)
8850.5	39.511	8.876	1016.85	30.635	8
8858.5	39.479	8.884	1016.6	30.595	6.5
8866.5	39.515	8.886	1020.3	30.629	6
8874.5	39.566	8.896	1019.4	30.67	4
8882.5	39.554	8.924	1017.35	30.63	8
8890.5	39.669	8.96	1017.1	30.709	6
8898.5	39.734	9.325	1015.25	30.409	3
8906.5	39.757	9.388	1013.75	30.369	7.5
8914.5	39.869	9.449	1012.35	30.42	7
8922.5	39.941	9.657	1010.2	30.284	6
8930.5	39.995	9.716	1008.75	30.279	5
8938.5	40.118	9.774	1009.2	30.344	3
8946.5	40.25	10.063	1007.1	30.187	7
8954.5	40.307	10.139	1006.9	30.168	7.5
8962.5	40.402	10.266	1008.2	30.136	9
8970.5	40.468	10.327	1009.45	30.141	7
8978.5	40.522	10.37	1012.55	30.152	9.5

7/29/89 - 8/7/89

time (hrs)	mat (cm)	water (cm)	pressure (mb)	mat-water	wind (knots)
9705.5	43.526	15.287	1015.75	28.239	10
9713.5	43.591	15.453	1014.8	28.138	6.5
9721.5	43.599	15.543	1016.8	28.056	7
9729.5	43.649	15.612	1018.3	28.037	11
9737.5	43.889	15.674	1018.45	28.215	11.5
9745.5	43.887	15.669	1020.25	28.218	6
9753.5	43.937	15.682	1022.95	28.255	6
9761.5	44.04	15.757	1022.55	28.283	6
9769.5	44.055	15.773	1021.95	28.282	4
9777.5	44.136	15.768	1022.8	28.368	9
9785.5	44.217	16.567	1019.55	27.65	4
9793.5	44.247	16.585	1018.15	27.662	8
9801.5	44.317	16.601	1016.5	27.716	3
9809.5	44.423	16.772	1012.35	27.651	4.5
9817.5	44.481	16.833	1009.85	27.648	5
9825.5	44.613	17.004	1009.75	27.609	8
9833.5	44.739	17.259	1009.2	27.48	6
9841.5	44.817	17.292	1008.7	27.525	5
9849.5	44.928	17.463	1006.75	27.465	10
9857.5	45.004	17.571	1004.15	27.433	7.5
9865.5	45.067	17.617	1002.95	27.45	7
9873.5	45.155	17.734	1002	27.421	10
9881.5	45.396	17.865	1003.05	27.531	5
9889.5	45.416	17.87	1005.2	27.546	5
9897.5	45.456	17.879	1005.6	27.577	7
9905.5	45.471	17.9	1002.2	27.571	7.5
9913.5	45.458	17.91	1004	27.548	4
9921.5	45.513	17.99	1005.2	27.523	7
9929.5	45.632	18.161	1003.95	27.471	9.5

APPENDIX E

Propane and Methane Profiles from Propane Tracer Tests

			PROPANE		
	10/11/90		11/16/90		
DEPTH	PROFILE 3	PROFILE 4	PROFILE 1	PROFILE 2	PROFILE 3
0-2.4 CM	6.69E-04	6.03E-04	4.35E-05	5.48E-05	5.44E-05
2.4-4.8 CM	1.03E-03	9.55E-04	5.11E-05	7.68E-05	1.69E-04
4.8-7.2 CM	1.13E-03	1.19E-03	6.11E-05	1.38E-04	5.16E-04
7.2-9.6 CM	2.08E-03	1.55E-03	6.57E-05	2.34E-04	3.59E-03
9.6-12 CM	2.91E-03	2.70E-03	9.38E-05	3.23E-04	2.56E-02
12-14.4 CM	7.89E-03	6.13E-03	1.09E-04	5.09E-04	2.88E-02

		METHANE			METHANE		
	10/25/90	11/1/90			11/16/90		11/16/90
DEPTH	PROFILE 1	PROFILE 1	PROFILE 2	PROFILE 3	PROFILE 1	PROFILE 2	PROFILE 3
0-2.4 cm	9.48E-07	3.57E-06	3.54E-06	3.50E-06	8.90E-07	9.32E-07	1.18E-06
2.4-4.8 cm	1.06E-06	3.80E-06	3.82E-06	3.68E-06	1.09E-06	1.04E-06	1.49E-06
4.8-7.2 cm	1.05E-06	3.85E-06	3.91E-06	3.98E-06	1.21E-06	1.51E-06	1.64E-06
7.2-9.6 cm	1.25E-06	3.82E-06	3.92E-06	3.91E-06	1.34E-06	1.82E-06	2.04E-06
9.6-12 cm	1.38E-06	4.02E-06	4.08E-06	4.09E-06	2.42E-06	2.19E-06	3.22E-06
12-14.4 cm	1.66E-06	5.04E-06	4.31E-06	4.42E-06		5.16E-06	3.51E-06